VPI-E-73-9
March 1973

An Evaluation of the Three-dimensional Split-film Anemometer for Measurements of Atmospheric Turbulence

H. W. Tieleman and K. P. Fewell
Department of Engineering Science and Mechanics

H. L. Wood
Department of Mechanical Engineering

This research was supported by the National Aeronautics and Space Administration, Washington, D. C., under Grant No. NGL 47-004-067.

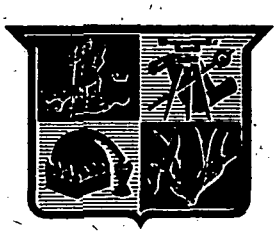

College of Engineering
Virginia Polytechnic Institute and State University

AN EVALUATION OF THE THREE-DIMENSIONAL SPLIT-FILM ANEMOMETER FOR MEASUREMENTS OF ATMOSPHERIC TURBULENCE

H. W. Tieleman*

K. P. Fewell**

H. L. Wood***

Department of Engineering Science and Mechanics
College of Engineering
Virginia Polytechnic Institute
and State University
Blacksburg, Virginia 24061

*Associate Professor
**Graduate Research Assistant
***Professor

ABSTRACT

The Thermo-Systems, Inc., Model 1080D three-dimensional split-film anemometer was tested in non-turbulent flow in the VPI&SU stability wind tunnel as well as in a turbulent flow downstream from a turbulence grid in the same wind tunnel.

Calibration constants were reevaluated and changes were made in the T.S.I.-suggested method of analysis (computation of the velocity components in the sensor-oriented coordinate system). An alternate method was introduced where the computation of the velocity components is based on the ratio of the heat transfer from the two films on the same sensor. With the latter method, the sensor yaw angles, ϕ, are obtained through geometric relations from the sensor pitch angles, θ, which in turn depend on the heat transfer ratio of the two adjacent films.

The two methods of analysis were compared and it was found that the new method or the so-called θ-method was somewhat more accurate than the improved T.S.I.-suggested method. However, errors of approximately $\pm 10\%$ can be expected depending on the angle of attack. Only when the probe is operated with zero angle of attack or when the mean velocity vector is parallel to the probe axis can an accuracy of approximately 3% be expected with the ϕ-method (improved T.S.I. method).

The data obtained with this probe in the turbulence behind a grid indicated that the measured turbulence intensities are somewhat lower than the intensity measured with the conventional hot-wire anemometry, which was to be expected as a result of the finite dimensions of the sensor array. In addition, the probe yaw angle can be determined within a three degree accuracy. This angle is necessary in order to obtain the statistical

averages in a coordinate system determined by the mean-wind direction, and the vertical and the lateral directions.

TABLE OF CONTENTS

LIST OF FIGURES

LIST OF TABLES

LIST OF APPENDICES

LIST OF SYMBOLS

A	Constant in Collis and Williams heat-transfer formula (2-1).
A_θ	Factor in correlation expression (5-31).
a	Surface area of hot wire.
a_f	Surface area of hot film.
B	Constant in Collis and Williams heat-transfer formula (2-1).
C	Constant in heat-transfer formula (2-5).
CF	Temperature correction factor (5-15).
D	Constant in heat-transfer formula (2-5).
d	Diameter of hot wire or hot film.
E	Error as defined in 5-22, also DISA hot-wire anemometer output voltage.
E_I, E_{II}	Bridge voltages for films I and II, respectively.
$\sqrt{\overline{e^2}}$	Root mean square of voltage fluctuation.
h_f	Convective heat-transfer coefficient.
I	Heating current.
I_I, I_{II}	Heating current of films I and II, respectively.
K_I, K_{II}	Calibration constants for films I and II, respectively.
k	Constant in expression for effective cooling - velocity (2-10).

k_m	Heat conductivity of air measured at mean temperature, T_m.
L	Active length of hot wire or hot film.
Nu	Nusselt number.
n	Exponent in heat-transfer formula (2-1).
n_θ	Exponent in expression for sensor.
p	Atmospheric pressure.
p_s	Standard atmospheric pressure (14.7 psia or 29.92 in. Hg).
Q	Total heat transfer per unit time from one sensor.
Q_2/Q_1	Ratio parameter (3-16).
Q_{TOT}	Total heat transfer from cable and film.
q	Heat transfer per unit time from one film.
q_d	Heat transfer per unit time from downstream film.
q_u	Heat transfer per unit time from upstream film.
$(q_d/q_u)_{\theta=90°}$	Ratio of heat transfers per unit time for sensor pitch angle $\theta = 90°$.
R	Ratio of film voltages $\frac{E_I}{E_{II}}$ for zero sensor pitch angle.
R_I, R_{II}	Hot film resistance, for films I and II, respectively.
R_{A_I}, $R_{A_{II}}$	Resistance of bridge arm adjacent to film, for films I and II, respectively.
R_{B_I}, $R_{B_{II}}$	Total bridge resistance for films I and II, respectively.

R_{C_I}, $R_{C_{II}}$	Cable resistance, for films I and II, respectively.
R_{cold}	Cold resistance of film.
R_f	Film resistance.
R_{TOT}	Sum of cable resistance and film resistance.
Re_d	Reynolds number based on diameter of hot wire or hot film.
ΔR_c	Change in cable resistance.
S_u	Velocity sensitivity.
T_a	Ambient temperature.
T_f	Film operating temperature.
T_m	Mean temperature between film and air.
T_s	Standard atmospheric temperature.
ΔT	Difference between film operating temperature and ambient temperature.
U	Actual velocity
U_A, U_B, U_C	Velocity components in sensor-oriented coordinate system.
U_e	Effective cooling velocity.
$U_{es}(A)$, $U_{es}(B)$, $U_{es}(C)$	Effective cooling velocities for the three sensors A, B and C at standard conditions.
U_{ps}	Velocity measured with pilot-static tube.
U_s	Total velocity at standard conditions.
u	Velocity fluctuation in streamwise direction.
$\sqrt{\overline{u^2}}$	Root mean square of velocity fluctuations.
V_T	Thermocouple voltage.

α	Probe pitch angle.
α_{cu}	Temperature coefficient of resistance for copper.
α_f	Temperature coefficient of resistance for the hot film.
α_s	Factor for second approximation in T.S.I. method (3-12).
β	Probe yaw angle.
β_s	Factor for second approximation in T.S.I. method (3-12).
θ	Sensor pitch angle.
ρ	Density of air.
ρ_s	Density of air at standard conditions.
ϕ	Sensor yaw angle.

Subscripts

A, B, C	Reference to the three mutually-perpendicular sensors.
I, II	Reference to the two films on the same sensor.
s	Reference to standard conditions.
1	Reference to T.S.I. calibration conditions.
2	Reference to ambient conditions for the hot films.
3	Reference to ambient conditions for the cable.

Superscripts

1	Reference to improved accuracy in the T.S.I.-method and θ-method of analysis.

Chapter I

INTRODUCTION

The need for accurate measurements of atmospheric turbulence has become increasingly apparent in the several years. A knowledge of the structure of turbulence in the atmospheric boundary layer is necessary for use in many practical applications, such as air-pollution control, the launching of missiles, the design of aircraft, and the design of bridges and other engineering structures.

Many types of instruments have been developed to perform these measurements. The use of some of these instruments for meteorological measurements, however, has only become possible recently because of the rapid growth of the electronics industry.

One of the most widely used instruments in meteorology is the cup anemometer, which is most frequently used in conjunction with a vane for direction measurements. Although a cup anemometer is very useful for measurements of mean wind speed, serious problems arise when one attempts to use either this instrument or the aerovane for turbulence measurements. Because of their large physical size and the attendant poor frequency response, it is doubtful that adequate response is possible with such large instruments for the measurement of atmospheric turbulence.

Drag-sphere anemometers are useful in some applications (8). However, these instruments are also relatively large and do not have

an exceptionally high-frequency capability. In addition, problems are encountered with the strain gages used on them. As indicated by Morrison (8), calibration is a rather long and complicated procedure.

The use of the sonic anemometer, a relatively new turbulence-measuring device, is becoming more widespread. However, in addition to its considerable cost, the sonic anemometer has the disadvantage of having a lower frequency limit determined by its size. Also, the sonic anemometer cannot be used for extremely low velocities and the measurements are dependent on local atmospheric conditions such as temperature and humidity.

There are many other types of anemometers currently available. The three-dimensional split-film anemometer (T.S.I.-1080D) was selected for use in this project because of the many advantages it has over the types mentioned above. First, this system may be used over a wide range of angles of attack, while the variations of the heat transfer from the sensor due to different angles of attack are being accounted for with the use of a specific correlation expression.

One of the major advantages of a split-film anemometer is that the magnitude of the velocity and thus, the velocity components, are calculated at any instant, thus eliminating the problems of non-linearity which are encountered in customary hot-wire anemometry. In addition, no assumption of $u<<\overline{U}$ need to be made which, for atmospheric applications, is not necessarily valid. Another advantage of the split-film anemometer is the film's characteristic small time

constant, especially as compared to the cup anemometer. This gives a frequency response up to 1000 Hz for this particular system.

Because of the orientation of the sensors on the T.S.I.-1080D and the two split films on each sensor, there is no ambiguity in the determination of the angle between the mean wind direction and the sensor. This is a major problem with other types of sensors.

Because of the high sampling rates which need to be used with the three-dimensional split-film anemometer system, a special data handling and analysis system had to be developed. This system will be discussed in detail in a later chapter.

In order to perform a complete evaluation of the accuracy of the anemometer, it was decided to first take measurements in turbulence free flow in the Virginia Tech 6-foot stability wind tunnel and obtain the necessary calibration constants from this data. Then, in order to check the response and accuracy of the system, the anemometer was tested in the turbulent flow field generated by a grid aligned perpendicular to the axis of the wind tunnel.

Chapter II

HOT-WIRE AND HOT-FILM ANEMOMETRY

2.1 Types of Anemometers

The hot-wire or hot-film anemometer is the most reliable and accurate and the most widely used instrument for the measurement of turbulence which has been developed to date. The detecting element of the anemometer is either a short, thin wire suspended between two supports, or, in the case of a hot-film anemometer, a thin metal film fused to a quartz rod and sometimes coated with a thin layer of quartz for protection. Either type is heated by an electric current.

There are two basic modes of operation of a hot wire: either constant current operation (Figure 1) or constant temperature operation (Figure 2). The constant-current type has the disadvantage in that compensation for the time constant must be adjusted manually during a test, while the thermal inertia of a wire or film operating in the constant-temperature mode is compensated for automatically by an amplifier operating in a feedback loop.

Because of the feedback-type operation, the constant temperature anemometer is also more useful in flows with high turbulence intensities, especially with the development of the linearizer. The problems mentioned in previous years in connection with the constant-temperature system and the stability of the amplifiers have been solved by recent developments in the field of electronics. Thus, the

constant-temperature anemometer is currently the most widely used type and it is the type used in the T.S.I.-1080D system.

2.2 Theoretical Aspects

The basic notion behind the operation of a hot-wire or hot-film anemometer is the transfer of heat from the detecting element to the surrounding environment. There are five factors that influence this heat transfer (4):

1. The angle of attack
2. The flow velocity
3. The physical properties of the surrounding fluid
4. The difference in temperature between the wire and the fluid
5. The dimensions and physical properties of the wire or film.

In the development of the general theory of operation of a hot-wire anemometer, it is assumed that there is no heat conduction to the supports and that there are no radiation losses. Any losses that do occur due to these factors (and under certain conditions they may be considerable) may be accounted for in the calibration process. In addition, only the effects of forced convection are considered, with free convection becoming important only at very low velocities, which are not of interest in this study.

The first theoretical solution for the heat transfer from a heated cylinder was developed by L. V. King in 1914 (5). King treated the case of two-dimensional, potential, incompressible and inviscid

flow. Collis and Williams (3) found that King's results did not take into account a sufficient temperature loading (see reference 3) correction. Their improvement to King's solution is given by,

$$Nu = (A + B\ Re_d^n)\ \left(\frac{T_m}{T_a}\right)^{0.17} \tag{2-1}$$

where T_m/T_a represents the temperature loading of the wire. The constants A, B, and n as found by Collis and Williams are given in Table I.

The heat transferred per unit time from a hot film is:

$$q = h_f a\ (T_f - T_a)$$

or introducing the Nusselt number

$$q = Nu\ k_m\ a\ (T_f - T_a)/d \tag{2-2}$$

where $a = \pi dL$. Substituting expression (2-1) into (2-2) yields

$$q = k_m \pi\ L\ (T_f - T_a)\left(\frac{T_m}{T_a}\right)^{0.17}\ (A + B\ Re_d^n). \tag{2-3}$$

And, since conduction and radiation losses are neglected,

$$I^2\ R_f = C\ k_m \pi\ L\ (T_f - T_a)\ \left(\frac{T_m}{T_a}\right)^{0.17}\ (A + B\ Re_d^n). \tag{2-4}$$

Now, the relation between the velocity of the fluid and the power required to operate the sensor at a given temperature in a specific fluid may be given by

$$\frac{I^2\ R_f}{T_f - T_a} = C + D\ (\rho U_e)^n \tag{2-5}$$

where U_e is the effective cooling velocity. Essentially, U_e is the normal velocity that would produce the same amount of cooling of the sensor as is produced by the actual velocity under some angle of attack.

For a split-film sensor (see section 3.1) where both films are operating at the same temperature,

$$\frac{I_I^2 R_I + I_{II}^2 R_{II}}{T_f - T_a} = C + D (\rho U_e)^n \tag{2-6}$$

where R_I and R_{II} are the hot resistances of the two films respectively.

Now, we must relate the effective cooling velocity to standard pressure and temperature (which will be taken to be p_s = 14.7 psia or 29.92 in. Hg and T_s = 530° R.). It is required that $\rho U_e = \rho_s U_{es}$.

From the equation of state for a perfect gas, we obtain

$$U_e = \frac{\rho_s}{\rho} U_{es} = \frac{p_s}{p} \frac{T}{T_s} U_{es} \tag{2-7}$$

where p is the barometric pressure and T is the ambient air temperature in °R. Now we have,

$$\frac{I_I^2 R_I + I_{II}^2 R_{II}}{T_f - T_a} = C + D (\rho_s U_{es})^n . \tag{2-8}$$

Since ρ_s is a constant, it may be incorporated into the coefficient D and equation (2-8) becomes

$$\frac{I_I^2 R_I + I_{II}^2 R_{II}}{T_f - T_a} = C + D U_{es}^n . \tag{2-9}$$

Until now, we have assumed that the ambient temperature remains constant. In the atmosphere, however, this is obviously not a valid assumption and a correction must be made to account for this change. The derivation of this correction will be treated in a subsequent chapter.

Next, we must investigate the case where the sensor is yawed with respect to the mean flow. As suggested by Hinze (4),

$$U_{es}^2 = U_s^2 \, (\cos^2 \phi + k^2 \sin^2 \phi) \tag{2-10}$$

where U_s is the magnitude of the velocity under standard conditions and ϕ is the angle of yaw. The factor k is used to indicate the contribution of the lateral velocity component to the total cooling velocity when the sensor is yawed with respect to the mean-velocity vector. Introducing equation (2-10) into equation (2-9), we obtain,

$$\frac{I_I^2 \, R_I + I_{II}^2 \, R_{II}}{T_f - T_a} = C + D \, U_s^n \, [\cos^2 \phi + k^2 \sin^2 \phi]^{\frac{n}{2}} \tag{2-11}$$

This equation yields a means for the calculation of the velocity U_s from known or measurable quantities.

Chapter III

THE T.S.I. MODEL 1080D THREE-DIMENSIONAL SPLIT-FILM ANEMOMETER SYSTEM

3.1 The Probe

The T.S.I. model 1080D probe is shown in Figure 3. It consists of three split-film sensors and a copper-constantan thermocouple for measurement of the ambient temperature. In addition, there are the necessary electrical leads and cable connections, a calibration shield and orifice, a pneumatic cylinder and valve for remote operation of the shield, and a mounting flange.

Each sensor consists of a 0.006 inch diameter quartz rod (Figure 4) which is coated with a platinum film of approximately 1000 Å in thickness. The sensor is coated with a thin quartz film for protection from contamination. The total sensor length is 0.200 inches while the active length is approximately 0.08 inches, giving an $\frac{L}{d}$ ratio of approximately 13.33. The ends of the sensor are gold plated.

The sensors are supported at only one end to avoid as much support interference as possible. The sensors are mounted on the probe in an orthogonal array as shown in Figure 5. The splits are arranged in such a way as to provide the octant determination necessary for proper data reduction. All three sensors, when mounted on the probe, fit into a 0.3 inch diameter sphere.

The reference junction for the copper-constantan thermocouple is mounted on an aluminum block enclosed in the chassis of the control circuit so that the reference temperature will remain virtually constant. Any reference temperature changes are cancelled by changes in the compensating circuit output. By proper adjustment of the "gain" and "zero" potentiometers, the operating range of the thermocouple may be varied. For use in this project, the potentiometers were set to provide zero volts output at 0° F and five volts output at 150° F. The output is slightly non-linear over the range of operation. However, the "zero" potentiometer may be set to compensate for this non-linearity over a small range of ambient temperatures.

The pneumatically operated calibration-shield is provided for the protection of the sensors and, with the built-in calibration nozzle is a quick means of checking the calibration.

3.2 The Control Circuit

The control circuit controls all of the six films on the probe. There are two printed circuit boards contained in the unit. The first is the "bridge" board which contains the amplifier bridges and the thermocouple amplifier. In addition, the supply busses, output lines, and the thermocouple leads from the reference junction compensator are wired to this board.

The second printed circuit board is the "amplifier" board which is connected to the bridge board and into which the cable is connected.

The "zero" and "gain" potentiometers for the six 0-5 volt outputs and the potentiometers for the temperature amplifiers are

located on the front panel. Also, the three "balance" potentiometers and the output pin jacks are found on this panel.

Amphenol connectors for the operation of the calibration and shield systems, the power cord, and the analog output amphenol-connectors are located on the rear panel of the chassis.

In addition to the above units, the cabinet contains a voltage regulator for the power supplied to the control circuit. The power switch, shield and calibrate control are located on the front panel of the regulator.

3.3 Output Devices

Each anemometer system has six 0-5 volt output pin jacks, six bridge voltage output pin jacks, one temperature output pin jack and corresponding amphenol connector output facilities. For turbulence-free flows in the wind tunnel, a digital voltmeter may be used to record the voltages used in the data reduction procedure. However, for most applications, some form of automated data acquisition system must be developed so that the voltages can be sampled simultaneously and high sampling rates may be used. The system developed for this project will be discussed in some detail in a later chapter. For a more detailed explanation of the anemometer see reference 10.

3.4 Theory of Operation

For the T.S.I.-1080D anemometer system, the voltages across each bridge are measured. For one sensor, let R_{B_I} and $R_{B_{II}}$ be the two total bridge resistances. Now, from the development in Chapter 2, equation 2-11 becomes,

$$\frac{\frac{R_I}{R_{B_I}^2} I_I^2 R_{B_I}^2 + \frac{R_{II}}{R_{B_{II}}^2} I_{II}^2 R_{B_{II}}^2}{T_f - T_a} = C + D\, U_s^n \left[\cos^2 \phi + k^2 \sin^2 \phi\right]^{\frac{n}{2}} . \quad (3\text{-}1)$$

Now,

$$R_{B_I} = R_I + R_{C_I} + R_{A_I} .$$

And, (3-2)

$$R_{B_{II}} = R_{II} + R_{C_{II}} + R_{A_{II}} .$$

where R_{A_I} and $R_{A_{II}}$ are the fixed resistances in the arm of the bridge which is adjacent to the cable and film arm, and R_{C_I} and $R_{C_{II}}$ are the cable resistances and R_I and R_{II} the film resistances. For this particular system,

$$R_{A_I} = R_{A_{II}} = 110\ \Omega .$$

Now, define

$$K_I = \frac{R_I}{R_{B_I}^2} \text{ and } K_{II} = \frac{R_{II}}{R_{B_{II}}^2} .$$

Since

$$I_I^2 R_{B_I}^2 = E_I^2$$

and

$$I_{II}^2 R_{B_{II}}^2 = E_{II}^2 ,$$

we obtain

$$\frac{K_I E_I^2 + K_{II} E_{II}^2}{T_f - T_a} = C + D\, U_s^n \left[\cos^2 \phi + k^2 \sin^2 \phi\right]^{\frac{n}{2}} . \quad (3\text{-}3)$$

The voltages E_I and E_{II} are the bridge voltages for films I and II respectively. The constants K_I and K_{II} also correct for area and resistance differences in the two films and must be determined experimentally.

For all velocities of interest in this study, the constant C may be eliminated by adjustment of K_I and K_{II}. All the split-film sensors will then obey the following equations:

$$\frac{K_I E_I^2 + K_{II} E_{II}^2}{\Delta T} = D U_{es}^n \tag{3-4}$$

and

$$(K_I E_I^2 + K_{II} E_{II}^2)/\Delta T = D U_s^n [\cos^2 \phi + k^2 \sin^2 \phi]^{\frac{n}{2}} \tag{3-5}$$

where $\Delta T = T_f - T_a$.

Since the quantity on the left-hand side of equations (3-4) and (3-5) is a measure of the total heat transfer, we may define

$$\frac{Q}{\Delta T} = \frac{K_I E_I^2 + K_{II} E_{II}^2}{\Delta T} .$$

Equations (3-4) and (3-5) then become

$$\frac{Q}{\Delta T} = D U_{es}^n \tag{3-6}$$

and the total heat-transfer for each sensor becomes

$$\frac{Q}{\Delta T} = D U_s^n [\cos^2 \phi + k^2 \sin^2 \phi]^{\frac{n}{2}} . \tag{3-7}$$

The constants D and n must be determined from calibration data. When the sensor is operated in a position normal to the flow, the sensor yaw angle, ϕ, is zero and the effective cooling velocity of the

sensor U_{es} and the standard velocity U_s are identical. From calibration curves showing the variation of total heat transfer with a change in the standard velocity for a zero yaw angle, values for the coefficients D and n can be obtained.

For operation with a non-zero yaw angle, the factor k in equation (3-7) must be known. As a first approximation a value of 0.2 is used as suggested by Champagne et. al. (2). The three sensors A, B and C are mounted in a mutually perpendicular manner. Because of this geometry, it can be shown that

$$\sin^2 \phi_A + \sin^2 \phi_B + \sin^2 \phi_C = 1$$

and

$$\cos^2 \phi_A + \cos^2 \phi_B + \cos^2 \phi_C = 2 .$$

These relations will be used in the data reduction procedure suggested by T.S.I. (10). An explanation of this procedure follows.

Recall that

$$U_{es} = U_s \left(\cos^2 \phi + 0.2^2 \sin^2 \phi\right)^{1/2} \qquad (3\text{-}8)$$

for each sensor. Taking the squares of the three cooling velocities, adding the results and using the above geometric relations, one obtains the following expression for the standard velocity:

$$U_s = \left[\frac{U_{es}^2 (A) + U_{es}^2 (B) + U_{es}^2 (C)}{2.04} \right]^{1/2} . \qquad (3\text{-}9)$$

The actual velocity can be found by making use of the equation of state for a perfect gas. Since the mass velocity ρU must be a constant,

$$U = \frac{\rho_s}{\rho} U_s = \frac{p_s}{p} \frac{T}{T_s} U_s \qquad (3\text{-}10)$$

where p_s and T_s are the standard pressure and temperature and p and T are the actual pressure and temperature, respectively.

Ultimately, the velocity components are required and as a result, the magnitude and sign of the three sensor yaw angles ϕ_A, ϕ_B and ϕ_C must be determined. Since the standard velocity is now known, equation (2-10) may be used to obtain the yaw angles.

$$\sin \phi_A = \left[\frac{1 - \frac{U_{es}^2 (A)}{U_s^2}}{0.96} \right]^{1/2} . \qquad (3\text{-}11)$$

Similar expressions for ϕ_B and ϕ_C can be obtained.

The signs of the yaw angles are determined by an examination of the geometry of the sensors and their arrangement on the probe in conjunction with a comparison of the heat transfers from the two films on one sensor. The signs of the sensor yaw angles ϕ_A, ϕ_B and ϕ_C are given by the following set of conditions:

If $E_{I_C} > R_C E_{II_C}$, $\phi_A > 0$; otherwise, $\phi_A < 0$.

If $E_{I_A} > R_A E_{II_A}$, $\phi_B > 0$; otherwise, $\phi_B < 0$.

If $E_{I_B} > R_B E_{II_B}$, $\phi_C > 0$; otherwise, $\phi_C < 0$.

where R_A, R_B and R_C are the ratios of the voltages when the velocity vector lies in the plane of the two splits of one sensor. If this is the case, the heat transfer from each film should be equal and as a result for zero sensor pitch angle, θ,

$$K_I \, E_I^2 = K_{II} \, E_{II}^2$$

and $$E_I = \left(\frac{K_{II}}{K_I}\right)^{1/2} E_{II}$$

or for example

$$E_{I_A} = R_A \, E_{II_A} \, .$$

After the magnitudes and signs of the angles are found, the velocity components in the sensor-oriented coordinate system may be calculated.

However, the correlation given by equation (2-11) does not fit the data well. It was found that the coefficient k is not only a function of the magnitude of the velocity, but a function of the sensor yaw angle ϕ as well. The ϕ-dependence turns out to be asymmetric as a result of support interference for sensor yaw angles of -90°.

T.S.I. suggested that the following correlation be used as a second approximation:

$$\frac{U_{es}^2}{U_s^2} = \cos^2 \phi + \alpha_s (U_s, \phi)\, k^2 (U_s) \sin^2 \phi$$

where

$$\alpha_s (U_s, \phi) = 1 + \beta_s (U_s) \cos^2 \phi$$

and

$$k (U_s) = 0.9 (U_s)^{-\frac{1}{2}} \quad \text{for } 0 < U_s < 20$$

$$k (U_s) = 0.2 \text{ for } 20 < U_s < 150.$$

For $\phi < 0$, (3-12)

$$\beta_s (U_s) = 0 \text{ for } 0 < U_s \leq 20$$

$$\beta_s (U_s) = -12 + 0.6\, U_s \text{ for } 20 < U_s \leq 30$$

$$\beta_s (U_s) = 5 + 0.033\, U_s \text{ for } 30 < U_s \leq 150$$

and for $\phi > 0$

$$\beta_s (U_s) = 0 \text{ for } 0 < U_s \leq 20$$

$$\beta_s (U_s) = -22 + 1.1\, U_s \text{ for } 20 < U_s \leq 30$$

$$\beta_s (U_s) = 9 + 0.067\, U_s \text{ for } 30 < U_s \leq 150.$$

The expression for the second approximation of the velocity is given by,

$$U_s^1 = \left[\frac{U_{es}^2 (A) + U_{es}^2 (B) + U_{es}^2 (C)}{2 + k^2 (U_s) \{\alpha_{s_A} \sin^2 \phi_A + \alpha_{s_B} \sin^2 \phi_B + \alpha_{s_C} \sin^2 \phi_C\}} \right]^{1/2} . \quad (3\text{-}13)$$

A second approximation for the sensor yaw angles can be found from

$$\sin \phi_A^1 = \left[\frac{1 - \frac{U_{es}^2 (A)}{U_s^2}}{1 - \alpha_{s_A} k^2 (U_s)} \right]^{1/2} . \quad (3\text{-}14)$$

Again, similar expressions can be obtained for the other sensor yaw angles ϕ_B and ϕ_C.

The signs of the yaw angles are the same as found previously. Because of the method used in obtaining the magnitudes and signs of the velocity components, there can be no ambiguity as to the quadrant in which the total velocity vector is located.

Olin and Kiland (9) suggested an alternate data analysis procedure which is based on the variation of the ratio of the heat flux of the downstream film to that of the upstream film with the sensor pitch angle θ. This variation is the result of the non-uniform heat-flux around the sensor. The three heat-flux ratios depend on the magnitude of the velocity, the yaw angles and the pitch angles. Olin and Kiland point out that a correlation expression of the form

$$\frac{q_d/q_u - (q_d/q_u)\theta = 90°}{1 - (q_d/q_u)\theta = 90°} = \left[1 - \frac{\theta}{90}\right]^2 \qquad (3\text{-}15)$$

can be used over a wide range of velocities and yaw angles. It turns out that the parameter

$$\frac{Q_2}{Q_1} = \frac{q_d/q_u - (q_d/q_u)\theta = 90°}{1 - (q_d/q_u)\theta = 90°} \qquad (3\text{-}16)$$

is independent of the velocity and yaw angle and is only a function of the sensor pitch angle θ. It should be noted that this is true even though the ratio q_d/q_u is not independent of velocity.

The signs of the three sensor pitch angles are determined by a comparison of the heat flux from the upstream film to that of the downstream film.

Once the magnitudes and signs of the three pitch angles have been determined, the three sensor yaw angles may be obtained by the use

of certain geometrical relationships that may be found between the pitch and yaw angles. Using the same method as was suggested by TSI, the magnitude of the velocity may be determined. Then the magnitudes and signs of the velocity components may be determined as before.

Besides the velocity components, it is necessary to calculate the ambient temperature so that velocity-temperature correlations can be obtained. The ambient temperature is calculated using the gain of the temperature amplifier. The operating range is decided upon (in this case it was 0 - 150° F.) and the gain is calculated as follows. Let T_{a_L} be the lower limit of the range and T_{a_H} the upper limit. Then, the gain is given by $(T_{a_H} - T_{a_L})/5$. The high temperature corresponds to five volts output and the lower temperature corresponds to zero volts output. The ambient temperature, T_a, is given by

$$T_a = \frac{T_{a_H} - T_{a_L}}{5} V_T,$$ where V_T is the voltage indicated. The output is slightly non-linear, but this may be accounted for in a small range by the adjustment of the "zero" potentiometer.

The object of this study is to analyze the results of data reduced by both methods and, if possible, to improve on either method and to adapt the T.S.I.-1080D three-dimensional split-film anemometer system for measurements of atmospheric turbulence in the planetary boundary layer.

Chapter IV

EXPERIMENTAL EQUIPMENT AND PROCEDURES

All experimental work in this study was carried out in the Virginia Polytechnic Institute and State University six-foot low-speed stability wind tunnel. The output data were initially read sequentially from a digital voltmeter. It was found, however, that due to small perturbations in the output, it was desirable to sample the outputs simultaneously. This was achieved using the data handling system which had been designed for taking turbulence data. The calibration data was sampled, multiplexed and recorded on digital tape and then printed on the teletype in octal form. The final data processing was performed by the IBM 370/155 digital computer after the data had been translated into decimal form and transferred to IBM cards.

4.1 Experimental Equipment

4.1.1 Wind Tunnel

The VPI&SU stability wind-tunnel has a 20-foot long, 6-foot square test section and is powered by a 600-horsepower motor which turns an 8-bladed propeller with a diameter of approximately 16 feet. The maximum test-section speed is approximately 370 fps and the minimum speed is approximately 10 fps. The test section speed is controlled by the use of two rheostats located on the operator's

console in the test-section area. The dynamic pressure, in inches of water, may be set at a predetermined magnitude and as a result, the test-section velocity may be set within a fraction of a foot per second of a predetermined value. Damping screens and a 3:1 entrance contraction produce a free stream turbulence intensity of approximately 0.1%. The flow angularity was measured at a point approximately 12 feet downstream from the test-section entrance and was found to be less than ±0.3°. A more detailed description of the stability wind tunnel can be found in reference 6.

4.1.2 Turbulence Grid

The grid used for turbulence measurements was located at the entrance to the test section. The grid was of the bi-planar type and was designed for maximum turbulence scale and maximum turbulence intensity while obtaining nearly isotropic turbulence and a uniform velocity profile at a distance of approximately 8 to 10 mesh lengths downstream from the grid. Vickery (11) indicates that a mesh size of one-fourth the tunnel width and a bar size of one-fifth the mesh size should give a near-uniform velocity as well as a near-uniform turbulence distribution within two tunnel widths (in this case 12 feet) downstream from the grid. A lateral scale of turbulence close to the bar size and an intensity of approximately 10% can be expected at this point. After examining Vickery's paper and one by Baines and Peterson (1), a mesh size of 18 inches and a bar size of 3.6 inches was decided upon. The "solidity ratio" of this grid was found to be about 0.40.

This should yield stable flow downstream according to Baines and Peterson. The turbulence grid and coordinate system are shown in Figure 6.

4.1.3 Probe Support Devices

Several different devices were used to support the probe, and all of them involved the angle-of-attack actuator. The basic component of the actuator system is a large steel turntable which may be made to rotate a full 360° with the use of a toggle-switch control on the operator's console. It is possible to control the angle of yaw of this turntable to within 0.01°. The turntable has been found to be inclined from the horizontal to an angle of less than three minutes. The support which is most frequently used is mounted on the turntable and is provided with a mechanism with which one may change the pitch angle of the probe. The control and readout for this mechanism is also located on the operator's console. However, it is difficult to set the angle of pitch accurately with the readout provided, and it was found easier to obtain a desired angle with the help of an inclinometer. This inclinometer was also used to check various other angles to insure proper alignment of the probe.

In addition to being used for general data acquisition in both fluctuating and non-fluctuating flows, this support system was also used when variations in sensor pitch angle were required. The probe was first mounted in a horizontal position so that alignment could be checked and then the probe pitch angle was changed until one of the sensors was in a vertical position. As can be seen from Figure 4, when the sensor is in this position, the sensor pitch angle θ may be

changed by simply rotating the turntable. For the location of the sensors with respect to the probe axis, the reader is referred to the Operating and Service Manual for the T.S.I. model 1080D total-vector anemometer (10).

While the previously discussed support-system was used most extensively during the tests, other methods of support were used at various times. One such method was designed to keep the anemometer's sensors located at the same point in the tunnel in order to eliminate effects of possible velocity variations across the tunnel. With this system, the probe pitch angle was changed by simply changing the angle of the support on which the probe was mounted. It was determined that any small velocity variations which did occur had no significant effect on the accuracy of the experiment. In addition, with this support system there was believed to be a significant blockage effect at high yaw angles.

The last method of probe support was used for calibrations where it was necessary to vary the sensor yaw angle, ϕ, a known amount. The support was mounted on the turntable as previously described and an index head was affixed to the support. The probe, when mounted in the index head, could be rotated about its axis in 15° increments. This allowed the sensors to be positioned in a horizontal plane, so that a rotation of the turntable produced the desired change in the sensor yaw angle.

4.1.4 Ambient Measurements

The static pressure in the tunnel was measured in millibars by a Kahlsico precision aneroid barometer. This instrument has a range of 900-1050 mb and can be read accurately to 0.01 mb.

The room temperature in the wind tunnel area was monitored constantly during the test periods. The temperature of the airflow at the tunnel wall was measured by means of a thermocouple which is permanently affixed to the wall.

4.1.5 Pitot-Static Tube Measurements

The dynamic pressure in the airflow was measured by a one-eighth inch Dwyer pitot-static tube which was mounted on a portable stand and placed as close as possible to the probe. The dynamic pressure was read on a Type 1023 Barocel electronic manometer which has a maximum pressure capability of 10 inches of water. The pressure data were read in inches of water on a meter on the front panel of the manometer. The accuracy of the readings from the panel meter is listed as ±2% of full scale on any operating range. There is approximately a 2% difference in reading over the entire range of this manometer when compared to the readings from the Meriam micromanometer also located in the tunnel area.

4.1.6 Turbulence Measurements

Velocity fluctuations were measured by means of a DISA type 55D01 constant-temperature hot-wire anemometer unit and a DISA type 55A22 general purpose probe. The sensor of the probe is a 1.2mm long, 5μm diameter platinum-plated tungsten wire.

This hot wire was located on the centerline of the tunnel and was calibrated under steady-flow conditions so that accurate values for the hot-wire bridge voltage could be obtained for several different velocities. These velocities ranged from 10 to 100 fps. From these results the velocity sensitivity, $S_u = \frac{\partial E}{\partial U}$, was obtained with the hot wire positioned normal to the flow. A standard spline interpolation method was used to fit a cubic equation between the experimental calibration points from which the slopes for different values of the velocity were obtained. From the root mean square measurements of the fluctuating output voltage of the hot-wire anemometer, the standard deviation of the streamwise velocity fluctuation can then be obtained from: $\sqrt{\overline{u^2}} = \frac{1}{S_u}\sqrt{\overline{e^2}}$.

4.2 Calibration Procedures for the T.S.I.-1080D Split-Film Anemometer

Before data may be taken with the T.S.I.-1080D anemometer, a short calibration check must be performed. The protective shield must be moved to its most forward position, and approximately 50 psi of air pressure is then applied to the calibration orifice through the pneumatic system. This orifice is designed to yield a flat velocity profile past the sensors for calibration purposes. The balance for each set of films (necessary to operate both films at the same temperature) is set to the value given by T.S.I. on the data sheet supplied with the anemometer. At this time, the total heat transfer from the sensor may also be checked. The calibrate air is now turned off and the shield moved back to the normal operating position.

4.3 Data Handling System

Because of the high sampling rates required, it was found necessary to develop a data handling system for the acquisition and processing of the seven output voltages from the TSI-1080D anemometer system. In addition, it was necessary that this system be capable of simultaneously recording data from up to 13 such anemometers.

The system multiplexes the seven signals from each anemometer and records the output on one channel of an analog tape recorder. When acquisition is halted, the output is played back, demultiplexed, digitized and stored on 9-track digital magnetic tape. The data is then processed either by a program written for the mini-computer or by one written for the IBM 370/155. The data acquisition and handling system is described in somewhat more detail in the following paragraphs and a schematic diagram of the entire system is presented in Figure 7.

Each voltage is fed into a constant band-width voltage-controlled oscillator (Data-Control Systems, Inc. Model GOV-5C). Each oscillator operates at a different center frequency and an input voltage of ±5 volts produces a deviation from the center frequency of ± 1 KHz. The outputs of the oscillators are then summed, along with the output of a 100 KHz reference oscillator, by a summing amplifier (Data Control Systems, Inc. Model GSA-5). The resulting output is a multiplexed signal of approximately three volts peak-to-peak. One such output signal is obtained for each anemometer. It should be noted that because of the voltage limitations of the voltage-controlled

oscillators, it is necessary to use the 0-5 volt output facilities of the anemometers as input to the system.

The multiplexed signal is then recorded on one of the channels of a 14-channel Bell and Howell, Model VR3700B, analog tape recorder. Thirteen channels may be used for the recording of the anemometer output signals, with the fourteenth channel used for time-of-day.

Time-of-day is generated by a Hermes Electronics Company system and is monitored by an Itek Electro-Products Co., Model 2124C remote display.

The data acquisition system has the capability of recording approximately one hour of continuous data. At this time, provisions are made for only two anemometers; however, it is possible to expand the system to accomodate the 13 desired anemometers.

In order to digitize the data, it is first necessary to demultiplex it. The desired output channel of the analog tape recorder is connected to the inputs of the eight discriminators (Data-Control Systems, Inc. Model GFD-16). The center frequency of each discriminator corresponds to the center frequency of one of the voltage-controlled oscillators (including the reference oscillator) and it produces an output voltage of ±5 volts for a frequency deviation of ±1 KHz. The recording is played into the discriminators and demultiplexed and the seven voltages are reproduced at the discriminator outputs. The reference discriminator can detect any variations in frequency of the 100 KHz reference signal and its output will correct the other seven discriminators.

The outputs of these discriminators are connected to low-pass filters (UTC Model LMI-100) which are matched for phase and amplitude response and which have cut-off frequencies of 100 Hz. This arrangement is necessary so that all frequency components above 100 Hz that might distort the turbulence spectra can be removed. The outputs of the filters are connected to the multiplexer and analog-to-digital converter.

The multiplexing analog-to-digital converter is a DEC Model AD01-D which was modified to allow higher scan rates. This 11-bit (plus sign) computer-controlled converter can make a conversion in about 5 microseconds. The total scan, settling and conversion time is approximately 50 microseconds per point.

The output of the tape channel on which the time of day is recorded is connected to a Hermes serial-to-parallel converter which produces a 32-bit binary-coded-decimal output. This converter is interfaced with the computer by a Digital Equipment Corporation custom-designed interface.

The basic component of the data acquisition and handling system is a Digital Equipment Corporation, Model PDP-11/20, 16-bit computer with an 8K memory. The computer controls the multiplexing analog-to-digital converter and two DEC, Model TR06-FB, digital tape units. Two programs have been written in assembly language: one for data processing and one for analog-to-digital conversion.

Conversion is begun by entering the desired time of day. After conversion, the data is stored in one of the four buffers

provided in the computer and held until the buffer is full. The buffer size is sufficient for 209 scans (approximately 1.045 seconds of data). When the first buffer is full, the second starts filling and the first is subsequently dumped onto digital tape. Any number of records may be digitized and recorded in this way.

In addition to writing the output on tape, the system has the capability of printing the recorded data on the teletype. This is quite useful for system calibration and for runs with low turbulence. System calibration may be checked by applying a known voltage to the entire system and checking this value against the one printed by the computer.

Although the conversion of the raw data to velocity components may be carried out using the IBM 370/155 computer, it was felt desirable to have the capability of processing the data in the PDP-11/20. This capability, in conjunction with the use of the digital-to-analog converters, is useful for checking the recorded sample for stationarity.

The data on the digital tape is read, one record at a time, into the computer memory. The temperature and three velocity components are calculated and recorded on a second magnetic tape.

The computed results can be monitored with the aid of two DEC, Model BA614, digital-to-analog converters which allow the display of any two calculated values.

Calibration constants and other necessary values are entered through the teletype. For checking computations, a "debug" mode of

operation is available in which computations made within the program are printed on the teletype. In addition, error messages are printed in the event an error occurs.

System noise is low, less than about 10 millivolts peak in 5 volts. System error is less than ±1% not including the anemometers.

4.4 Procedures for Non-fluctuating Velocities

In order that velocity components can be determined and can be compared with expected values, several pieces of information need to be recorded. For a particular tunnel velocity, a certain probe yaw angle, β, and a certain probe pitch angle, α, one needs the following:

1. Either six bridge voltages or six 0-5 v. output voltages.
2. The temperature output voltage.
3. The room temperature.
4. The atmospheric pressure.
5. The angles of attack, α and β.
6. The dynamic pressure from the pitot-static tube.

After the probe has been aligned with the tunnel axis and is located in the horizontal plane, the desired angles of pitch and yaw can be set on the operator's console. Data from the anemometer may be read from a digital voltmeter or may be obtained by the automatic data acquisition system. All other data (room temperature, atmospheric pressure, etc.) must be read and recorded manually.

The manual acquisition of the six bridge voltages and the output voltage of the thermocouple requires a digital voltmeter and each of the readings requires approximately 30 seconds. Therefore, about

three minutes is required to obtain a complete set of data for one specific set of conditions, and due to the fact that the tunnel is not completely sealed from the prevailing atmospheric conditions, the mean velocity of the airflow may have changed enough to significantly change the bridge voltages. In addition, for certain angles of pitch and yaw, one sensor will be directly upstream from another, and the downstream sensor will register the eddy shedding from the upstream sensor. As a result, it is difficult to obtain meaningful values for the velocity components. It was for this reason that it was decided to use the computer-controlled data-acquisition and handling system.

When the automatic data-acquisition system is used, two persons must be available; one in the tunnel area and one in the instrumentation trailer in which the system is located. The anemometer, which is also located in the trailer, is connected to the probe in the wind tunnel test section with a 350-foot cable. At the instant the automatic system records the voltages, the dynamic pressure must be read on the electronic manometer in the tunnel area. Since in non-fluctuating cases the seven octal numbers representing the seven voltage outputs are printed on the teletype, these numbers must be translated into decimal form before an analysis of the data can begin.

4.5 Procedures for Grid Turbulence

When turbulence data are taken, it is necessary to pass the seven output voltages through the voltage-controlled oscillators and the summing amplifier and to record the resulting signal on F.M. tape. Later, the recording is played back and sent through the discriminators

and the analog-to-digital converter for subsequent recording on digital tape. It is essential that the voltage-controlled oscillators and the discriminators be properly tuned and checked frequently as they are extremely sensitive to temperature changes within the instrumentation trailer. The entire system is calibrated for both zero and five volts input.

If frequency information up to 100 Hz is required, the sampling rate must be at least 200 samples per second and the higher frequency content of the sample must be filtered out. A sample length of three minutes was felt to be sufficient to provide a proper basis for statistical analysis.

Dynamic pressure, atmospheric pressure and room temperature were recorded. Because of the length of the sample, however, it is necessary to average these quantities over the length of the sample.

Chapter V

ANALYSIS AND DISCUSSION

5.1 Analysis of Turbulence-free Wind Tunnel Measurements with the T.S.I.-suggested Analysis

Since the T.S.I.-1080D three-dimensional split-film probes had never been used in an experimental program, it was decided to test them in turbulence-free flow in the wind tunnel for various probe pitch angles, α, and various probe yaw angles, β. The velocity was to range from 10 fps to 100 fps with a velocity of 30 fps being considered the most important. The first set of data was analyzed by the T.S.I.-suggested method previously described. The calibration constants needed for the calculation of the sensor yaw angle, ϕ, and the total velocity were provided by T.S.I. for each probe. The initial data were read sequentially as bridge voltages on a Fluke 8200A digital voltmeter. A FORTRAN computer program for the IBM 370/155 was developed to carry out the analysis and the results were printed for each α, β and velocity. The results obtained included the three sensor yaw angles, ϕ_A, ϕ_B and ϕ_C, the calculated standard velocity, the actual velocity and the velocity components in the tunnel-oriented coordinate system (see Figure 6 for the definition of this coordinate system).

The probe was mounted in a manner such that sensor A was located in a vertical plane which included the tunnel axis when α and β were both zero. The components in the sensor-oriented coordinate

system can be obtained by multiplying the sines of the respective sensor yaw angles, ϕ, with the actual velocity. Using a simple coordinate transformation, the velocity components in the tunnel-oriented coordinate system were calculated. Since the flow angularity in the tunnel was measured to be less than $\pm 0.3°$, one can expect the components in the y and z directions to be nearly zero, while the x-component of the velocity should be approximately equal to the velocity measured by the pitot-static tube which was placed next to the T.S.I. probe. In addition, for given probe yaw and pitch angles, the expected values of the sensor yaw angles can be computed by considering the fixed geometric arrangement of the sensors. The measured sensor yaw angles may then be compared to the expected sensor yaw angles.

In the analysis of the first set of data, error messages were obtained for many of the angles due to the fact that the quantity $1 - \frac{U_{es}^2}{U_s^2}$ in either equation (3-11) or equation (3-14) was, in these cases, less than zero. This, of course, leads to imaginary values of the sensor yaw angles and these cannot exist. The problem was corrected by setting $1 - \frac{U_{es}^2}{U_s^2}$ equal to zero when U_{es}^2/U_s^2 is greater than one.

In Figure 8, the percent error in total velocity is plotted for the velocity range from 10 fps to 100 fps for three different probe yaw angles: $\beta = 0°$, $-40°$ and $-90°$ with $\alpha = 0°$. As can be seen from this figure, the errors are excessive, especially for the case where $\beta = -90°$ and in the range of 20 to 30 fps where we expect to operate extensively when atmospheric measurements are made. In Figures 9, 10 and 11,

the error in sensor yaw angles ϕ_A, ϕ_B and ϕ_C is plotted for a probe yaw angle range of -150° to +150° and for a probe pitch angle of zero degrees and a velocity of 30 fps. As can be seen, the error in calculated sensor yaw angle exceeds 5° in most cases and the maximum deviation from the expected value is 20°. As a result, questionable values of the velocity components in the tunnel-oriented coordinate system were obtained. At this point, it was decided to work only with the components in the sensor-oriented coordinate system because they are the ones used in the statistical analysis of turbulence data.

In Figures 12, 13 and 14, results are presented for data taken to check the accuracy of the second approximation suggested by T.S.I. It can be seen that for positive sensor yaw angles, the experimental results are significantly different from those that would be predicted by the T.S.I.-suggested data reduction method. Also, a comparison of the three figures shows indications of a velocity dependence. The second approximation seems to work well for yaw angles from zero to -70°. Past this point, however, the comparison is not good at all. The portion of the curve from ϕ = -70° to ϕ = -90° is highly velocity dependent. These experimental data were taken for a sensor pitch-angle θ = +45°. For different θ angles the results as plotted in Figures 12, 13 and 14 can be expected to be slightly different because of a possible θ-dependence. According to T.S.I., however, these correlation curves are only slightly θ-dependent and the value of θ = +45° lies in the middle of the range of expected values of θ. Consequently, the T.S.I. correlation was only compared with data taken at a sensor pitch angle of +45°.

During the period that experiments were run, it was noticed that the values of $Q/\Delta T$ calculated from the calibration check did not agree well with the values given by T.S.I. An examination showed that at least part of the inaccuracy was due to the fact that the temperature was not the same as that at which the calibration was made.

Recall that,

$$\frac{K_I E_I^2 + K_{II} E_{II}^2}{T_f - T_a} = D U_{es}^n .$$

It was assumed in the discussion in which this equation was developed that the ambient temperature, T_a, did not change. In the atmosphere or in the VPI&SU wind tunnel, the ambient temperature cannot be controlled and, as a result, the quantity $\Delta T = T_f - T_a$ often varies drastically from the conditions at which T.S.I. calibrated the probe.

For example, assume that the local ambient temperature is greater than that at which the probe was calibrated by T.S.I. The heat transferred from the sensor will then be too low. The cooling velocity and the ratio U_{es}/U_s will be too low. In addition, changes in cable resistance must be taken into account because these changes will affect the resistance of the film and thus the operating temperature of the film and the heat transfer. As a result, a correction factor must be introduced to raise the magnitude of $Q/\Delta T$ to its proper value. If this is not done, it would be necessary to use a different calibration curve for each ambient temperature. Consequently a correction factor needs to be established in order to take care of variations in ambient temperature as well as variations in cable resistance as a result of ambient temperature changes.

The total heat transfer from the cable and film combined will be,

$$Q_{TOT} = I^2 R_C + I^2 R_f. \tag{5-1}$$

For the T.S.I. calibration conditions (denoted by the subscript "1"),

$$I_1^2 R_{f_1} = h_f a_f (T_{f_1} - T_{a_1}) \tag{5-2}$$

assuming there are no conduction or radiation losses and that only forced convection is important. At the local conditions (denoted by the subscript "2"),

$$I_2^2 R_{f_2} = h_f a_f (T_{f_2} - T_{a_2}). \tag{5-3}$$

Dividing equation (5-3) by equation (5-2), we obtain

$$\frac{I_2^2 R_{f_2}}{I_1^2 R_{f_1}} = \frac{T_{f_2} - T_{a_2}}{T_{f_1} - T_{a_1}}. \tag{5-4}$$

In a balanced bridge the resistance of each arm remains constant including the arm with the cable and the film and therefore

$$R_{TOT} = R_{f_1} + R_{C_1} = R_{f_2} + R_{C_2} \tag{5-5}$$

and,

$$R_{f_2} = R_{f_1} + (R_{C_1} - R_{C_2}) = R_{f_1} + \Delta R_C . \tag{5-6}$$

From this and expression (5-4)

$$RI_2 = \left[\frac{R_{f_1}}{R_{f_1} + \Delta R_C} \frac{T_{f_2} - T_{a_2}}{T_{f_1} - T_{a_1}}\right]^{1/2} RI_1$$

or

$$E_2 = \left[\frac{R_{f_1}}{R_{f_1} + \Delta R_C} \frac{T_{f_2} - T_{a_2}}{T_{f_1} - T_{a_1}}\right]^{1/2} E_1 . \tag{5-7}$$

So,

$$E_1 = \left[\frac{R_{f_1} + \Delta R_C}{R_{f_1}} \frac{T_{f_1} - T_{a_1}}{T_{f_2} - T_{a_2}}\right]^{1/2} E_2 \tag{5-8}$$

Now to first order accuracy for the resistance of the film, one may write the following,

$$R_{f_2} = R_{cold_1} [1 + \alpha_f (T_{f_2} - T_{a_1})]$$

and

$$R_{cold_2} = R_{cold_1} [1 + \alpha_f (T_{a_2} - T_{a_1})]. \tag{5-9}$$

It follows that,

$$T_{f_2} - T_{a_2} = \frac{R_{f_2} - R_{cold_2}}{\alpha_f R_{cold_1}}$$

and also

$$T_{f_1} - T_{a_1} = \frac{R_{f_1} - R_{cold_1}}{\alpha_f R_{cold_1}} . \tag{5-10}$$

Substituting the equation (5-10) into equation (5-8), one obtains

$$E_1 = \left[\frac{R_{f_1} + \Delta R_C}{R_{f_1}} \frac{R_{f_1} - R_{cold_1}}{R_{f_2} - R_{cold_2}}\right]^{1/2} E_2 . \tag{5-11}$$

For the cable resistance one can write that

$$R_{C_2} = R_{C_1} \{1 + \alpha_{cu} (T_{a_2} - T_{a_1})\}. \tag{5-12}$$

Subtracting R_{C_1} from each side of equation (5-12), one obtains

$$-\Delta R_C = R_{C_2} - R_{C_1} = R_{C_1} \alpha_{cu} (T_{a_2} - T_{a_1}). \tag{5-13}$$

For wind tunnel operation, however, the cable may be at a different temperature than ambient temperature at which the probe is operating. If we denote the ambient temperature at which the cable is operating by the subscript "3", we obtain

$$-\Delta R_C = R_{C_1} \alpha_{cu} (T_{a_3} - T_{a_1}). \tag{5-14}$$

The resistances and temperatures at which the probe was calibrated are supplied by T.S.I. as calibration data.

We may now define the correction factor, CF, as

$$CF = \frac{R_{f_1} + \Delta R_C}{R_{f_1}} \frac{R_{f_1} - R_{cold_1}}{R_{f_2} - R_{cold_2}}. \tag{5-15}$$

It should be noted that there will be one correction factor required for each film. The expression for the heat transferred from one sensor of the probe becomes

$$\frac{Q}{\Delta T} = \frac{K_I \, CF_I \, E_I^2 + K_{II} \, CF_{II} \, E_{II}^2}{\Delta T} \tag{5-16}$$

where $\Delta T = T_f - T_{a_1}$ = constant.

The correction factor was applied to data which had been obtained from the calibration check when the shield is moved over the sensors and the probe is exposed to the calibrate air. For the same mass flow rate, the introduced correction factor for operation at temperatures other than those used by T.S.I., the calculated heat transfer rates compare within one percent to those predicted by T.S.I.

The next step taken to improve the accuracy of the data-analysis method was to change the second approximation itself. The case where the sensor yaw angle, ϕ, is greater than zero is discussed first.

The equation for the TSI second approximation is

$$U_{es}^2 = U_s^2 \left[\cos^2\phi + k^2(U_s)\alpha_s(\phi,U_s) \sin^2\phi\right].$$

It is easily seen from the above equation that, when $\phi = 90°$,

$$U_{es}^2/U_s^2 = k^2 \alpha_s . \tag{5-17}$$

A new form for α_s was found by trial and error and is given by

$$\alpha_s = 1 + \beta_s \cos^3 \phi \sin^2 \phi. \tag{5-18}$$

Therefore, at $\phi = 90°$,

$$k = U_{es}/U_s . \tag{5-19}$$

A functional relationship for k in terms of U_s can be found from the experimental data. The values of β_s were found for each velocity by trial and error, then functional relationships for β_s in terms of U_s were found.

The values of β_s and k which fit the experimental data for both probes the best are:

$$
\begin{aligned}
&\text{for } U_s \geq 75 \text{ fps} && k = 0.2 \text{ and } \beta_s = 30.0 \\
&40 \leq U_s < 75 && k = 0.36 - 0.0021\ U_s \\
& && \text{and } \beta_s = -18.7 + 0.6493\ U_s \\
&25 \leq U_s < 40 && k = 0.36 - 0.0021\ U_s \\
& && \text{and } \beta_s = 21.068 - 0.3448\ U_s \\
&20 \leq U_s < 25 && k = 0.045 + 0.0105\ U_s \\
& && \text{and } \beta_s = -6.285 + 0.7347\ U_s \\
&8.6 \leq U_s < 20 && k = 0.39 - 0.0064\ U_s \\
& && \text{and } \beta_s = -6.285 + 0.7347\ U_s \\
&U_s < 8.6 \text{ fps} && k = 0.39 - 0.0064\ U_s \\
& && \text{and } \beta_s = 0\ .
\end{aligned}
\qquad (5\text{-}20)
$$

Now we consider the case where the sensor yaw angle is less than zero. For the range from $\phi = 0°$ to $\phi = -70°$, the T.S.I. second approximation is sufficiently accurate except where U_s was greater than 70 fps or less than 23 fps. In the first case ($U_s > 70$ fps), k was found to be 0.175. When $U_s \leq 23$ fps, k = 0.25 and Champagne's expression fits the data adequately.

The expressions in the range $-90° \leq \phi \leq -70°$ are somewhat more complicated. The expressions found by T.S.I. can be used in an altered form. A graph was made of the error, E, against the angle ϕ where

$$E = (U_{es}/U_s)^2_{\text{measured}} - (U_{es}/U_s)^2_{\text{calculated}} \qquad (5\text{-}22)$$

$$\text{where } (U_{es}/U_s)^2_{\text{calculated}} = (\cos^2\phi + k^2\ \alpha_s\ \sin^2\phi) \qquad (5\text{-}23)$$

as above, and where $(U_{es}/U_s)^2_{\text{measured}}$ is obtained experimentally. The expressions for E were found by trial and error and were:

$$\begin{aligned} &\text{For } U_s \geq 70 \text{ fps}, && E = \tan^2 (|\phi| - 70°) \\ &23 < U_s < 70 && E = 0.375 \tan^2 (|\phi| - 60°) \\ &23 \leq U_s && E = 0. \end{aligned} \qquad (5\text{-}24)$$

The final expression for the second approximation to $(U_{es}/U_s)^2$ for $\phi < 0$ is,

$$\frac{U_{es}^2}{U_s^2} = \cos^2 \phi + k^2 \alpha_s \sin^2 \phi + E. \qquad (5\text{-}25)$$

Figures 15, 16 and 17 show the results for velocities of 16, 25.2 and 38.7 fps, respectively. A great improvement over a large part of the range of angles is observed. The exception is in the range $-90° \leq \phi \leq -70°$. These angles, however, are well outside the range of normal operation, so no effort was made to further improve the accuracy of the approximation in this region.

An examination of data taken at probe yaw angles of ±90° indicated that the assumption that the dependence of the velocity measurement on the sensor pitch angle, θ, was negligible might not hold true. Consequently, tests were performed in which the sensor pitch angle was varied. Data was taken for several different mean velocities and the results were plotted as shown in Figures 18, 19 and 20. As can be easily seen from these figures, there is a rather significant θ-dependence. It is interesting to note that the general form of the curve is the same for all velocities, when dealing with one particular sensor.

It was hoped that a change in the values of K_I and K_{II} would reduce this θ-dependence, so a method was devised to accomplish this. First, it is necessary that the balance, which keeps the two films on

a sensor operating at the same temperature, be checked frequently. A value of θ is selected for each sensor which gives approximately zero velocity error and the $\frac{Q}{\Delta T}$ versus U_s curves are plotted for those angles. Since the heat transfers from the two films on a sensor must be equal when the velocity vector is directed at the split, i.e. that

$$K_I \, E_I^{\,2} = K_{II} \, E_{II}^{\,2},$$

it is easily seen that

$$\frac{K_I}{K_{II}} = \frac{E_{II}^{\,2}}{E_I^{\,2}} \tag{5-26}$$

for $\theta = 0°$. The average value of the ratio $E_{II}^{\,2}/E_I^{\,2}$ is found for this angle for each sensor.

Next, the voltages for each film are found for a particular velocity, in this case 30 fps for the θ angle chosen. The correction factors are also calculated, and a value of $Q/\Delta T$ for the velocity desired is obtained from the fixed calibration curve as is shown in Figure 21. Now the magnitude of the K's can be obtained by solving two simultaneous equations with the K's as unknowns. The two equations for sensor A of probe #1193 are

$$\frac{K_I}{K_{II}} = 0.9437$$

and

$$\frac{K_{I_A} \, CF_{I_A} \, E_{I_A}^{\,2} + K_{II_A} \, CF_{II_A} \, E_{II_A}^{\,2}}{\Delta T_A} = 0.568.$$

The values of K_I and K_{II} found for this case are:

$$K_{I_A} = 2.178$$
$$K_{II_A} = 2.308$$

$$K_{I_B} = 2.065$$
$$K_{II_B} = 2.276$$

$$K_{I_C} = 2.195$$
$$K_{II_C} = 2.180.$$

The procedure is repeated for each probe.

The values of R_A, R_B and R_C necessary for the determination of the signs of ϕ_A, ϕ_B and ϕ_C must now be found. When the velocity is directed at the split,

$$E_{I_A} = R_A E_{II_A}$$

or
$$R_A = \frac{E_{I_A}}{E_{II_A}} . \tag{5-27}$$

It is easily seen that

$$R_A = \left[\frac{K_{II_A}}{K_{I_A}} \right]^{1/2} . \tag{5-28}$$

The values of the R's determined for this case are

$$R_A = 1.02941$$
$$R_B = 1.04985$$
$$R_C = 0.99658.$$

Next, data obtained for various probe yaw angles between $-135° \leq \phi \leq +135°$ and zero probe pitch angle was plotted to test the effects of the improvements on the $\frac{U_{es}}{U_s}$ vs ϕ correlations. It is seen from Figure 22 that the data fits well for angles from $\phi = -45°$ to $\phi = +40°$. After that point, the data for sensors B and C varies widely from the correlation. This is due to the effects of heat being convected from the upstream sensor to the downstream sensor when the probe yaw angle is either +90° or -90°. This causes the downstream sensor to operate at a higher ambient temperature than is indicated by the thermocouple. Under these conditions, the calculated correction factor will not be sufficient to correct the heat transfer of the downstream sensor. Thus the effective cooling velocity found will be too small. This will also affect the calculation of the total velocity, U_s, although to a lesser extent. For each position of the probe (for fixed values of probe yaw angle β and probe pitch angle α) the values of the three sensor yaw angles ϕ_A, ϕ_B and ϕ_C can be calculated. In figures 23, 24 and 25 the error in sensor yaw angle as calculated by the T.S.I. method, first approximation is plotted as a function of probe yaw angle β with $\alpha = 0$. As can be seen, errors larger than 10 percent occur in several instances. In figures 26, 27 and 28 the error in sensor yaw angle as calculated by the improved method is plotted as a function of probe yaw angle β with $\alpha = 0$. It is interesting to note that the results for this "improved" correlation (recall the results for U_{es}/U_s vs. ϕ) are actually worse than those obtained either from the T.S.I. first or second approximation. Note also that

for angles of $\beta = +40°$ or $\beta = -40°$, errors occur in either sensor B ($\beta = +40°$) or sensor C ($\beta = -40°$). These are due to the fact that the sensor yaw angle ϕ approaches zero degrees.

In the case a sensor yaw angle has a small value, the value of the ratio $\frac{U_{es}}{U_s}$ is approximately one. In order to estimate the sensor yaw angle to a certain degree of accuracy in this case, the value of $1 - \left(\frac{U_{es}}{U_s}\right)^2$ has to be estimated accurately (see equation 3-14). The latter is nearly impossible, especially when one realizes that a definite ϕ-dependence occurs. The value for $1 - \left(\frac{U_{es}}{U_s}\right)^2$ for small sensor yaw angles can only be estimated with a relatively low degree of accuracy. The problems with the estimation of sensor yaw angle when one sensor is located directly downstream from the other and when the sensor yaw angle is near zero can be easily inferred from the experimental results as given in Figures 26, 27 and 28.

The data for the percentage error in total velocity for the improved ϕ-method are shown in Figure 29. When these data are compared to those shown in Figure 8, the effects of the changes are clearly shown. A similar graph was made to determine the accuracy of the total velocity determined by the first approximation (Figure 30). It is seen from a comparison of the data that the first approximation is somewhat better than the second.

A comparison of the velocity components determined by the first approximation (Figures 31, 32 and 33) and by the ϕ-method (Figures 34, 35 and 36) reveals that the first approximation performs as well as the ϕ-method overall. As can be seen from the results in these graphs,

large errors of 15% or more can be expected in certain regions. The results of these tests were clearly disappointing and it was decided to try the alternate data-analysis procedure as suggested by Olin and Kiland (9). This method will be referred to from here on as the θ-method.

5.2 Analysis of Turbulence-free Wind Tunnel Measurements with the θ-method of Analysis

None of the methods of data reduction discussed above had the accuracy that was desired. In addition, both the T.S.I.-suggested method and the φ-method are quite long and complicated. It was hoped that the θ-method proposed by Olin and Kiland (9) would provide the desired accuracy and in addition be shorter.

When using the θ-method, it is important that the balance of the output voltage of each two films on the same sensor be checked frequently. Failure to do this results in unreliable data since proper balance ensures that no heat transfer takes place from one film to its neighbor through conduction.

The heat transfers, effective cooling velocities and the total velocity are determined by the same methods as used for the T.S.I.-suggested method. The only differences between the two methods are in the calculation of the sensor yaw angles, φ, and in the fact that there is no second approximation for the θ-method.

As previously discussed, Olin and Kiland (9) suggested the following correlation for θ:

$$\frac{q_d/q_u - (q_d/q_u)\theta = 90°}{1 - (q_d/q_u)\theta = 90°} = \left(1 - \frac{\theta}{90}\right)^2. \qquad (5\text{-}29)$$

Tests were performed to evaluate the heat-transfer ratio for various sensor pitch angles. First, the ratio of the heat transfer from the downstream film (q_d) to that of the upstream film (q_u) were obtained by changing the sensor pitch angle, θ, as well as the velocity. A typical graph of the ratio q_d/q_u for $\theta = 90°$ for various velocities is shown in Figure 37.

If the computer is used for data analysis an equation must be obtained for the curve shown. It was felt that the data reduction process would be too complicated if the equation was to fit the entire curve exactly. Consequently, the curves were each broken up into several segments. Straight-line approximations were used for the ranges when $U_s < 10$ fps and $U_s > 40$ fps. The range $10 \leq U_s \leq 40$ fps was divided into three segments and a spline interpolation method was used to fit cubic equations to the experimental points. The equations developed for the entire range appear to work rather well, but are somewhat complicated.

The ratio parameter

$$\frac{Q_2}{Q_1} = \frac{q_d/q_u - (q_d/q_u)\theta = 90°}{1 - (q_d/q_u)\theta = 90°} \qquad (5\text{-}30)$$

is plotted against the sensor pitch angle in Figures 38 and 39 for sensors A and B of probe #1192. It was at this point that problems developed with the above ratio parameter. The ratio should achieve a value of unity at $\theta = 0°$ and $\theta = 180°$. For most of the sensors, this

occurred as expected. However, as can be seen from Figure 39, for sensor C probe #1192, the point at which q_d/q_u becomes equal to one does not occur at $\theta = 180°$ as expected. It is possible to force the "location" of the upstream split to be at the upstream stagnation point where $\theta = 0$. However, no such adjustment is possible for the downstream split at the same time. As a result, the position of the splits of the films on the sensor is most critical and their placement seems to have been in error for sensor C. It is possible, however, that one film simply covers more than half of the sensor.

Expressions were obtained for the curves shown in Figures 38 and 39 and others similar to them and an examination of these expressions indicates that a more general form of the correlation for θ would be

$$\frac{q_d/q_u - (q_d/q_u)_{\theta = 90°}}{1 - (q_d/q_u)_{\theta = 90°}} = \left(1 - \frac{\theta}{A_\theta}\right)^{n_\theta} \qquad (5\text{-}31)$$

where the values of n_θ and A_θ are constant within specific ranges of θ. If the angles of operation can be limited to a smaller region, one can use a much simpler expression:

$$\frac{q_d/q_u - (q_d/q_u)_{\theta = 90°}}{1 - (q_d/q_u)_{\theta = 90°}} = \left(1 - \frac{\theta}{90}\right)^{n_\theta} . \qquad (5\text{-}32)$$

The signs of the pitch angles can be obtained by comparison of the heat-transfer of the two films on the same sensor. That is:

$\theta > 0$ when $E_I > R\, E_{II}$

and $\theta < 0$ when $E_I < R\, E_{II}$

(see Figures 4 and 5).

In order to determine whether θ_A lies in the range larger than +90° or in the range between 0 and +90°, one has to compare the heat transfers of the films on sensor B (see Figure 5).

That is: $\theta_A > 90°$ when $E_{I_B} < R_B E_{II_B}$

and $\theta_A < 90°$ when $E_{I_B} > R_B E_{II_B}$.

Similar comparisons can be made for the signs and magnitudes of the other sensor pitch angles.

Next, a relationship between θ and ϕ must be found. We know that,

$$U_A = U \sin \phi_A$$

$$U_B = U \sin \phi_B$$

$$U_C = U \sin \phi_C.$$

From the geometry of the sensors it is seen that,

$$\sin \theta_A = \frac{U_B}{U \cos \phi_A} \qquad \cos \theta_A = \frac{U_C}{U \cos \phi_A}$$

$$\sin \theta_B = \frac{U_C}{U \cos \phi_B} \qquad \cos \theta_B = \frac{U_A}{U \cos \phi_B} \qquad (5\text{-}33)$$

$$\sin \theta_C = \frac{U_A}{U \cos \phi_C} \qquad \cos \theta_C = \frac{U_B}{U \cos \phi_C}.$$

Now

$$U^2 = U_A^2 + U_B^2 + U_C^2$$

or

$$\frac{U_A^2}{U^2} + \frac{U_B^2}{U^2} + \frac{U_C^2}{U^2} = 1 \ .$$

By substitution, it follows that

$$1 = \cos^2 \theta_B \cos^2 \phi_B + \cos^2 \theta_C \cos^2 \phi_C + \cos^2 \theta_A \cos^2 \phi_A.$$

Substituting,

$$1 = \sin^2 \phi_A + \frac{\cos^2 \theta_C \sin^2 \phi_A}{\sin^2 \theta_C} + \cos^2 \theta_A - \cos^2 \theta_A \sin^2 \phi_A$$

or

$$\sin^2 \theta_A = \sin^2 \phi_A (\sin^2 \theta_C + \cos^2 \theta_C - \sin^2 \theta_C \cos^2 \theta_A).$$

Finally

$$\sin \phi_A = \frac{\sin \theta_A \sin \theta_C}{\sqrt{1 - \sin^2 \theta_C \cos^2 \theta_A}} . \tag{5-34}$$

In a similar manner one can find that

$$\sin \phi_B = \frac{\sin \theta_A \sin \theta_B}{\sqrt{1 - \sin^2 \theta_A \cos^2 \theta_B}} \tag{5-35}$$

and

$$\sin \phi_C = \frac{\sin \theta_B \sin \theta_C}{\sqrt{1 - \sin^2 \theta_B \cos^2 \theta_C}} . \tag{5-36}$$

By following the same steps, but substituting other expressions at the beginning of the development, an alternate set of equations for the evaluation of the sensor yaw angles is obtained.

$$\sin \phi_A = \frac{\cos \theta_B \cos \theta_A}{\sqrt{1 - \sin^2 \theta_A \cos^2 \theta_B}} \tag{5-37}$$

$$\sin \phi_B = \frac{\cos \theta_C \cos \theta_B}{\sqrt{1 - \sin^2 \theta_B \cos^2 \theta_C}} \tag{5-38}$$

and

$$\sin \phi_C = \frac{\cos \theta_A \cos \theta_C}{\sqrt{1 - \sin^2 \theta_C \cos^2 \theta_A}} . \tag{5-39}$$

After a complete examination of results analyzed by the two different expressions for calculating ϕ_A, ϕ_B and ϕ_C, it was found that the best results were obtained when a combination of the two methods was used. The formula to be used is determined by an examination of the magnitude of the denominators of these expressions. It turned out that those expressions with the larger denominator gave the least error for the sensor yaw angle, ϕ.

The signs of ϕ_A, ϕ_B and ϕ_C as well as the velocity components may now be obtained in the same manner as for the other methods.

Graphs showing the errors in the velocity components for data analyzed by the θ-method are given in Figures 40, 41 and 42. The results from sensors A and B are quite good; however, the results for sensor C are somewhat less accurate. In addition, the data from sensor C show that some difficulty in calculating small ϕ angles is still present. Otherwise one can conclude that these results are better than the results obtained with the ϕ-method.

A comparison of the above data with that analyzed by the ϕ-method and the first approximation, however, shows that, on the whole, the θ-method gives better results for the velocity components. In general, the large errors present at probe yaw angles of $\beta = \pm 40°$ and those caused by the heat convection from the upstream sensor to the downstream sensor are not found in data analyzed by this method.

The same comparisons as have been made above of the methods for probe #1193, can also be made for probe #1192. The results shown in Figures 43-51 are much the same as above, except that the angle

errors at $\beta = \pm 40°$ and $|\beta| \geq 60°$ are not as large for this probe. This is possibly due to the fact that the sensors on probe #1192 were spread farther apart than on #1193. This decreases the upper frequency-measuring limit of the probe slightly, but appears to increase the overall accuracy.

5.3 Analysis of Grid Turbulence Measurements

Data was taken in a turbulent flow field created with a grid at a point approximately 10.5 feet downstream from the grid. The results were analyzed using the θ method. Hot-wire measurements were made near the position of the probe at $\alpha = 0°$ and $\beta = 0°$. To check the uniformity of the turbulence across the test section, other measurements were made at different points for the same velocities. The uniformity was found to be good.

The results for the hot-wire measurements with a DISA anemometer and the measurements by the T.S.I.-1080D probe are given in Table II. It is seen that positive angles are calculated rather accurately, but that negative angles have rather large errors. At $\beta = 0°$, the calculated intensity is found to be somewhat lower than that found by the hot-wire measurement. The same is true at other angles; however, some of this is caused by the fact that the T.S.I. sensor cannot measure the small scale or high frequency turbulence and as a result a lower intensity can be expected. The above results are also verified at the other velocities tested.

5.4 Temperature Measuring Errors

It was noticed early in the study that when the probe was tilted up from the horizontal plane (when α is negative), the temperature indicated by the thermocouple can differ as much as 16° from that indicated by the wall thermocouple. This is due to the effect of heat being transferred to the thermocouple from sensor A. The former is located directly upstream from the thermocouple when the probe is in this position. This effect, however, occurs only in a narrow range of angles, generally within 5° from when $\beta = 0°$. In addition, McMahon (7) has found some errors in temperature when a sweep is made within the horizontal plane. These errors are not as large, however. Any errors made in the measurements of temperature will adversely affect the accuracy of the velocity measurements.

Chapter VI

CONCLUSIONS AND RECOMMENDATIONS

A definite need exists for reliable and high frequency measurements of low-level atmospheric turbulence. Many different types of instrumentation have been developed to perform these measurements. However, most do not have the desired degree of accuracy or have limitations as far as frequency is concerned or measure only the two horizontal components which make these types of instrumentation less desirable. This study was initiated to evaluate the measurements made in a low-speed wind tunnel by the T.S.I. Model 1080-D three-dimensional split-film anemometer. Measurements were made to test this instrument in the low-speed wind tunnel and to compare the results with expected values. It was found that the instrument did not have the required accuracy as was anticipated. The method of data analysis (calculation of the velocity components in the sensor-oriented coordinate system) suggested by T.S.I. was tested for many different angles of attack and it was concluded that changes in the data-analysis method were necessary in order to improve the accuracy. Changes were made for the so-called "improved accuracy" correlation expressions. Also a temperature correction was introduced to correct the output voltages when the probe is operating at different ambient temperatures and when the resistance of the connecting cable is changed due to varying

environmental temperatures. After these changes were made, the probes were tested again over a range of probe yaw angles of $-150° < \beta < 150°$ and probe pitch angles of $-20° < \alpha < 20°$ and a velocity range of 10 fps < U < 100 fps. The results of these tests were truly disappointing. The desired accuracy over the above range of operation was not obtained uniformly. As a matter of fact, only in very rare occasions was the percentage of error less than 5 percent (Figures 34, 35 and 36). The high percentage of error was due to the following problems which were prominent over different ranges where the probe was anticipated to operate:

a. θ-dependence. This is a problem which occurs for any angle of attack (Figures 18, 19 and 20). Not only are errors made due to θ-dependence in the evaluation of the cooling velocities and total velocity but also in the evaluation of the sensor yaw angles (Figures 26, 27 and 28).

b. Large errors were obtained in the estimation of the sensor yaw angle ϕ in regions where the absolute value of this angle is less than 10°. This occurs when the probe yaw angle is approximately plus or minus 40°.

c. Convection of heat from an upstream sensor to a sensor located directly downstream. In this case the downstream sensor senses a higher ambient temperature and as a result a lower cooling velocity is estimated. This occurs when the probe yaw angle is either plus or minus 90°. When $\beta = +90°$ sensor C lies directly downstream from sensor B and when the probe yaw angle $\beta = -90°$, sensor B lies directly

downstream from sensor C. The points which do not follow the correlation curve in Figure 22 are obtained from measurements taken when β was either plus or minus 90°.

d. When the probe pitch angle is changed so that sensor A is directly upstream from the thermocouple, the latter senses an ambient temperature which is too high. This results in additional error in the actual velocity because the ambient temperature is measured too high.

e. It was assumed that the sensors are mutually perpendicular and that the entire sensor array is situated with respect to the probe axis as described by the T.S.I. manual. How accurately the geometry of the sensor array really is, is an open question. However, it is undoubtedly possible that changes in the geometry due to production limitations or due to frequent usage in the field will result in inaccuracies in either the calculated yaw angles or the calculated velocity components.

Since the ϕ-method did not give the desired accuracy over the range in which we wanted the probe to operate, especially when it is mounted on a meteorological tower, the alternate method as suggested by Olin and Kiland (9) was tried. This method gave results which were somewhat more accurate over a wider angle range than the results obtained with the ϕ-method. Still, the newly developed method does not give the desired accuracy of less than 3%. As a matter of fact, the θ-method calculates velocity components within 10% accuracy except for a few isolated points (see Figures 40, 41, 42, 49, 50 and 51).

The data from the grid turbulence measurements indicate that the measured turbulence intensity is somewhat lower than measured with the conventional hot-wire anemometer. This can be expected since the sensor array of the T.S.I. probes has a finite dimension and thus high frequency turbulence with a small wave length cannot be measured with this probe. In addition,the probe yaw angle can be determined within a 3° accuracy.

From all these results one can come to the conclusion that the T.S.I.-1080 split-film probe cannot measure the velocity magnitude and direction over the full 360° solid angle in three-dimensional flow fields within the accuracy as was claimed by T.S.I. It seems that the θ-method gives better results but the drawback of this method is that the calculations are longer and more complicated. Over a limited range between $-150° < \beta < +150°$ and $-20° < \alpha < +20°$ the results show an accuracy of not less than 10% for the θ-method. For the same range, the T.S.I.-method and the ϕ-method (improved T.S.I.-method) does not give generally the same degree of accuracy.

In conclusion, it was decided to use the T.S.I.-1080 probe in conjunction with a rotating mechanism so that the probe is always nearly directed into the wind or the average probe yaw angle will be nearly zero. This means that the probe is operated in a very limited range only, say from $-30° < \beta < +30°$ and $-15° < \alpha < +15°$. From atmospheric turbulence data it was determined that the standard deviation of the vertical angle of attack is approximately 7°. Assuming that the turbulence is a normally-distributed random process, one can expect that

95% of the time the vertical velocity fluctuations and, as a first approximation, the lateral velocity of fluctations will fall well within the above angle ranges. If the probe is always to be operated in the above range the values of the calibration constants K may be altered slightly when the ϕ-method is used so that in this range the velocity errors vary about zero percent.

Therefore, the major conclusion of this report is that the T.S.I.-1080 split-film probe can only be used for small probe pitch angles and small probe yaw angles when the mean velocity vector is parallel to the probe and varies only small amount as far as the direction is concerned. Under these conditions, the ϕ-method will give better results especially when the calibration constants are varied slightly by trial and error. If a larger range of operation is required, the θ-method gives better results than the ϕ-method.

REFERENCES

1. Baines, W. D. and Peterson, E. G., An Investigation of Flow Through Screens. Report to the Office of Naval Research by Iowa Inst. of Hydraulics, July, 1949.

2. Champagne, F. H., Sleicher, C. A., and Wehrmann, O. H., Turbulence Measurements with Inclined Hot Wires. Journal of Fluid Mechanics. 28: 153-175, 1967.

3. Collis, D. C. and Williams, M. J., Two-Dimensional Convection from Heated Wires at Low Reynolds Numbers. Journal of Fluid Mechanics. 6: 357-378, 1959.

4. Hinze, J. O., Turbulence: An Introduction to Its Mechanism and Theory. McGraw-Hill Book Company, Inc., New York, 1959.

5. King, L. V., On the Convection of Heat from Small Cylinders in a Stream of Fluid. Phil. Trans. Roy. Soc. A214: 373, 1914.

6. Marchman III, J. F., Non-aeronautical Wind-tunnel Testing in the V.P.I. 6-foot Tunnel. Virginia Polytechnic Institute, Blacksburg, Virginia, May, 1970.

7. McMahon, H., Personal communication, September, 1972.

8. Morrison, J. G., Installation for Field Measurements of Wind Structure. Symposium on Instrumentation and Data Processing for Industrial Aerodynamics, National Physical Laboratory, Teddington, Middlesex, November, 1968.

9. Olin, J. G. and Kiland, R. B., Split-film Anemometer Sensors for Three-dimensional Velocity-vector Measurement. Symposium on Aircraft Wake Turbulence, Seattle, Washington, September 1970.

10. Thermo-Systems, Inc., Operating and Service Manual for Model 1080D Total Vector Anemometer. Saint Paul, Minnesota, 1970.

11. Vickery, B. J., On the Flow Behind a Coarse Grid and Its Use as a Model of Atmospheric Turbulence in Studies Related to Wind Loads on Buildings. NPL Aero Report 1143, March, 1965.

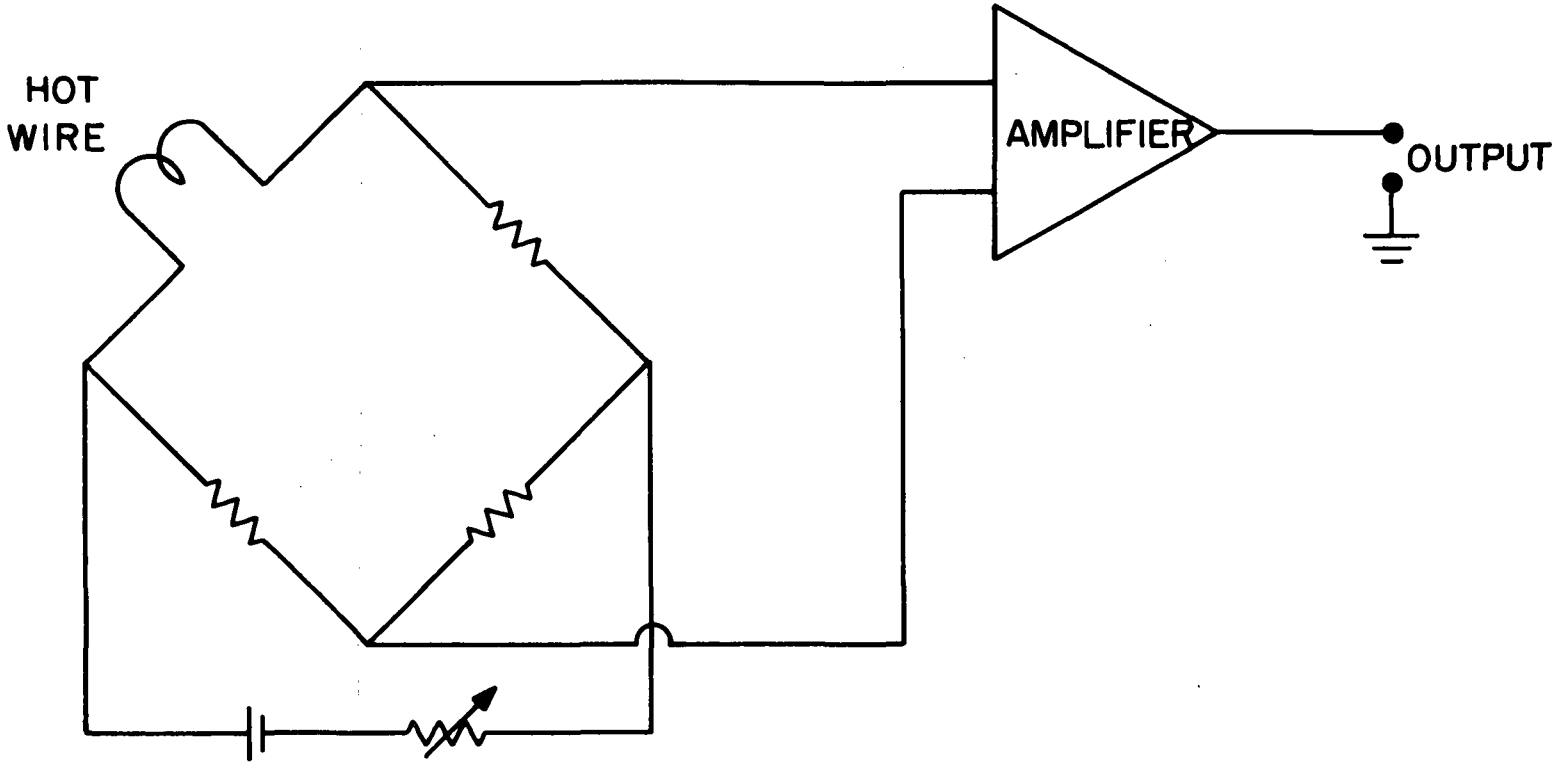

Figure 1: Schematic Diagram of a Constant-Current Anemometer.

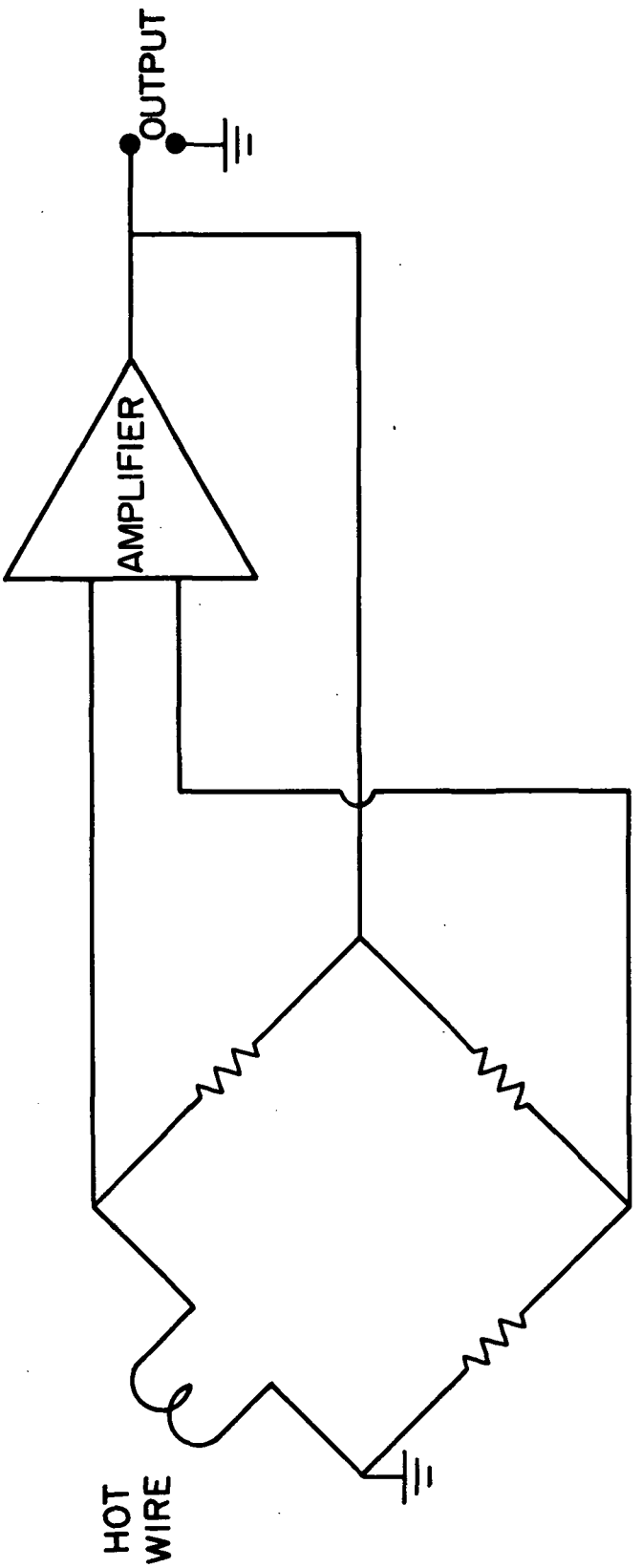

Figure 2: Schematic Diagram of a Constant-Temperature Anemometer.

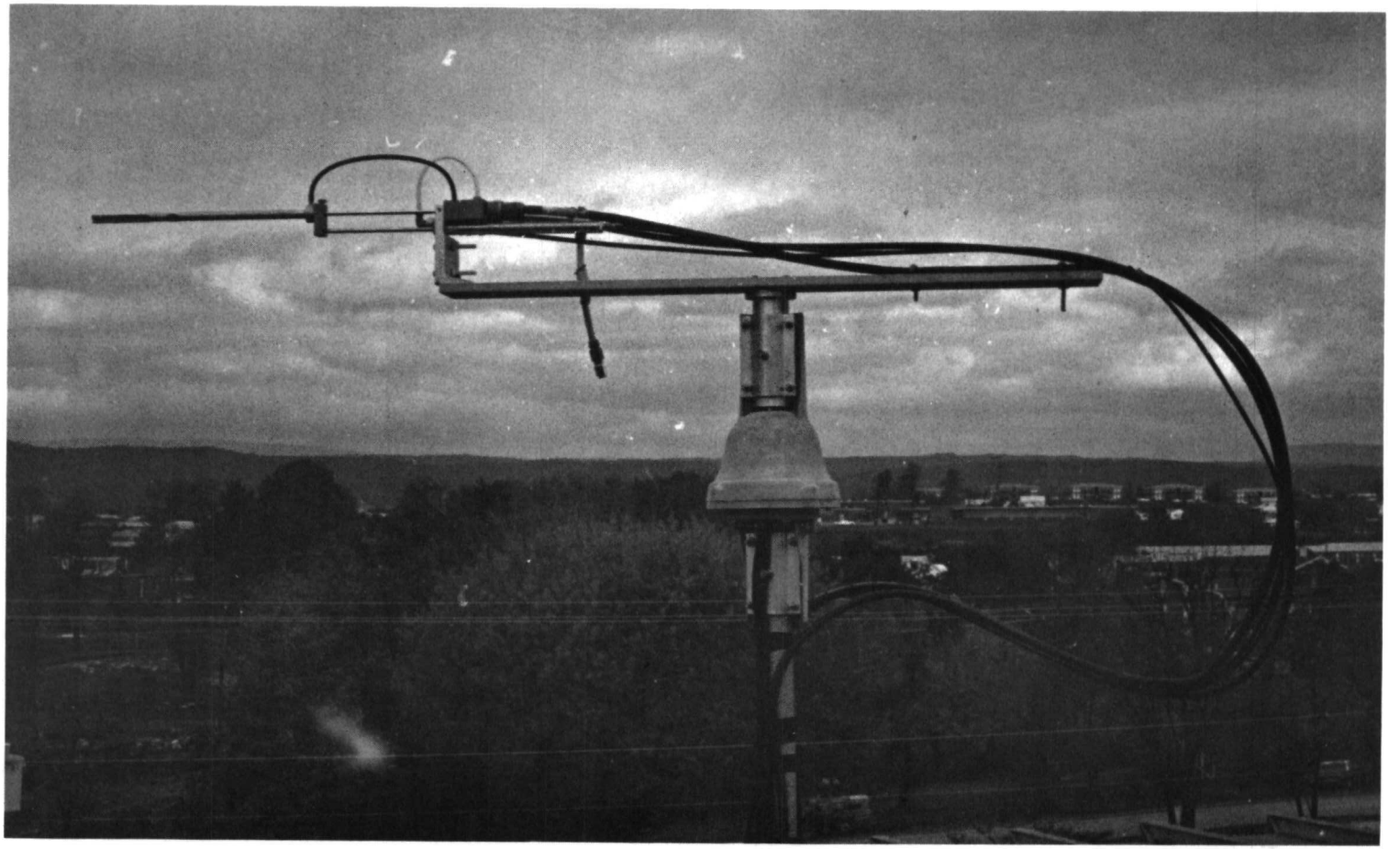

Figure 3: The T.S.I. Model 1080D Probe.

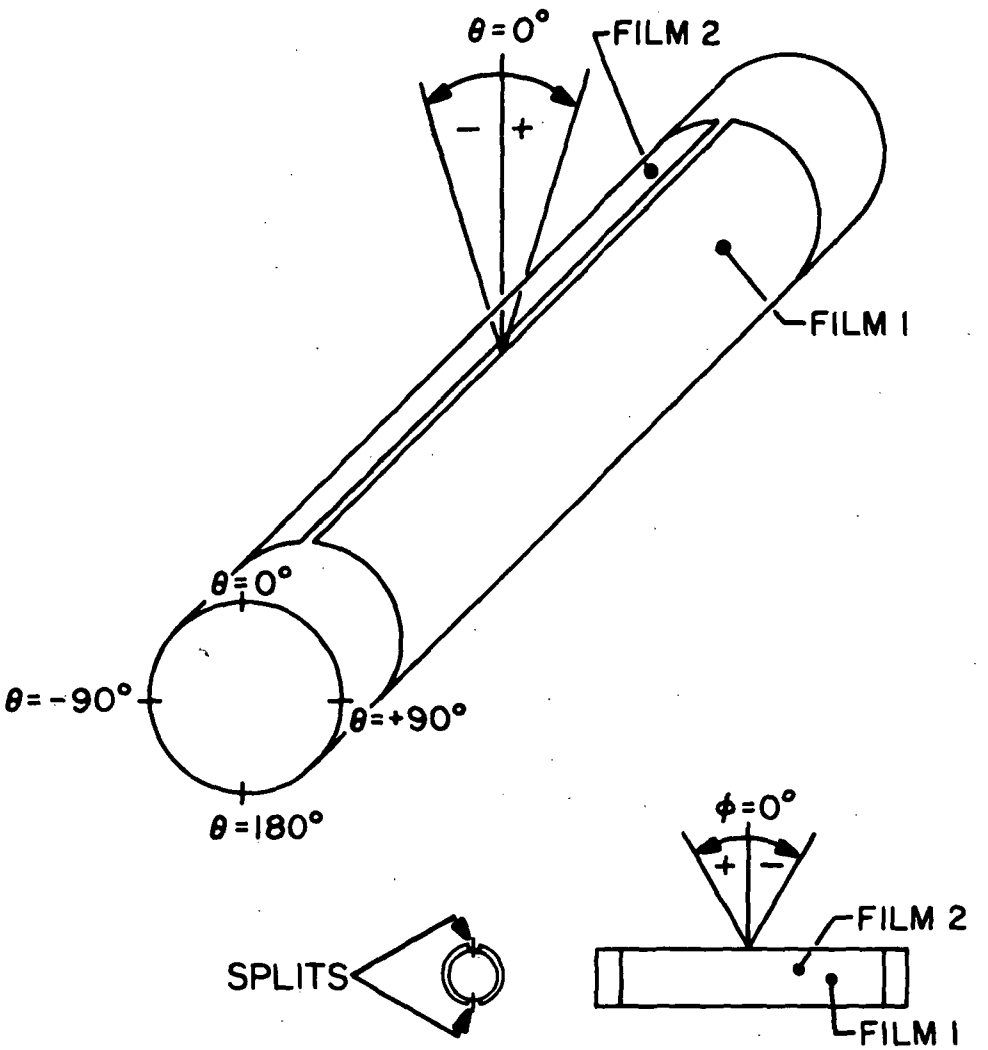

Figure 4: Single Split-Film Sensor with Definitions of θ and ϕ angles.

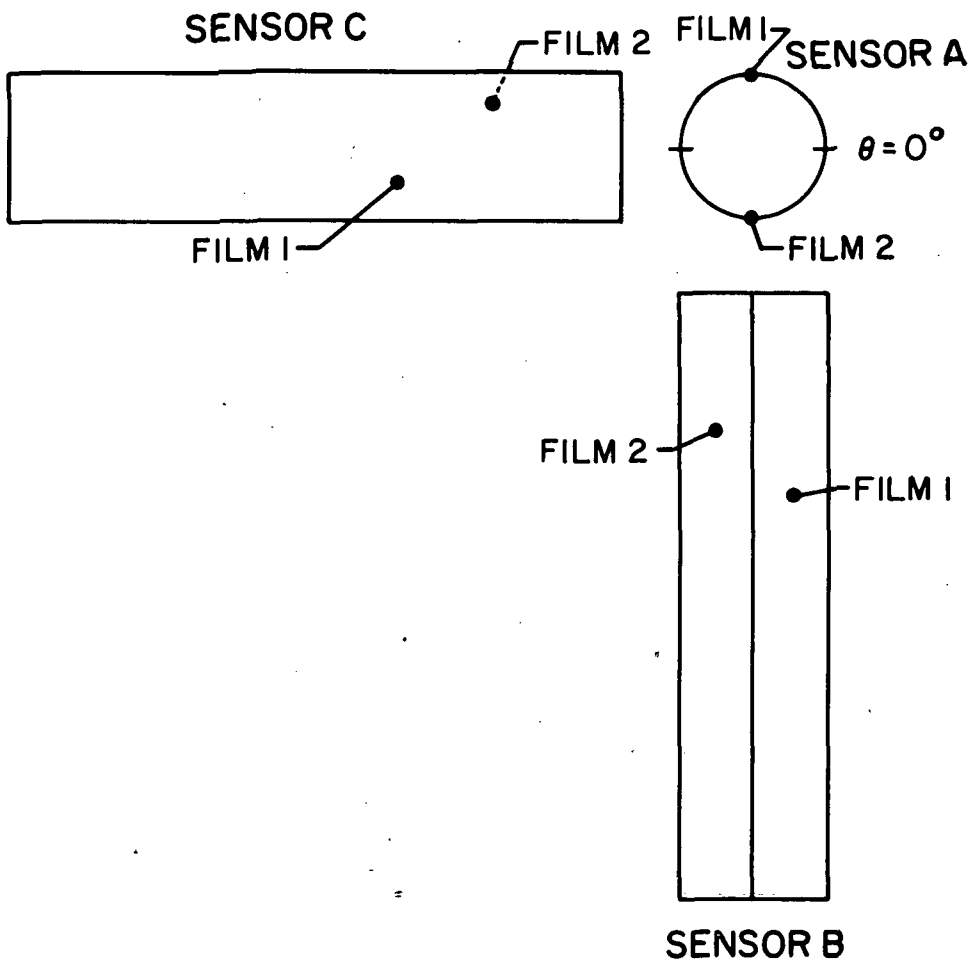

Figure 5: View of Orthogonal Array of Sensors.

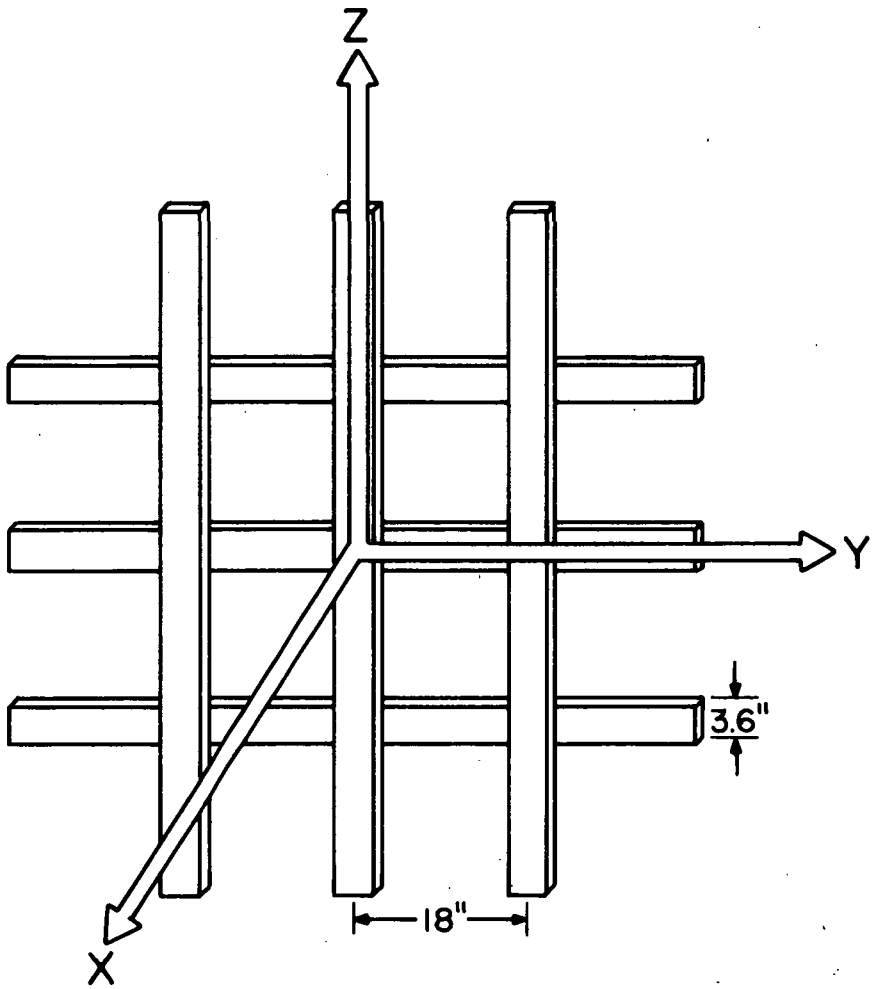

Figure 6: Turbulence Grid and Coordinate System. Tunnel axis coincident with coordinate X.

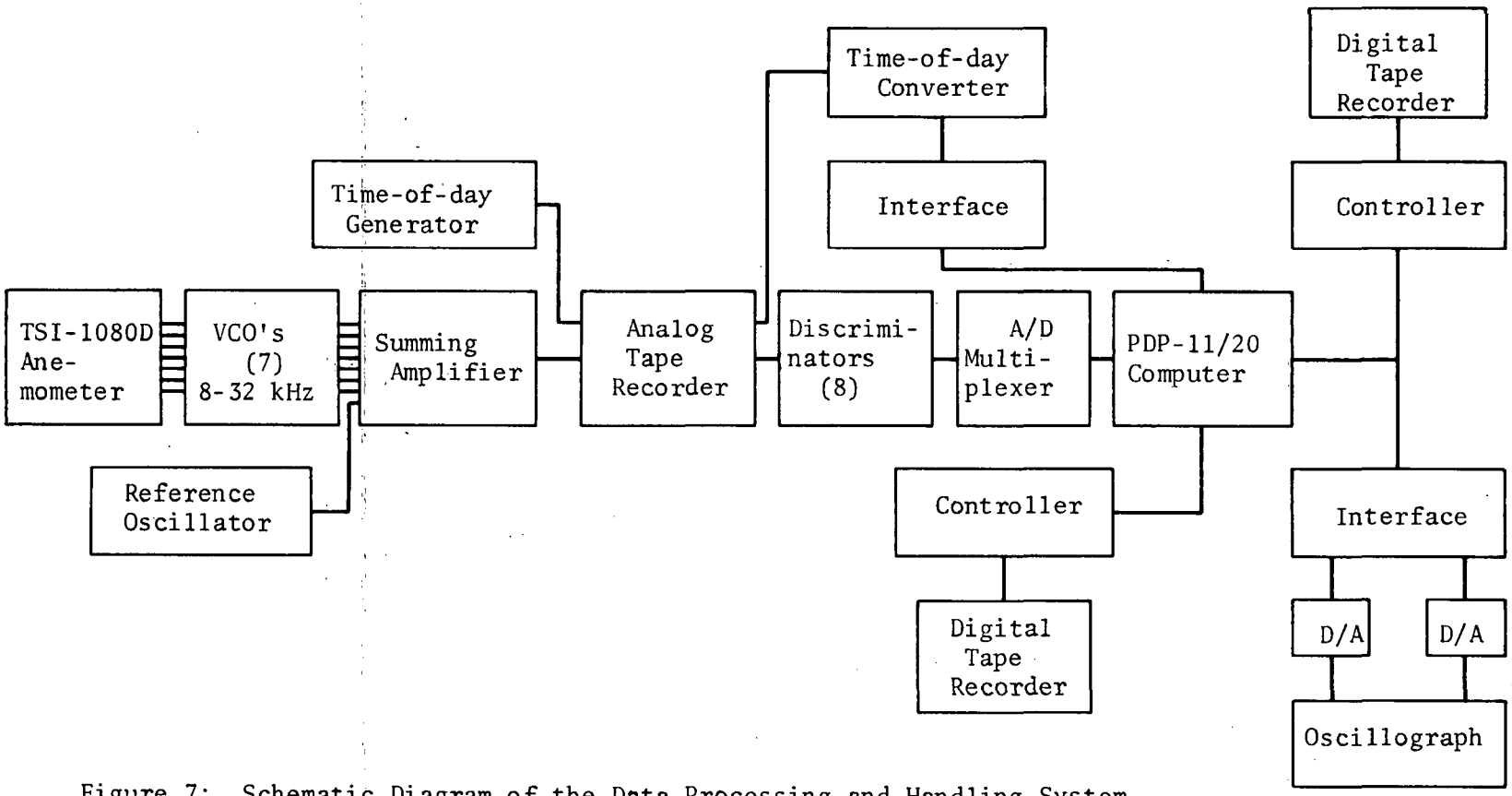

Figure 7: Schematic Diagram of the Data Processing and Handling System.

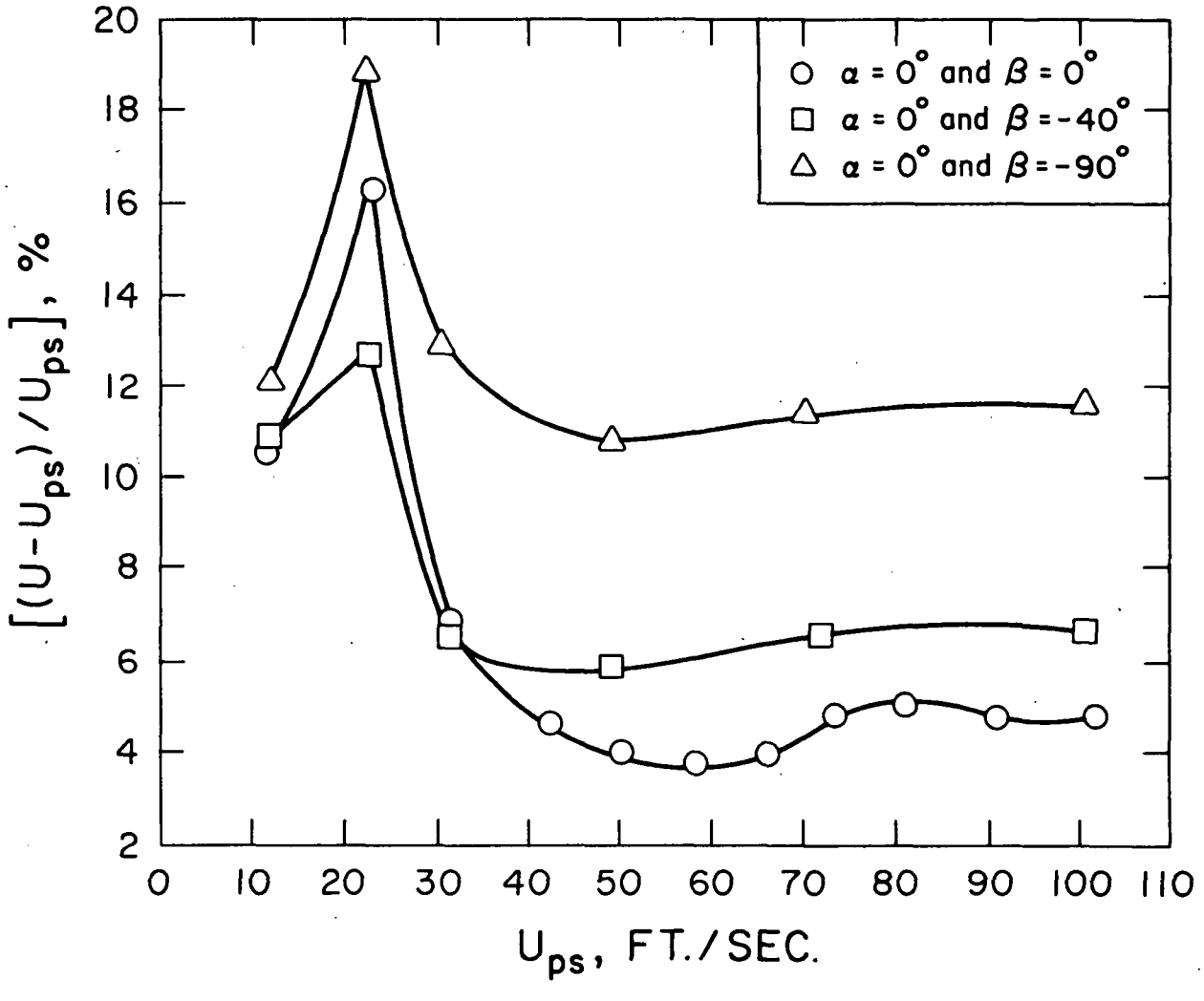

Figure 8: Percentage Error in Total Velocity for the T.S.I.-suggested Analysis. Probe #1192.

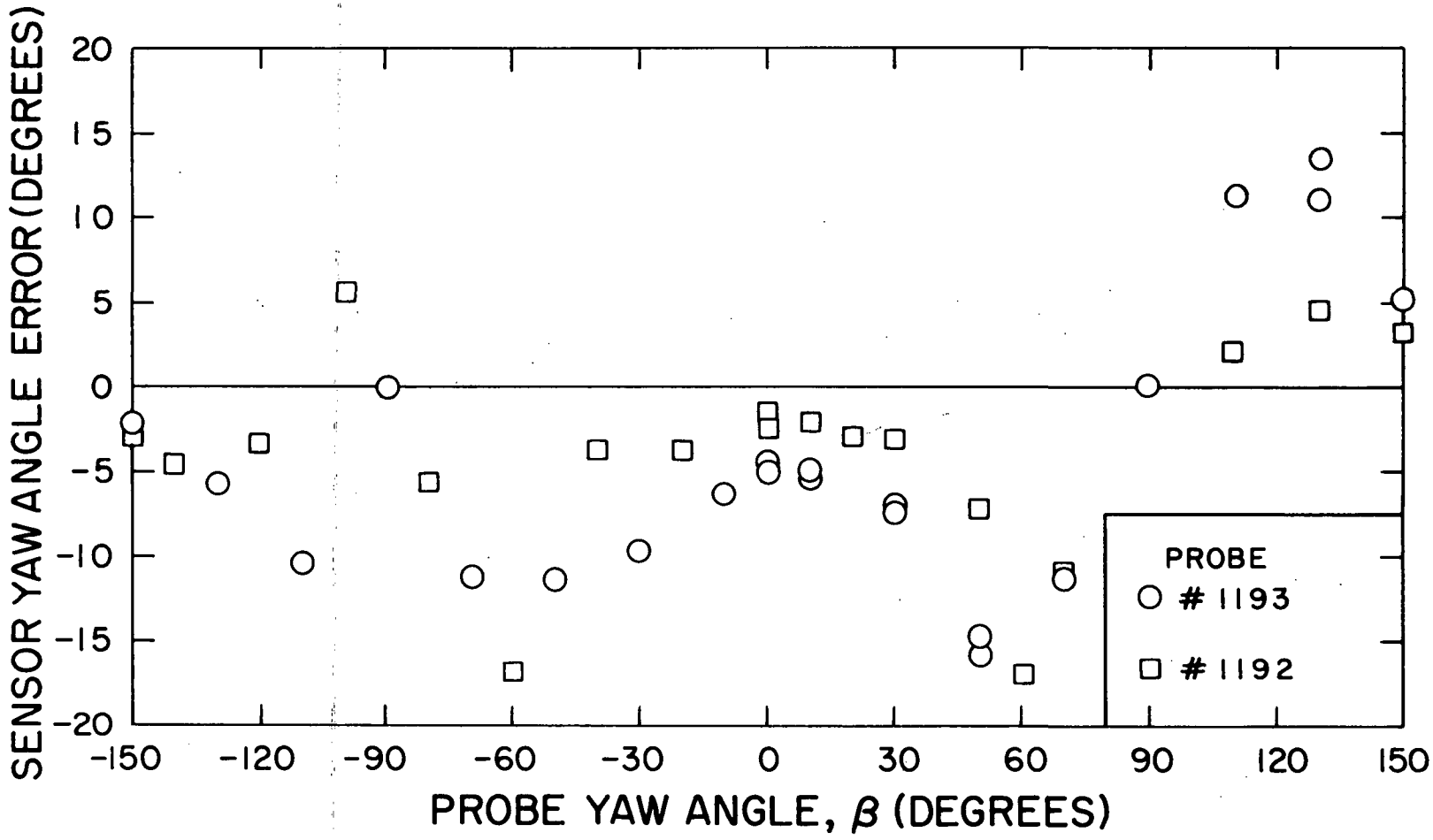

Figure 9: Error in Sensor Yaw Angle, ϕ_A, for the T.S.I. Suggested Analysis. $U \simeq 30$fps and $\alpha=0$.

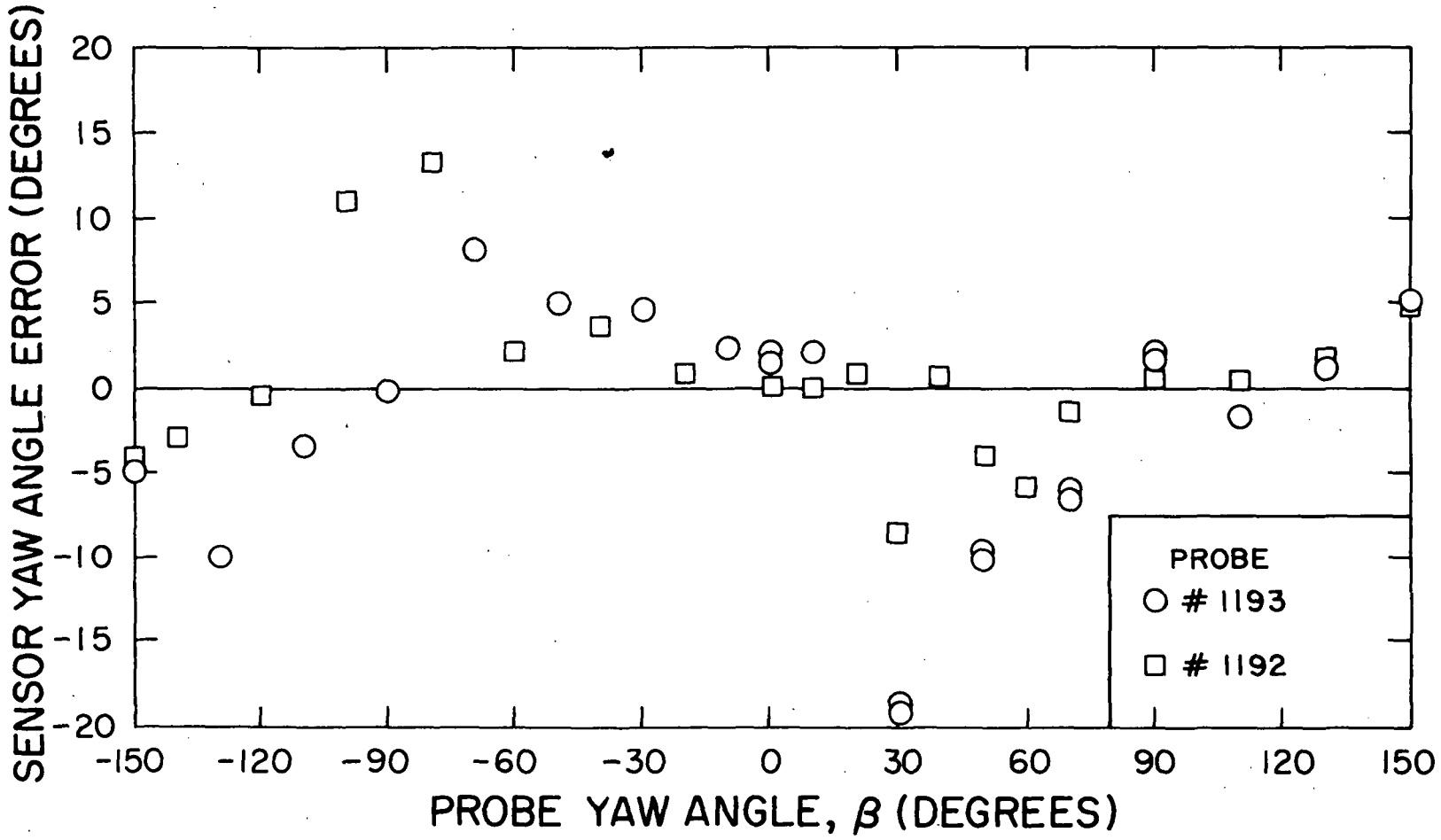

Figure 10: Error in Sensor Yaw Angle, ϕ_B, for the T.S.I. Suggested Analysis U $\simeq$ 30fps and α=0.

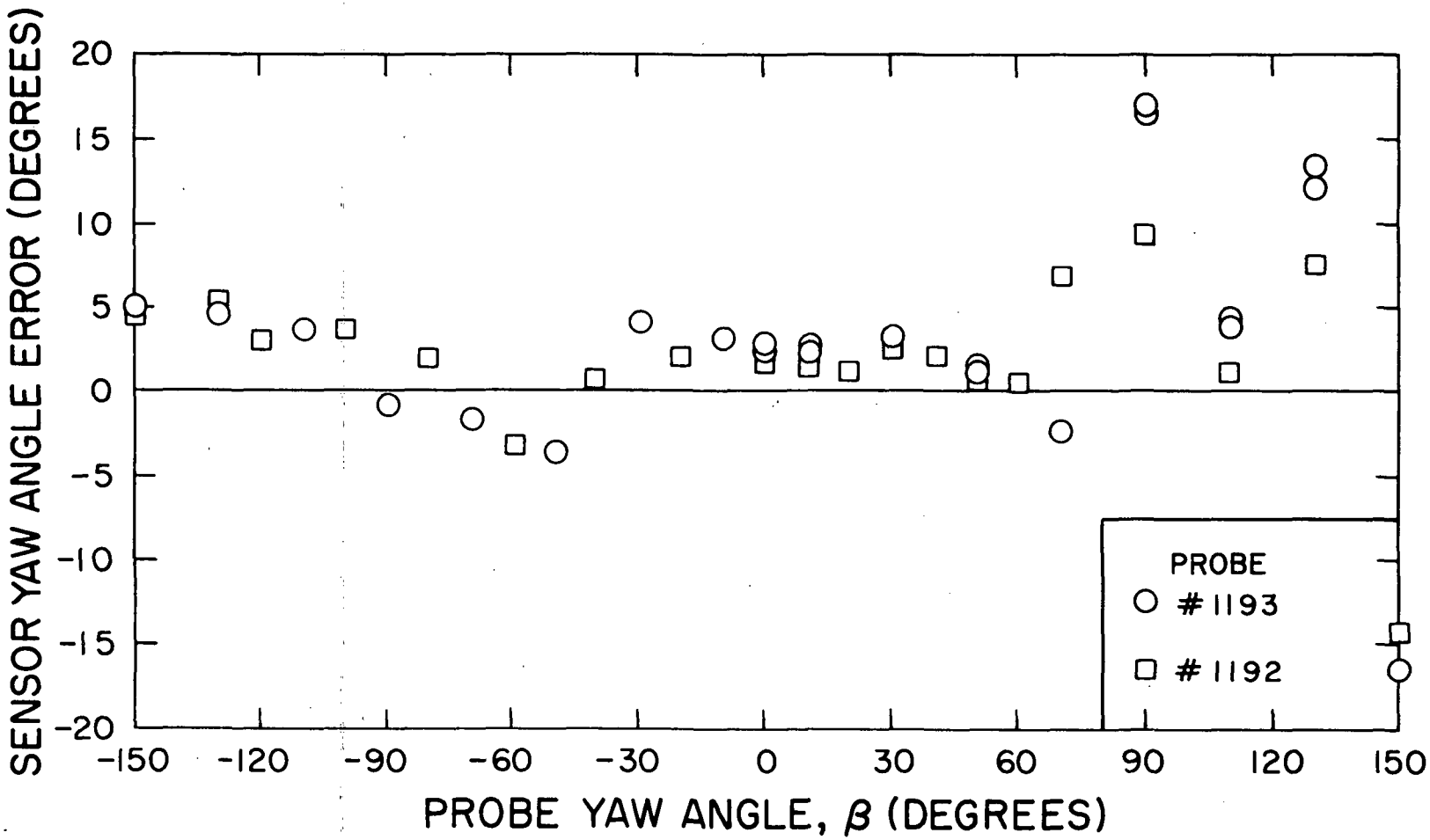

Figure 11: Error in Sensor Yaw Angle, ϕ_C, for the T.S.I. Suggested Analysis U $\simeq$ 30fps and α=0.

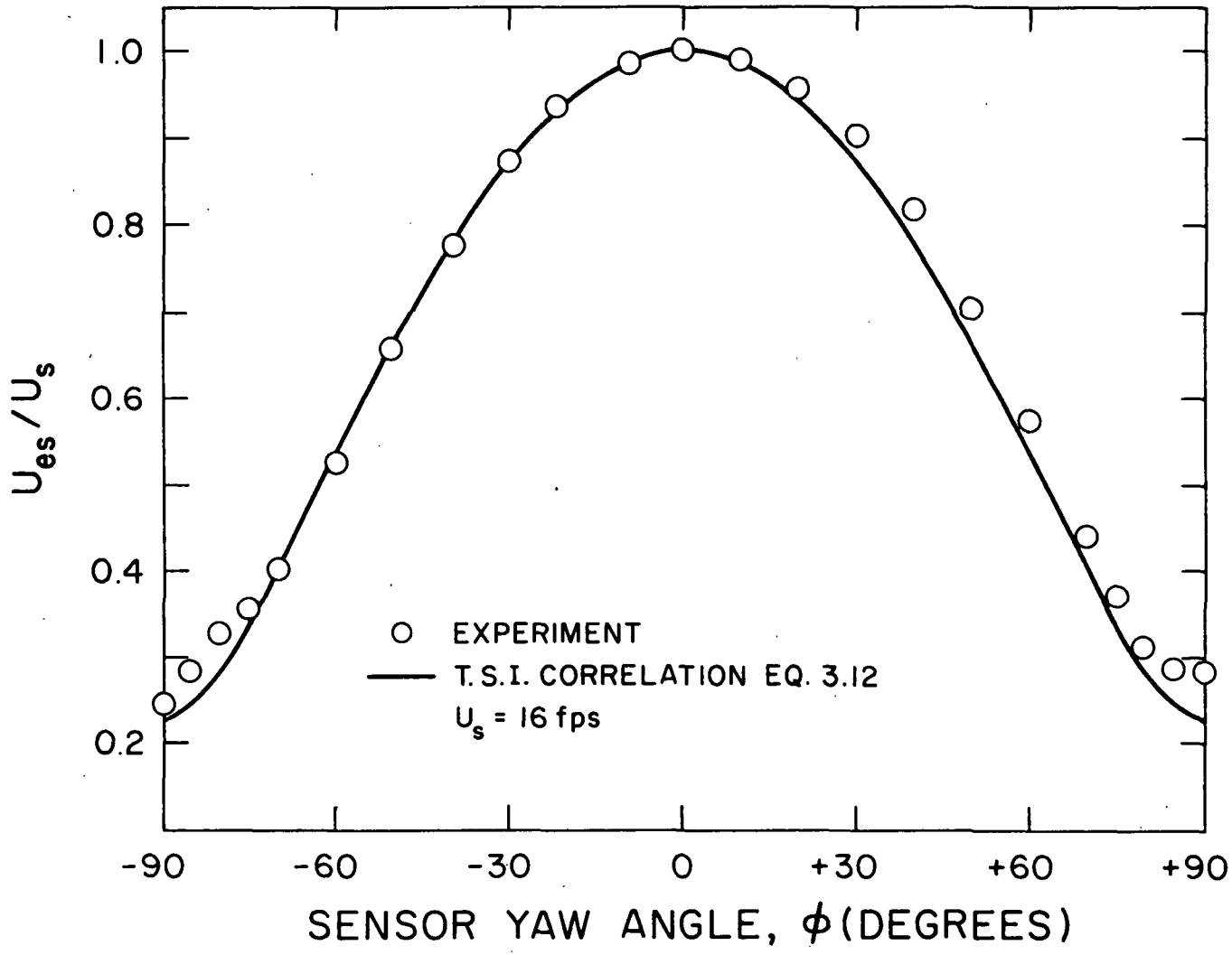

Figure 12: Comparison of Experimental Values of U_{es}/U_s with T.S.I. Suggested Correlation.

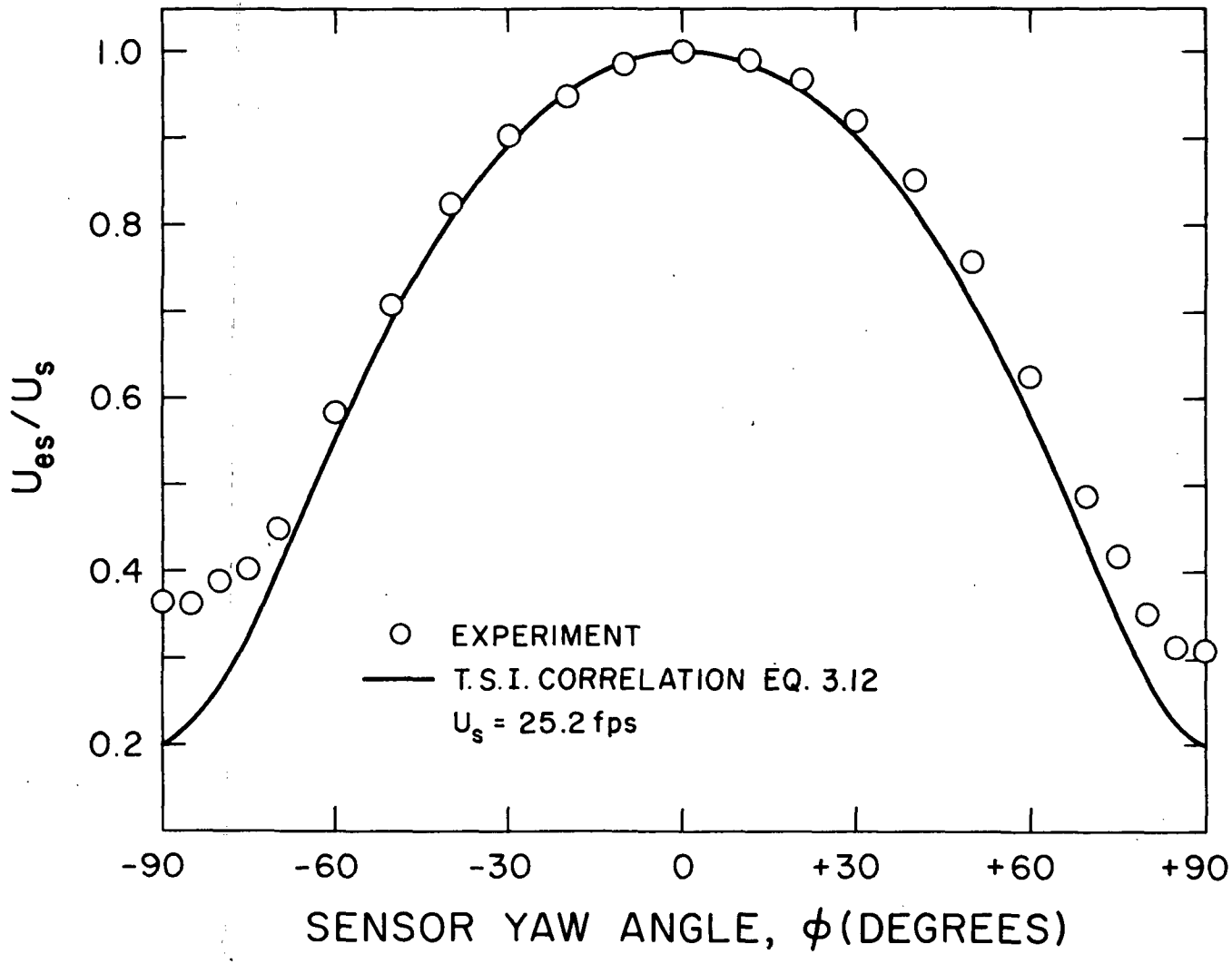

Figure 13: Comparison of Experimental Values of U_{es}/U_s with T.S.I. Suggested Correlation.

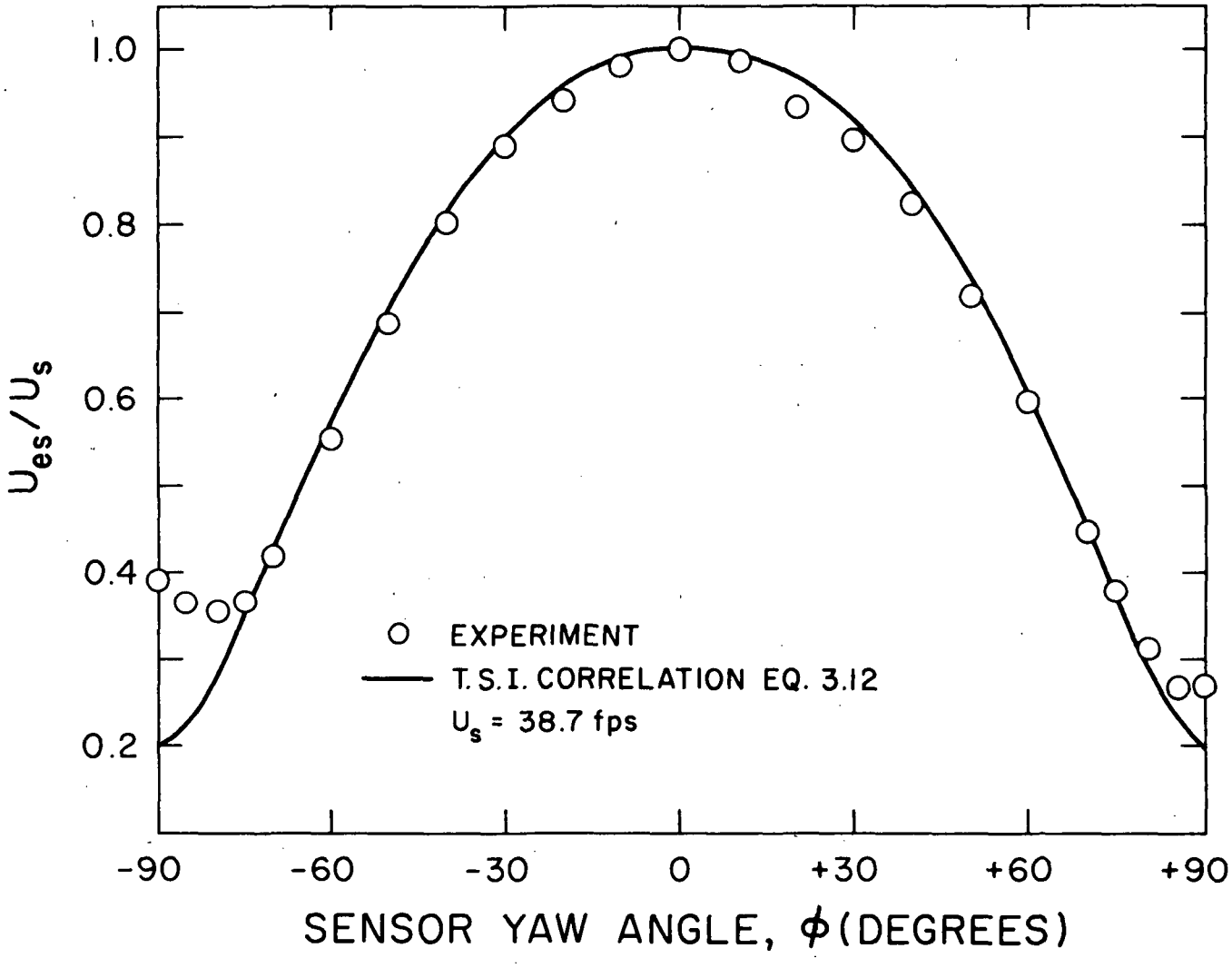

Figure 14: Comparison of Experimental Values of U_{es}/U_s with T.S.I. Suggested Correlation.

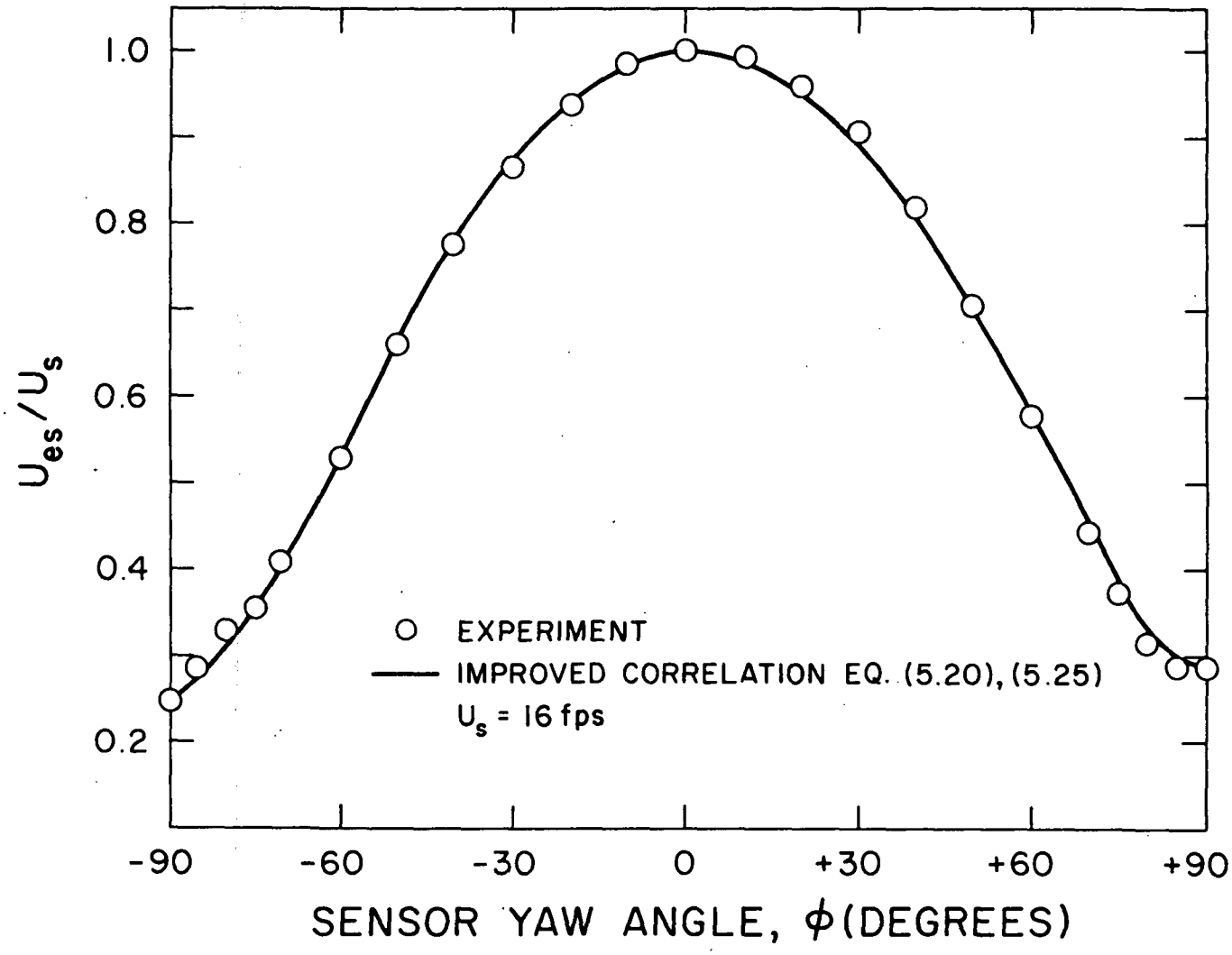

Figure 15: Comparison of Experimental Values of U_{es}/U_s with Improved Correlation.

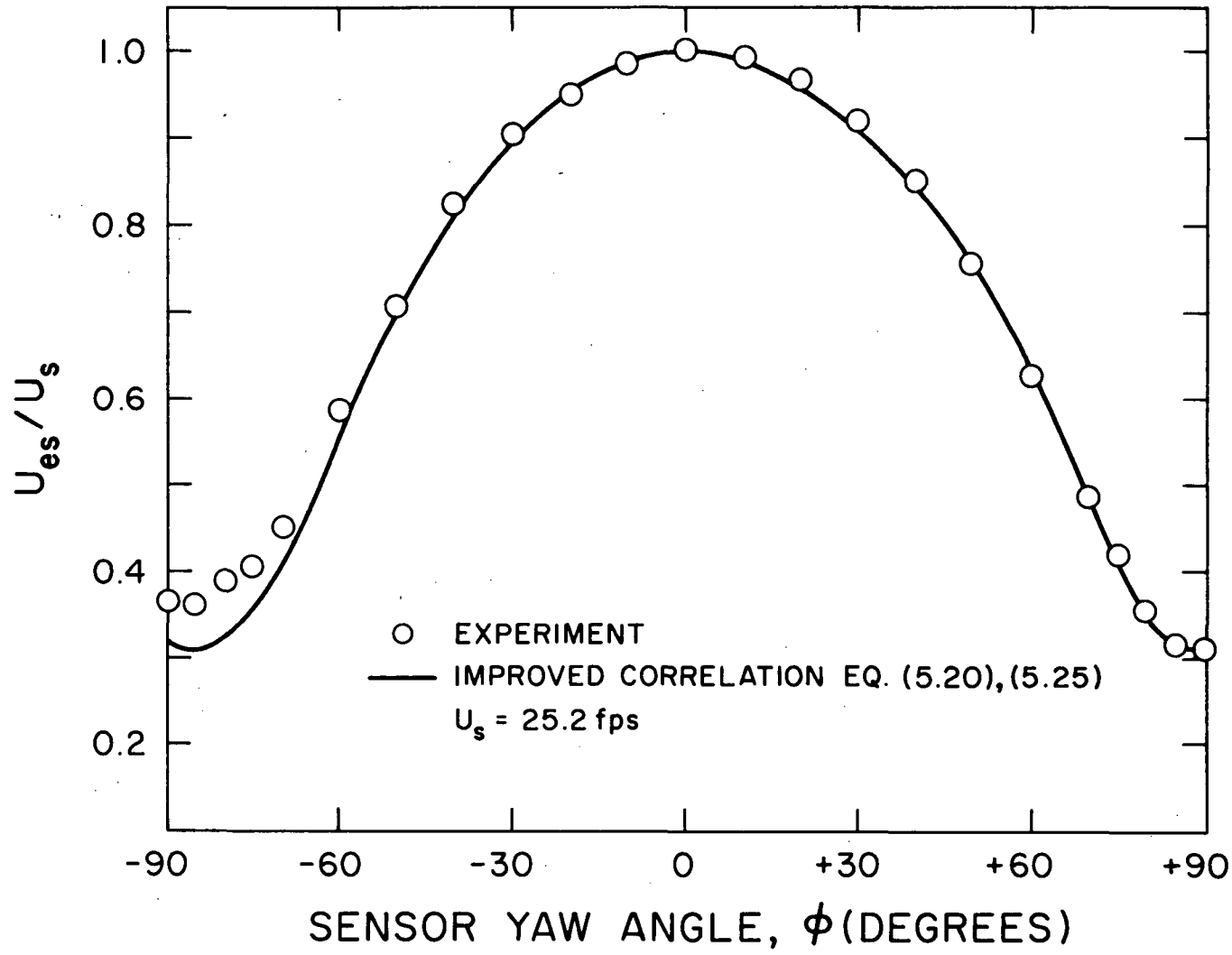

Figure 16: Comparison of Experimental Values of U_{es}/U_s with Improved Correlation.

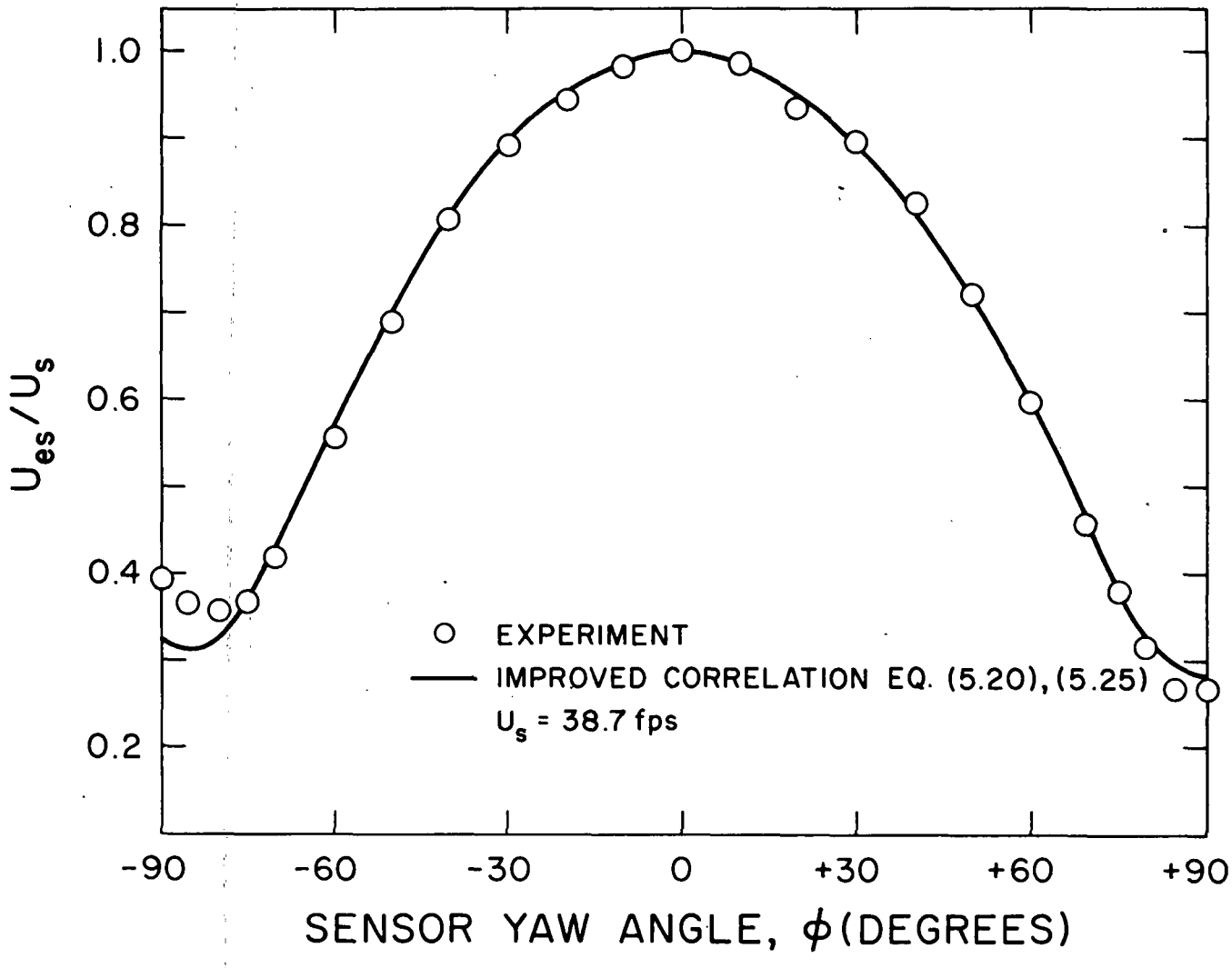

Figure 17: Comparison of Experimental Values of U_{es}/U_s with Improved Correlation.

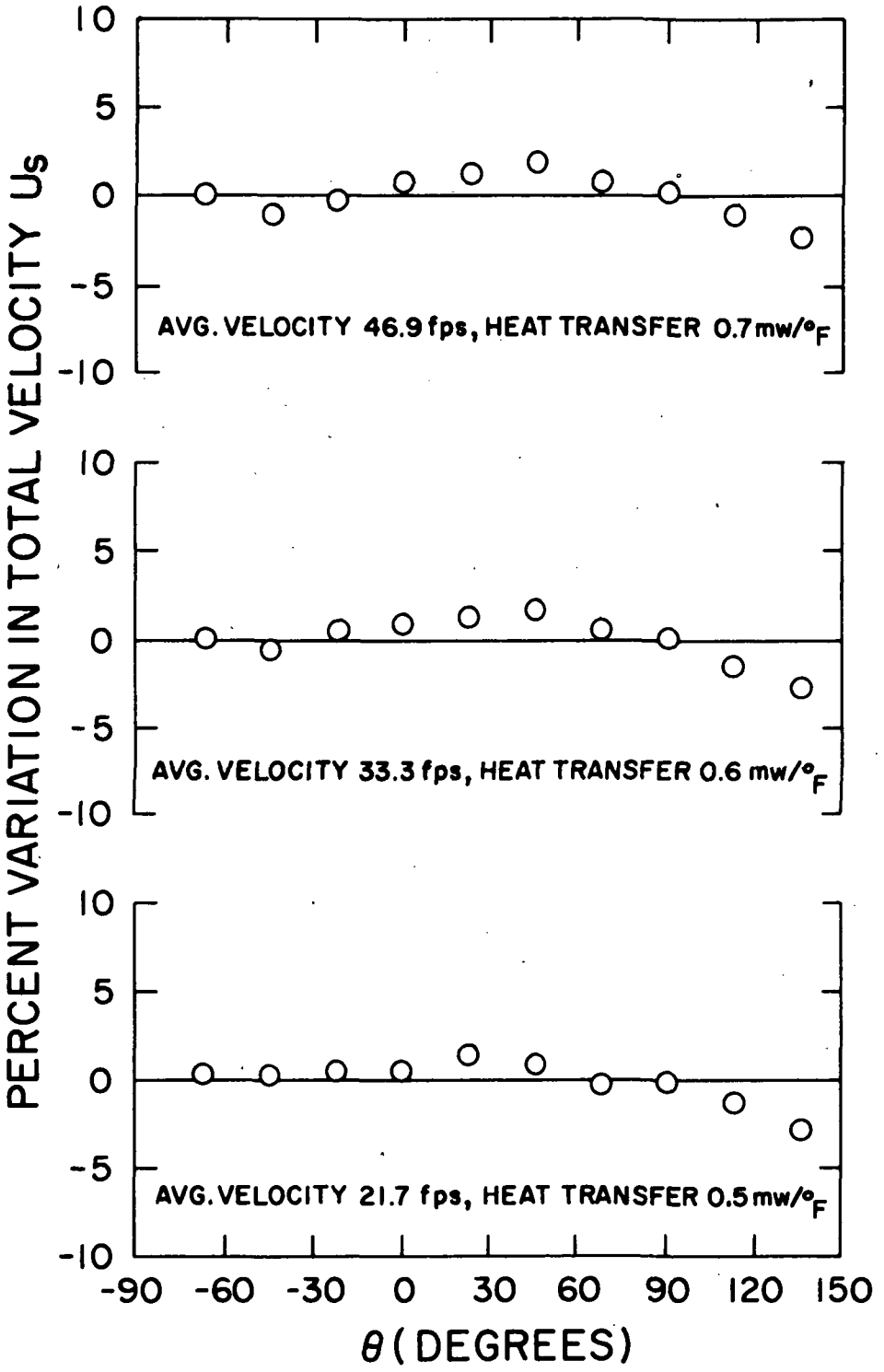

Figure 18: Error in Velocity Vs. Sensor Pitch Angle. Sensor A, #1193.

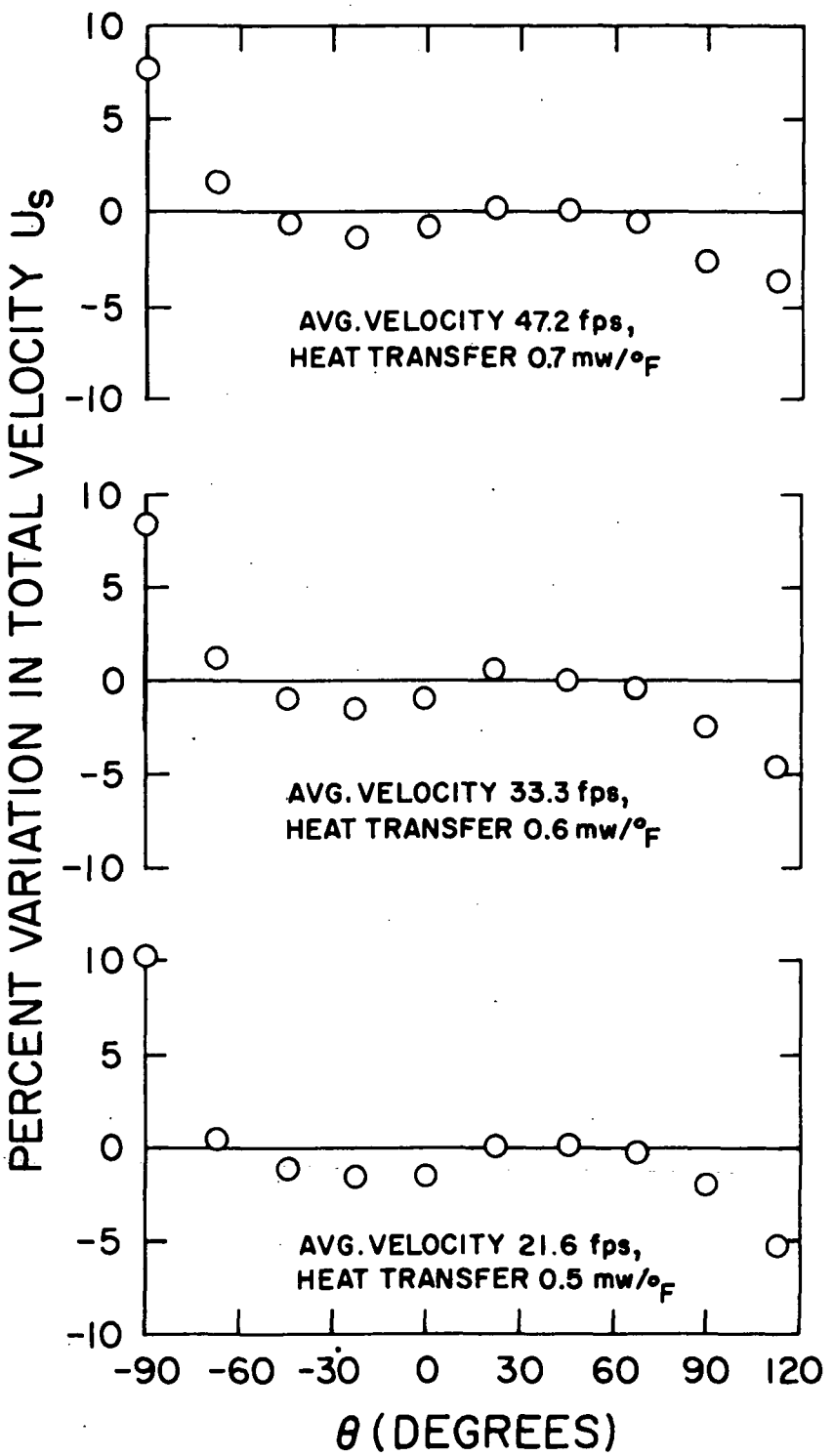

Figure 19: Error in Velocity Vs. Sensor Pitch Angle. Sensor B, #1193.

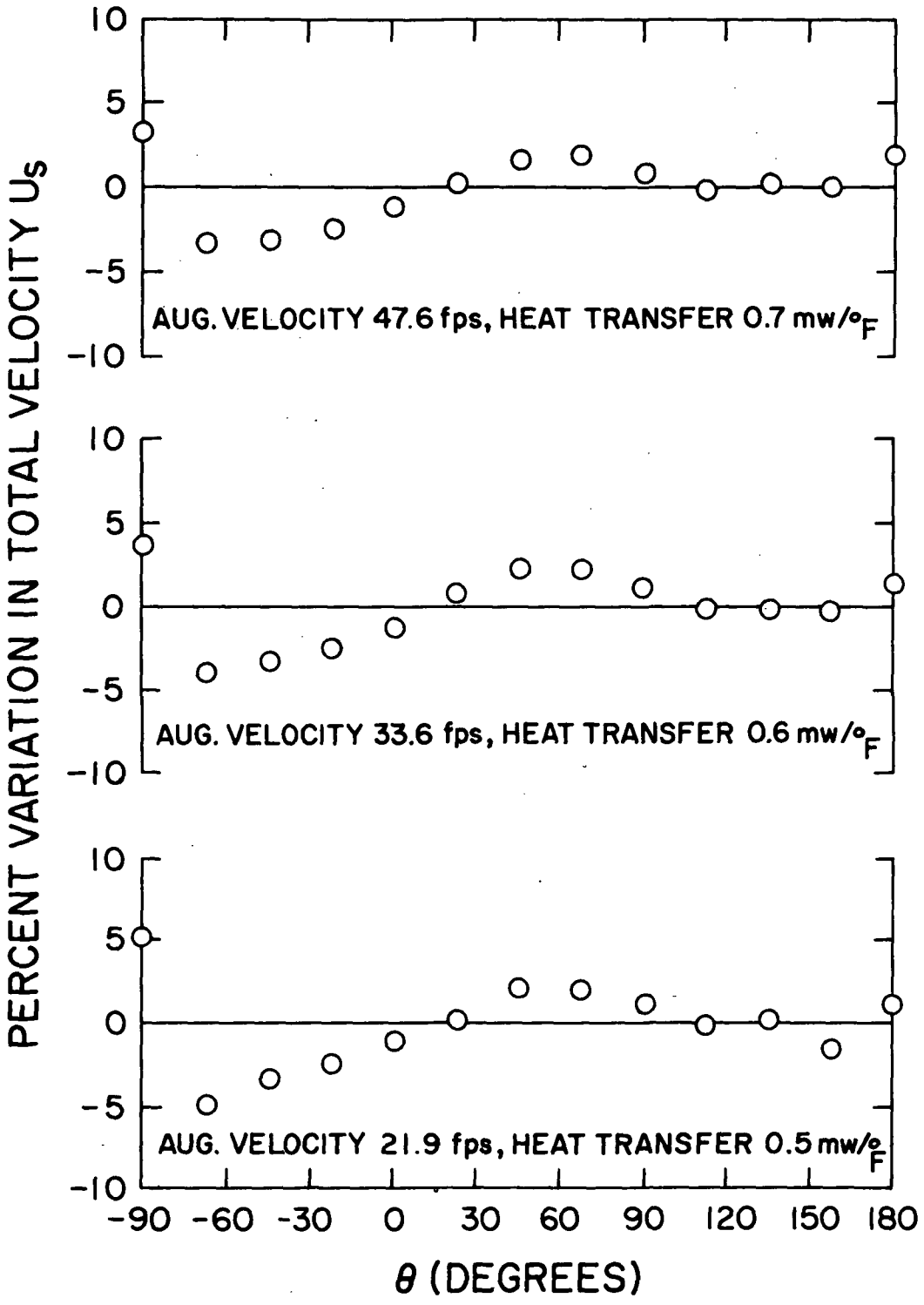

Figure 20: Error in Velocity Vs. Sensor Pitch Angle. Sensor C, #1193.

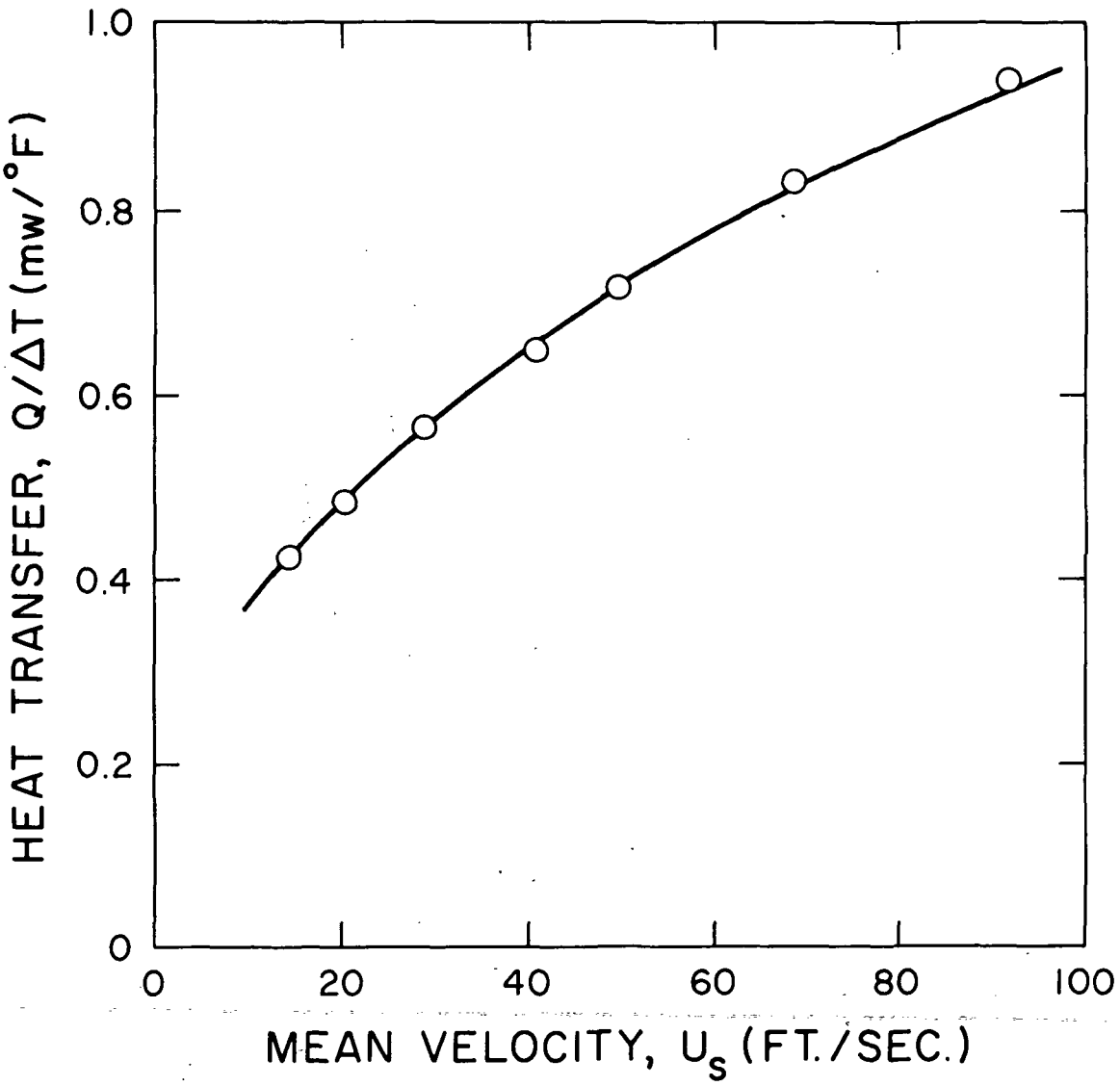

Figure 21: Typical Calibration Curve for Heat Transfer Vs. Mean Velocity.

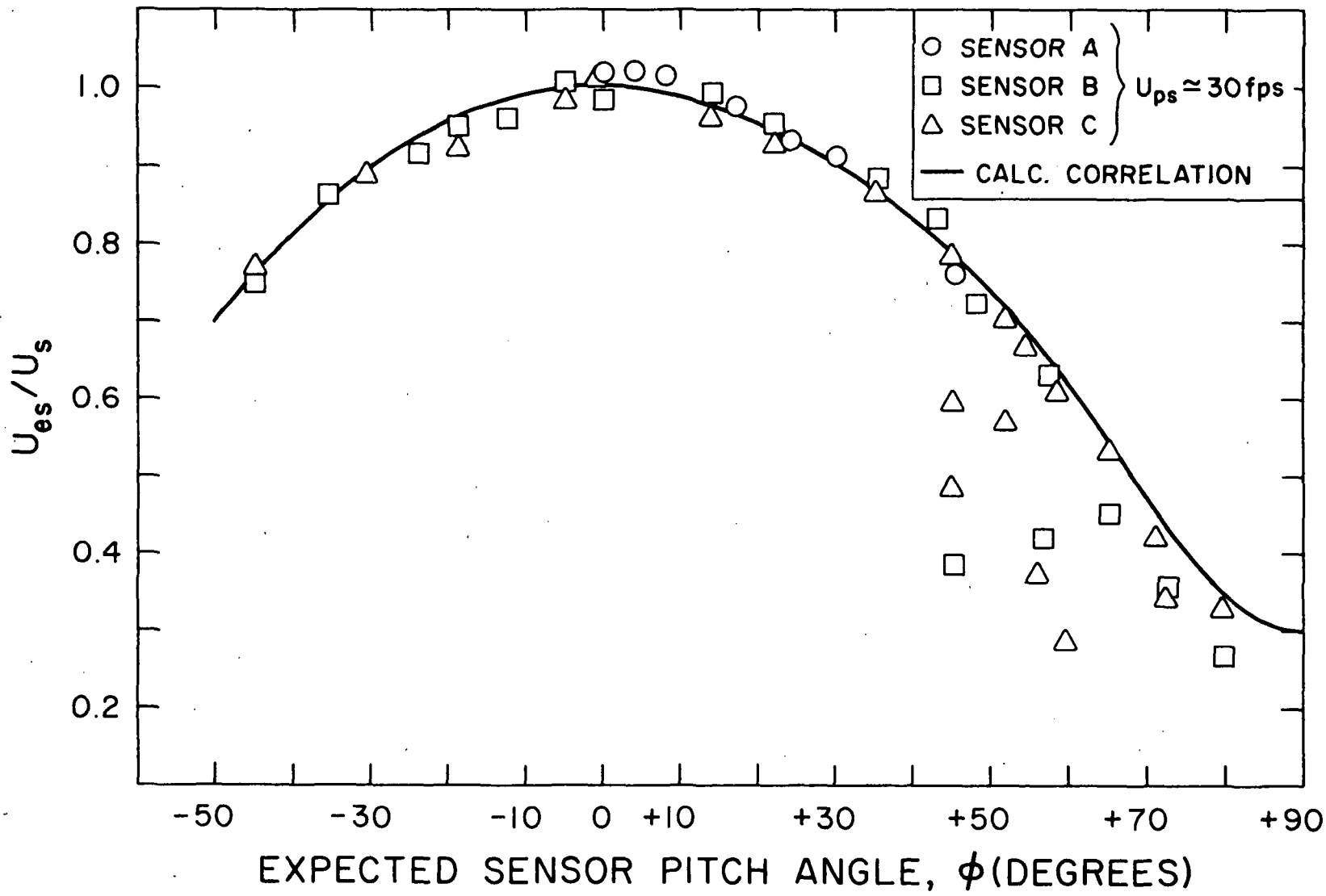

Figure 22: Comparison of Calculated Values of U_{es}/U_s with Expected Correlation.

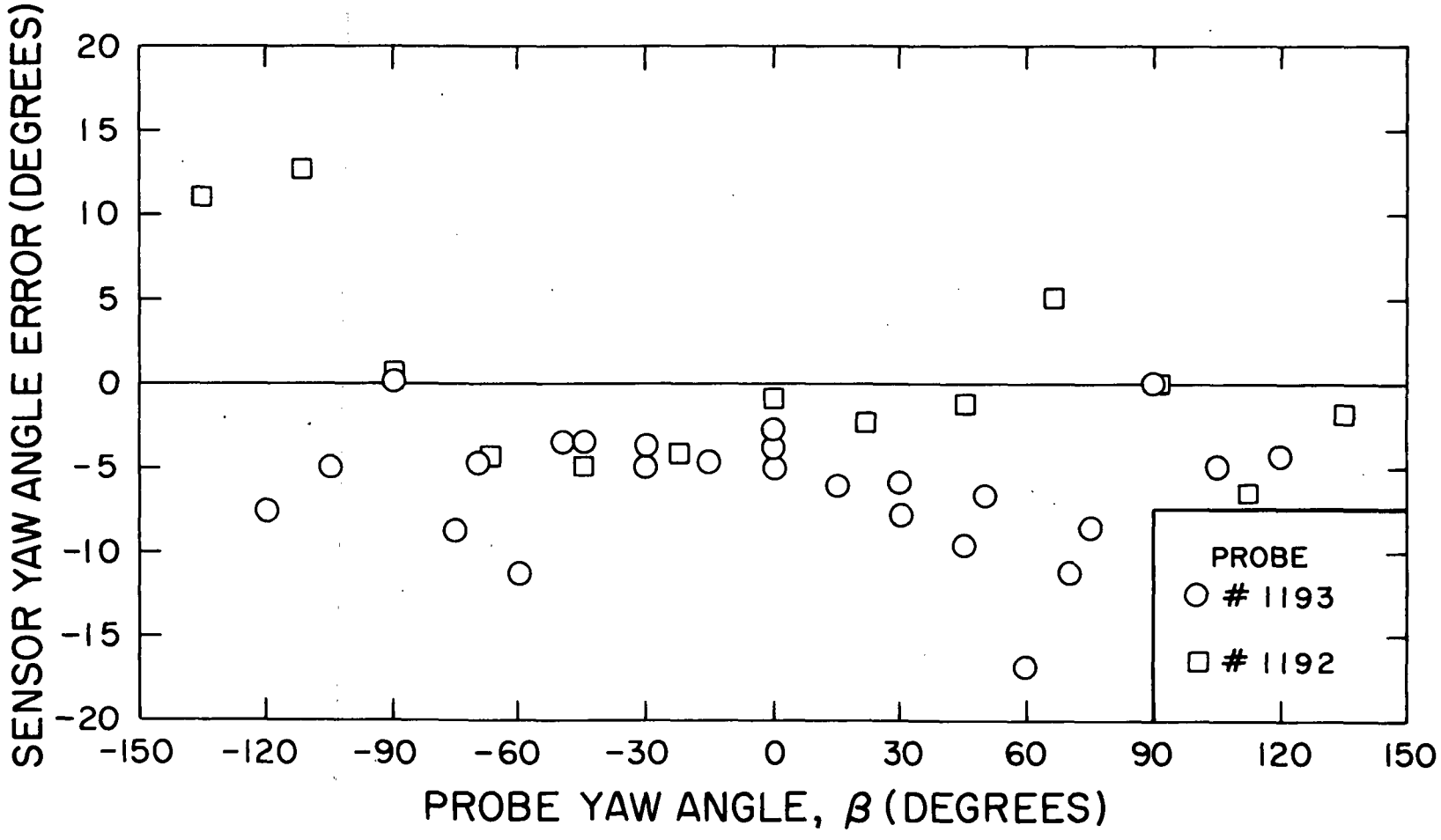

Figure 23: Error in Sensor Yaw Angle, ϕ_A for the T.S.I. Method (1st Approximation) $U \simeq 30$fps, $\alpha=0°$.

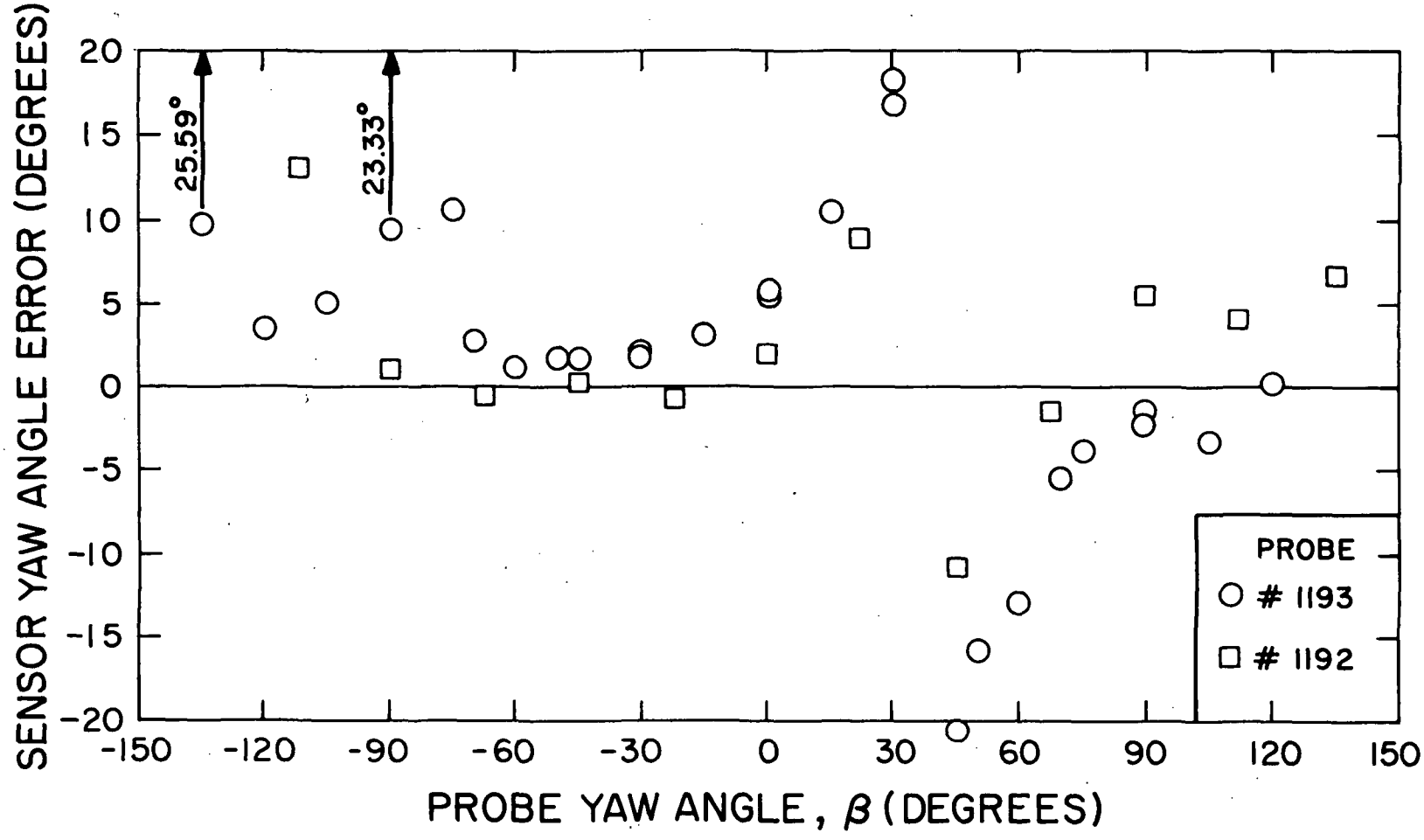

Figure 24: Error in Sensor Yaw Angle, ϕ_B for the T.S.I. Method (1st Approximation) $U \simeq 30$fps, $\alpha=0°$.

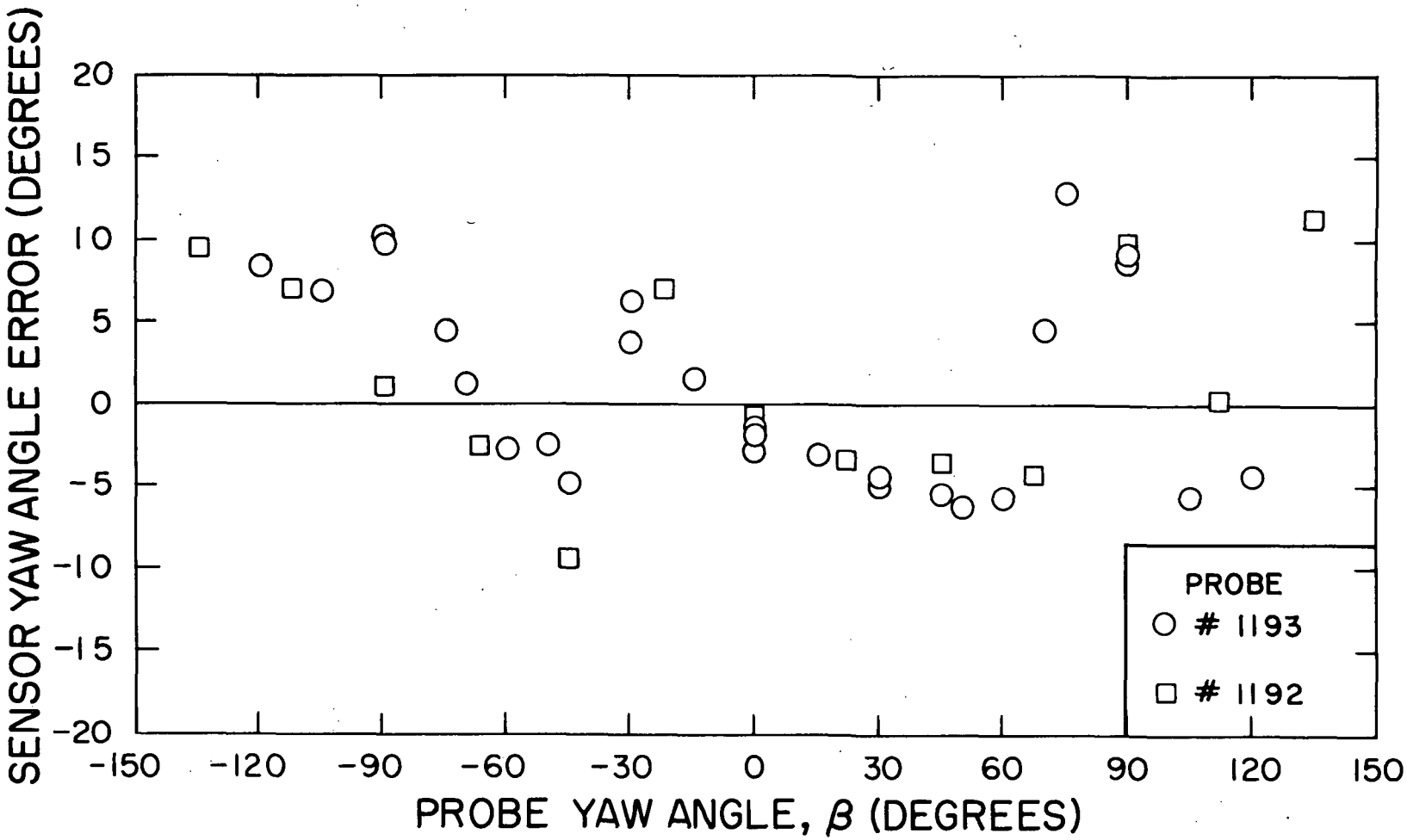

Figure 25: Error in Sensor Yaw Angle, ϕ_C for the T.S.I. (1st Approximation) $U \simeq 30$fps, $\alpha=0°$.

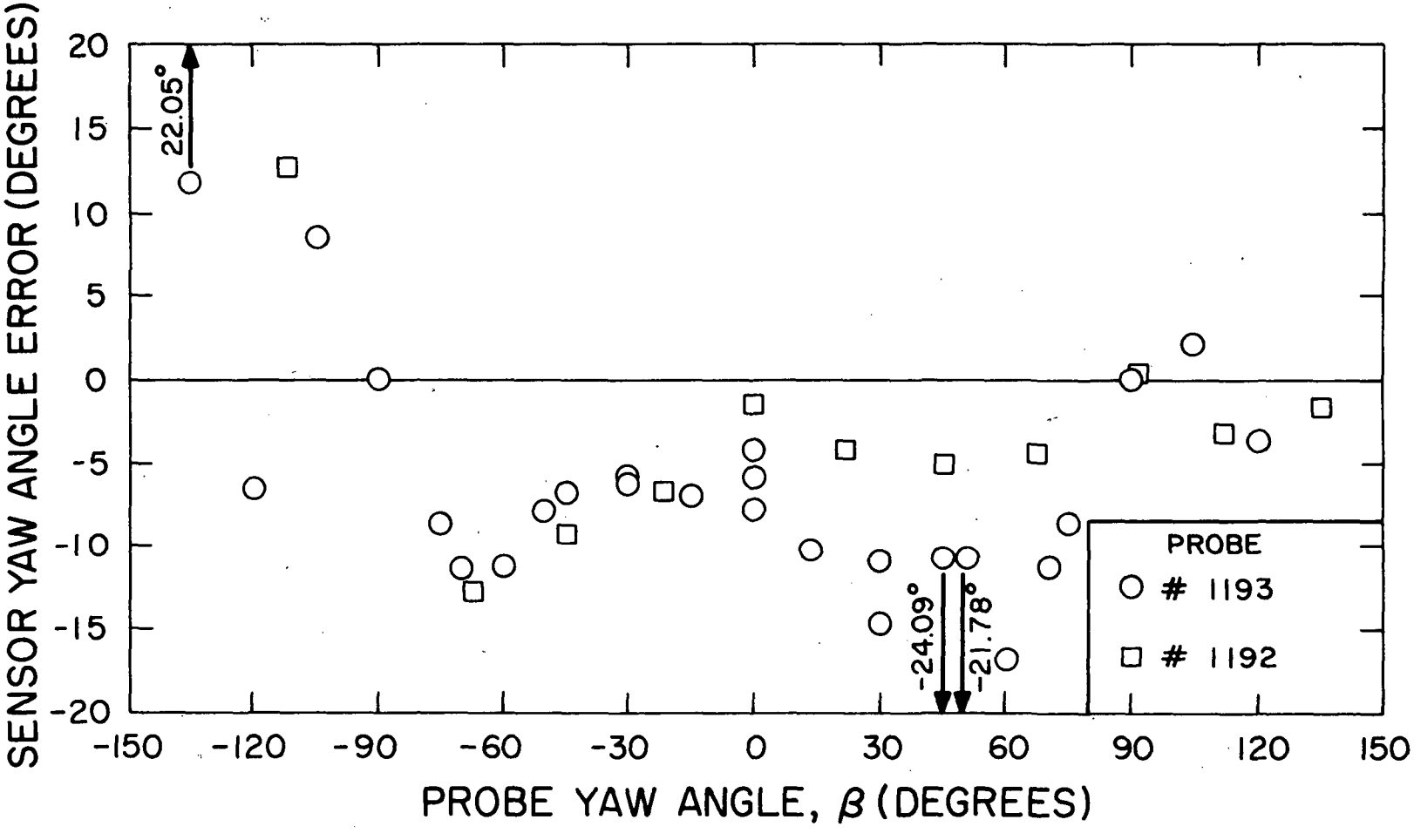

Figure 26: Error in Sensor Yaw Angle, ϕ_A for the Improved ϕ-Method U $\simeq$ 30fps and α=0°.

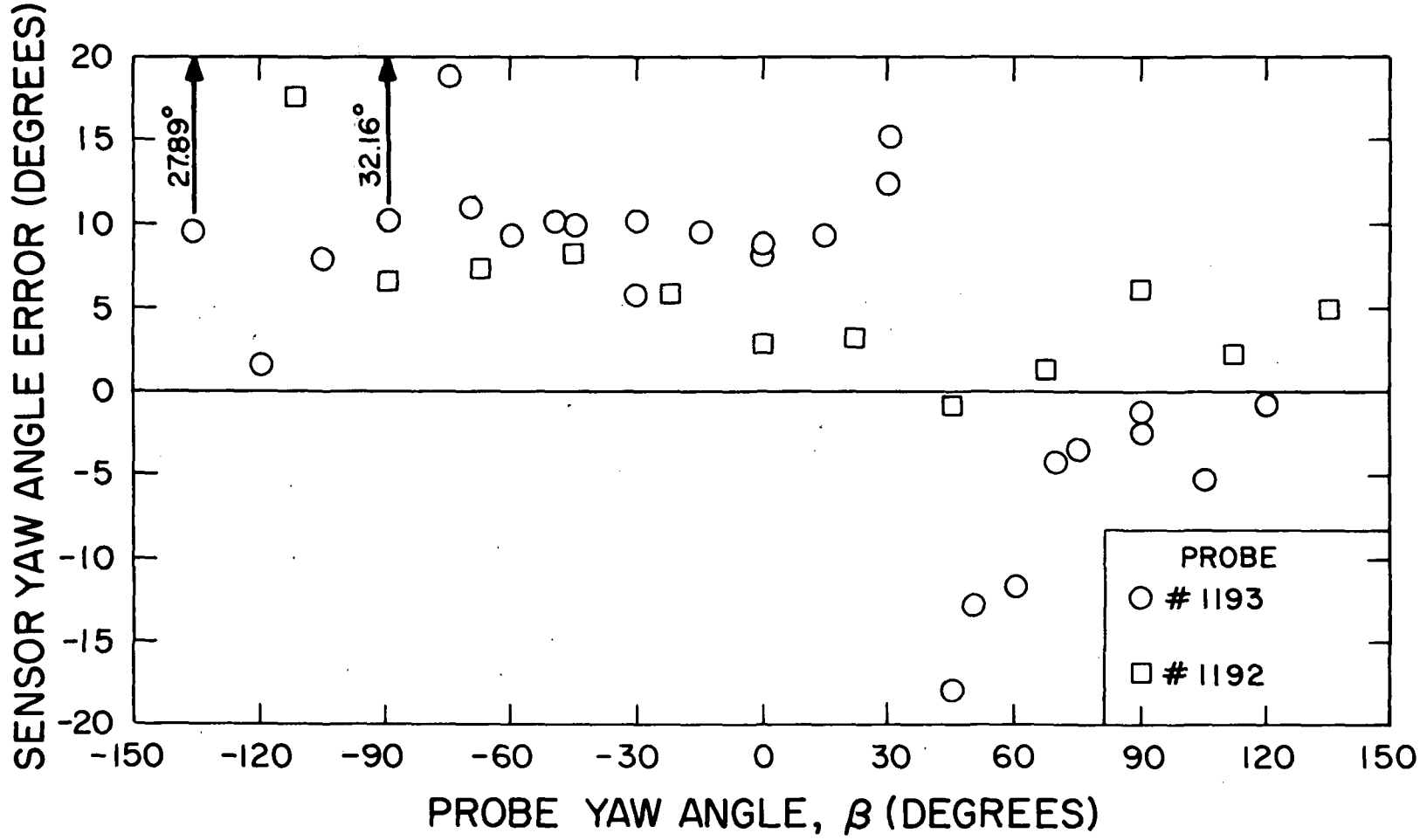

Figure 27: Error in Sensor Yaw Angle, ϕ_B for the Improved ϕ-Method U $\simeq$ 30fps and α=0°.

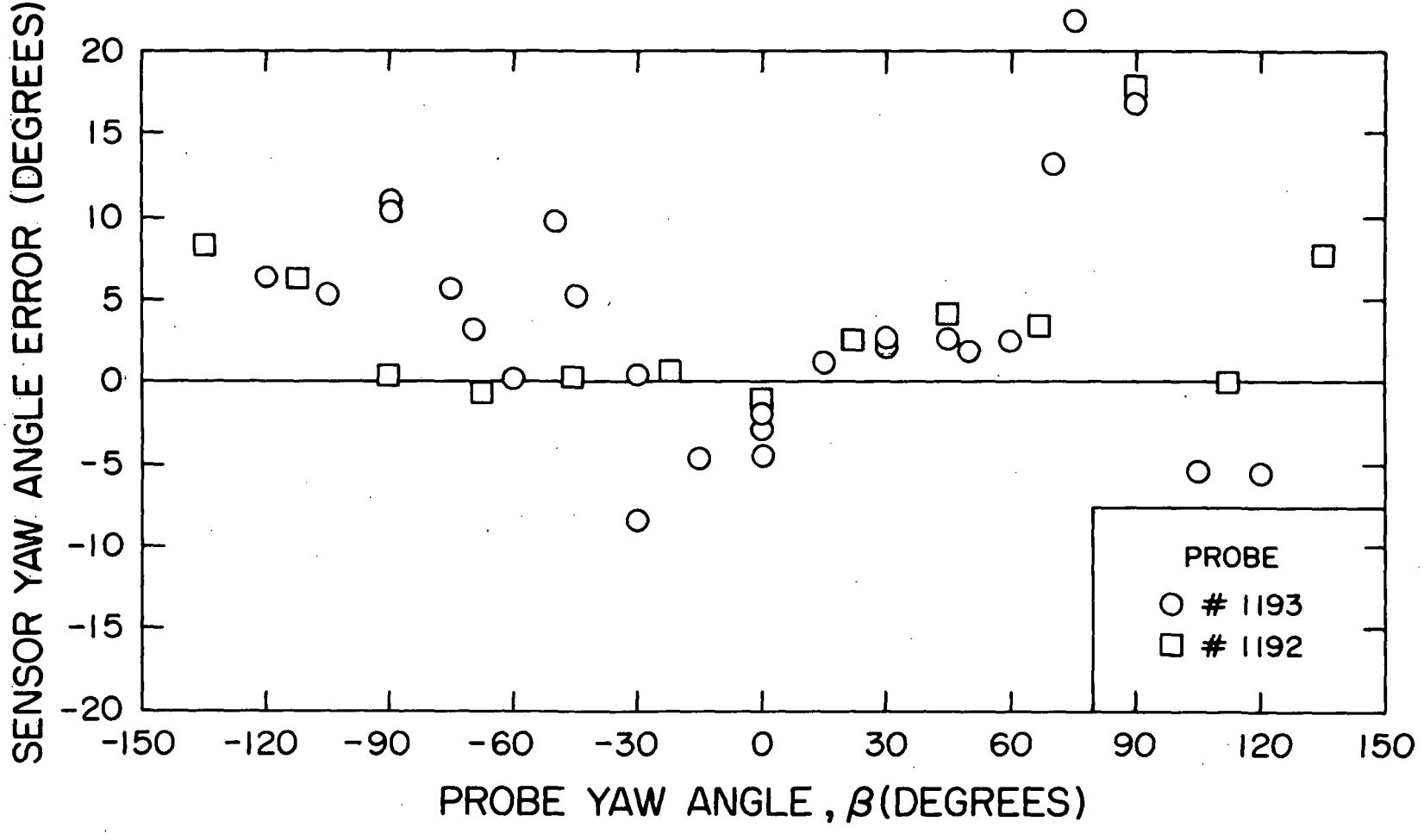

Figure 28: Error in Sensor Yaw Angle, ϕ_C for the Improved ϕ-Method $U \simeq 30$fps and $\alpha=0°$.

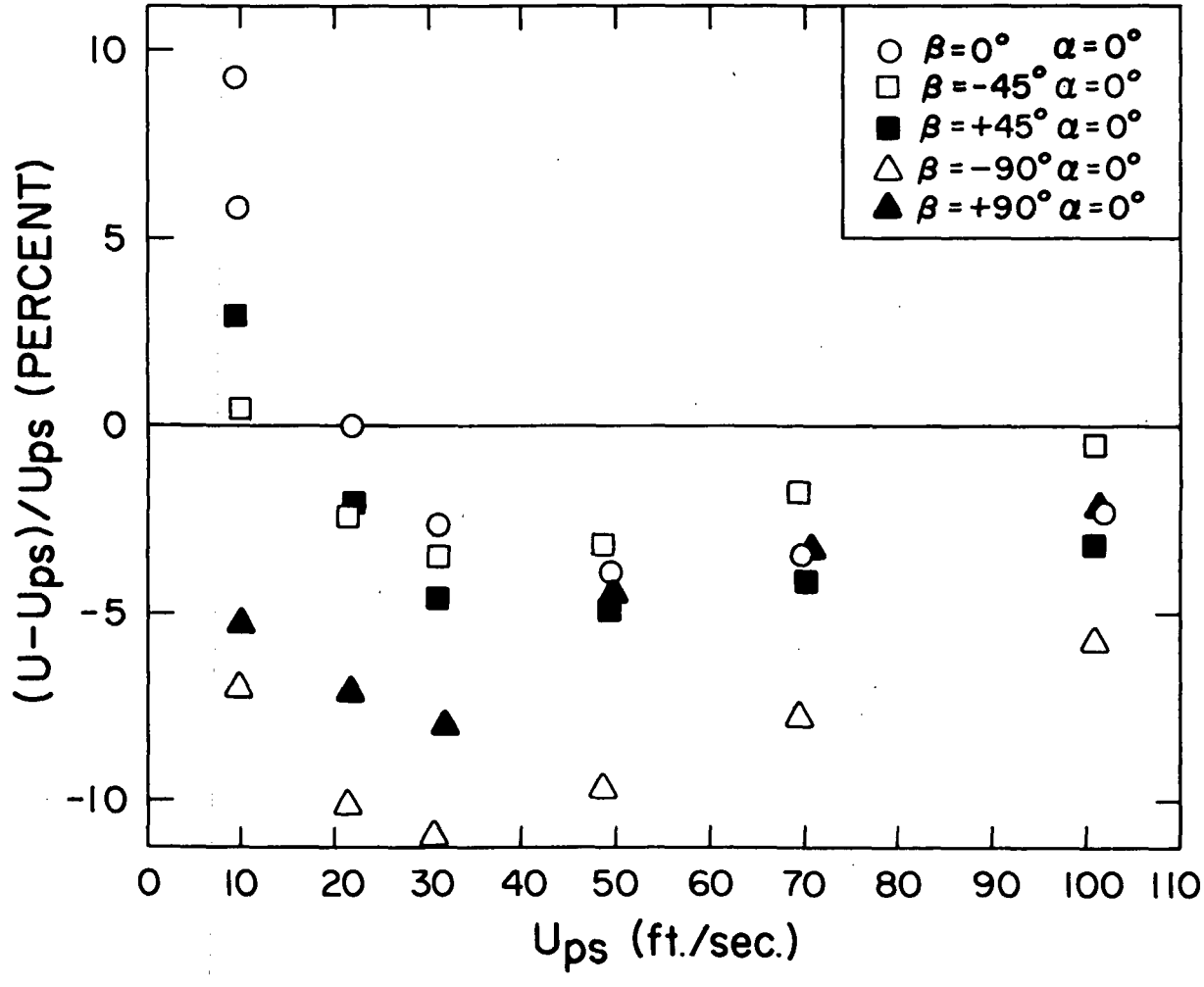

Figure 29: Percentage Error in Total Velocity for the Improved ϕ-Method, Probe #1193.

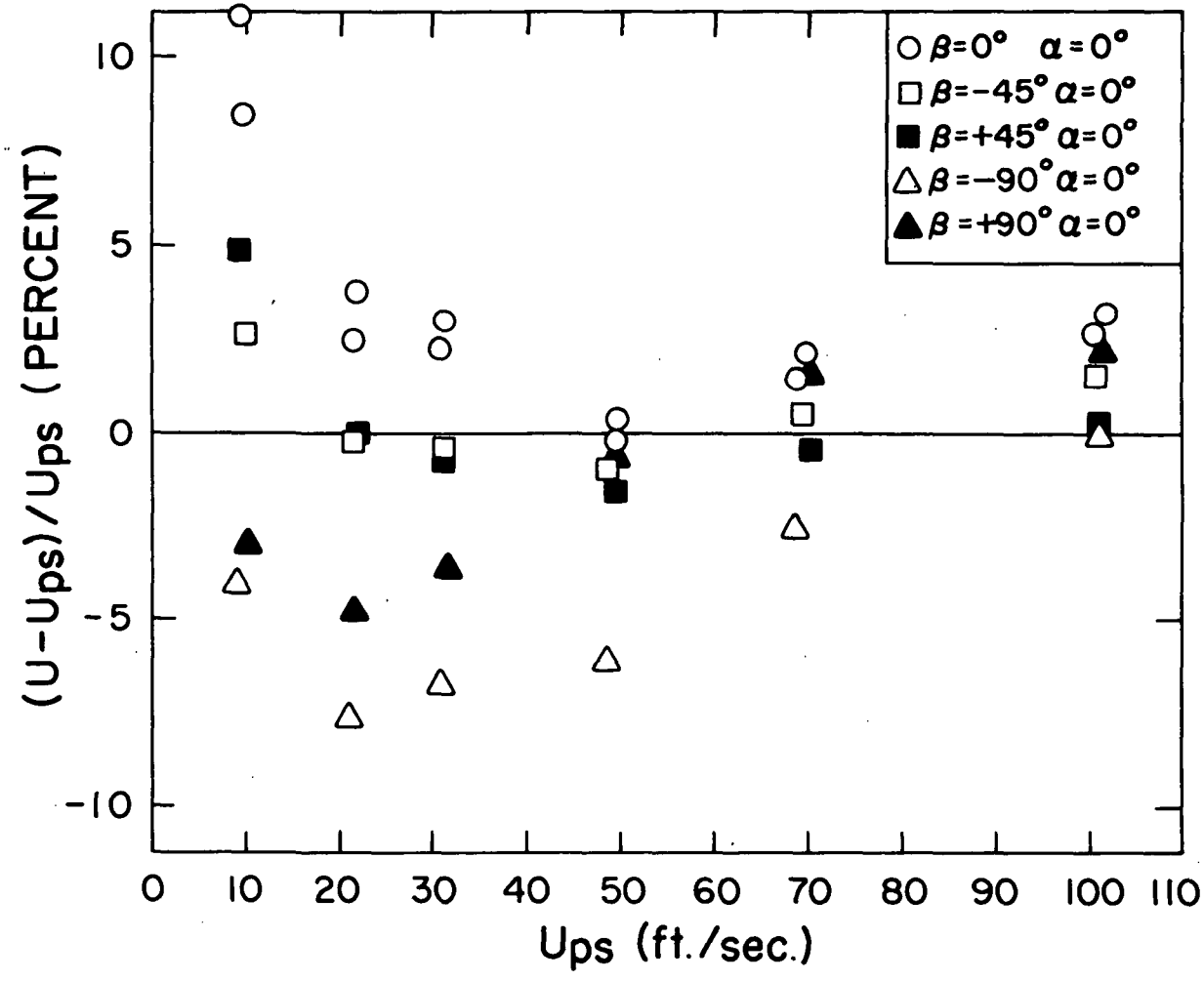

Figure 30: Percentage Error in Total Velocity for the T.S.I. Suggested First Approximation. Probe #1193.

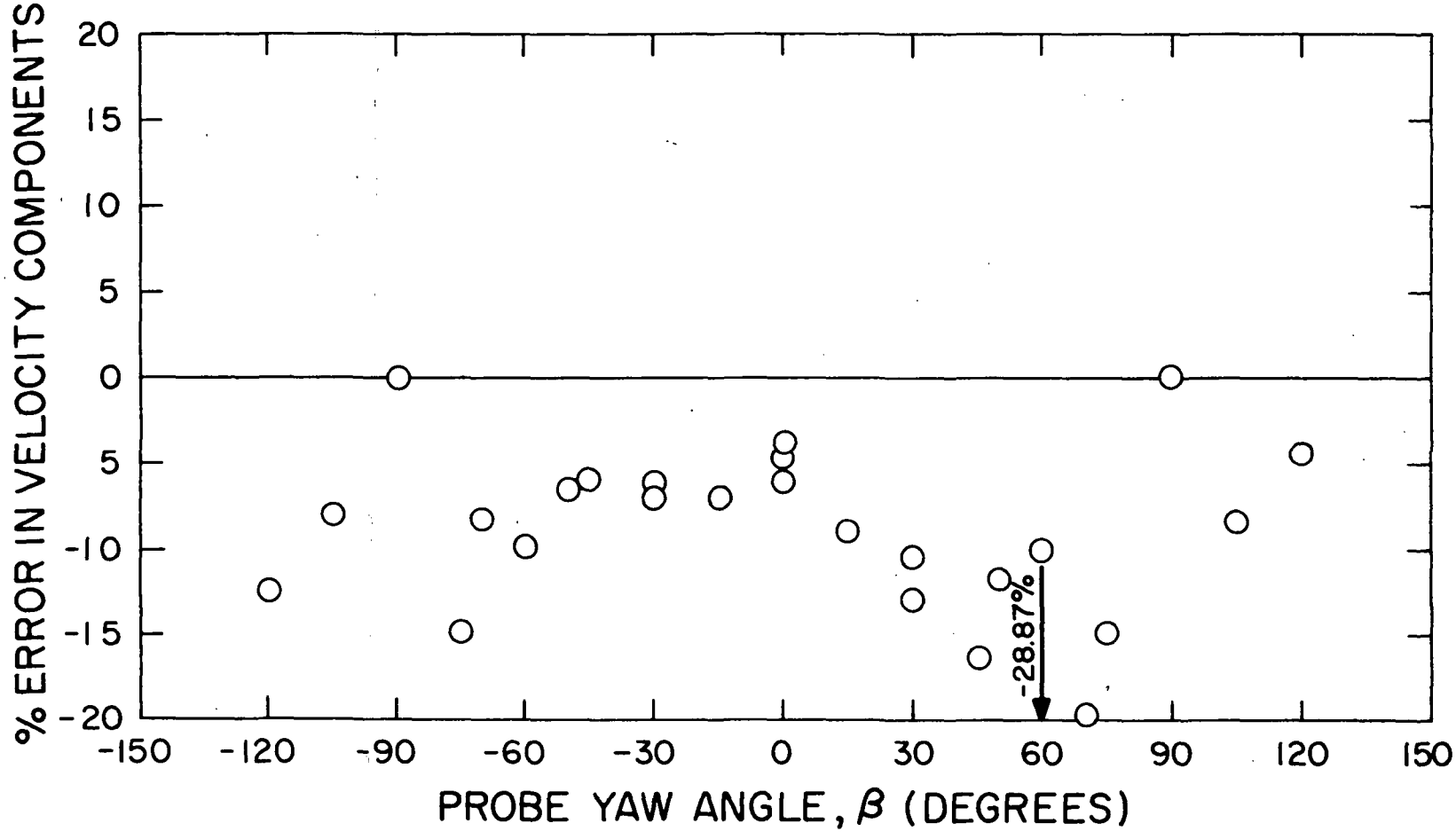

Figure 31: Percent Error in Velocity Component, U_A for First Approximation of the T.S.I. Method $U \simeq 30$fps, $\alpha=0°$. Probe #1193.

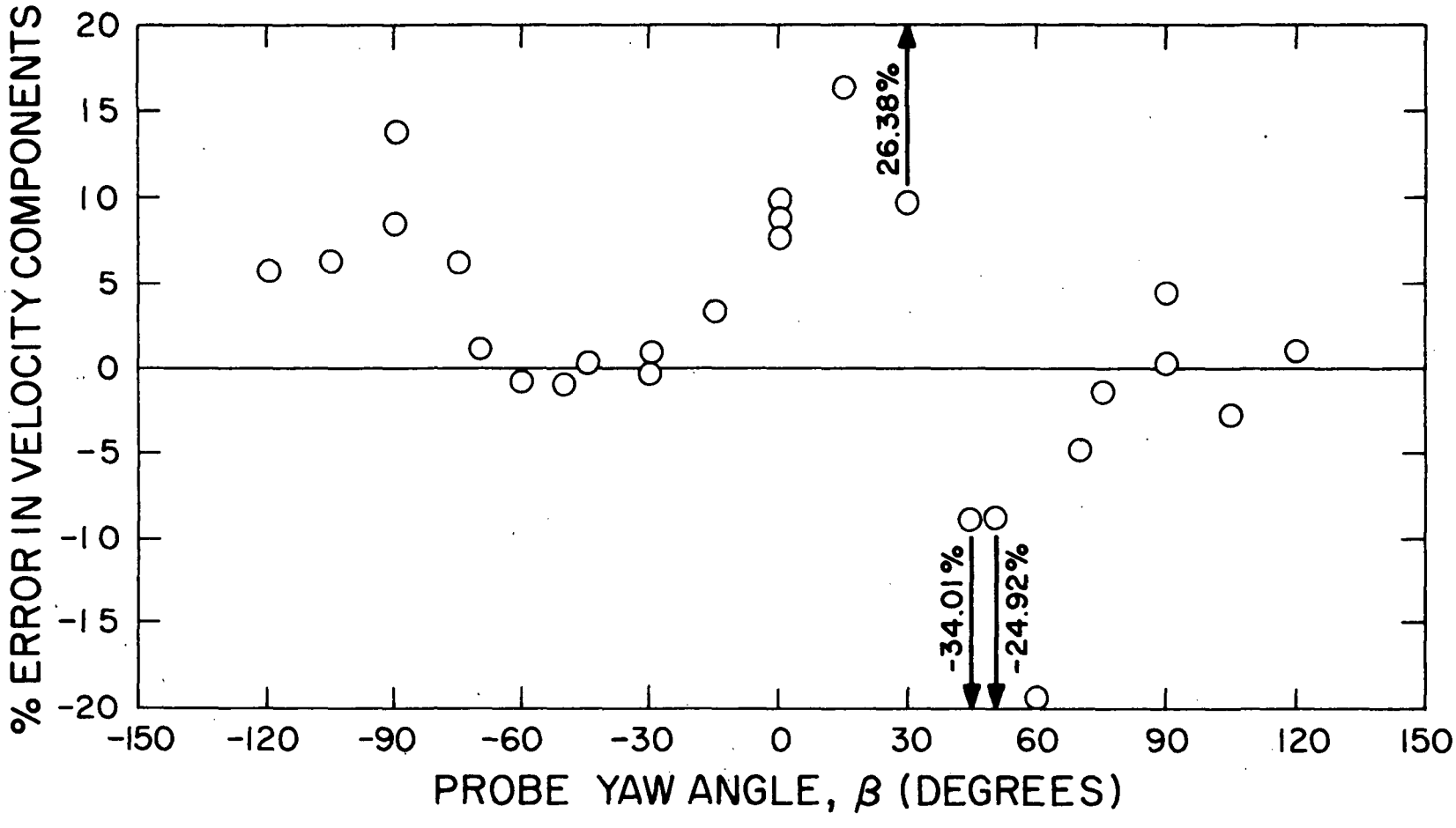

Figure 32: Percent Error in Velocity Component U_B for First Approximation of the T.S.I. Method $U \simeq 30$fps, $\alpha=0°$. Probe #1193.

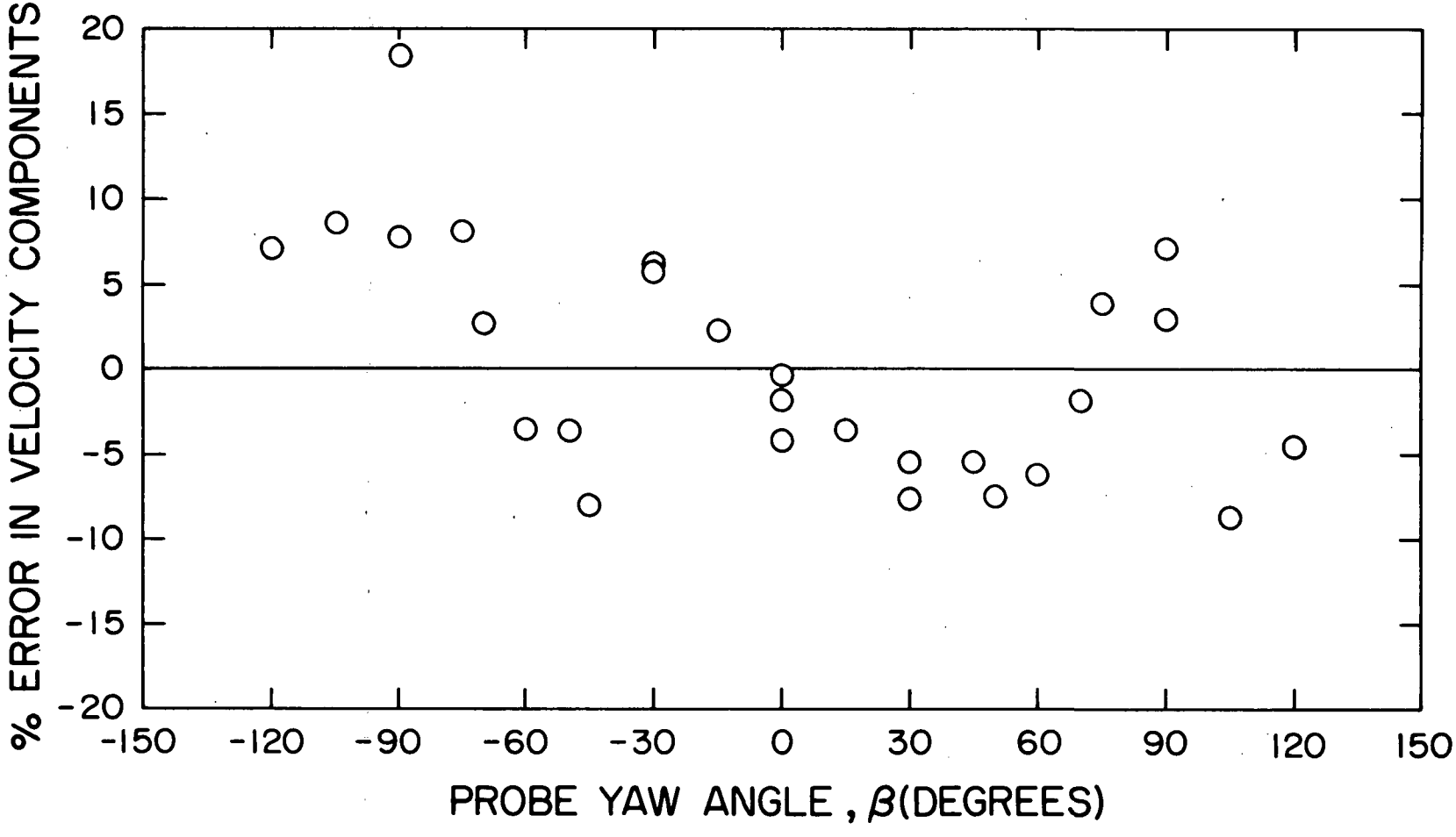

Figure 33: Percent Error in Velocity Component, U_C for First Approximation of the T.S.I. Method $U \simeq 30$fps, $\alpha=0°$. Probe #1193.

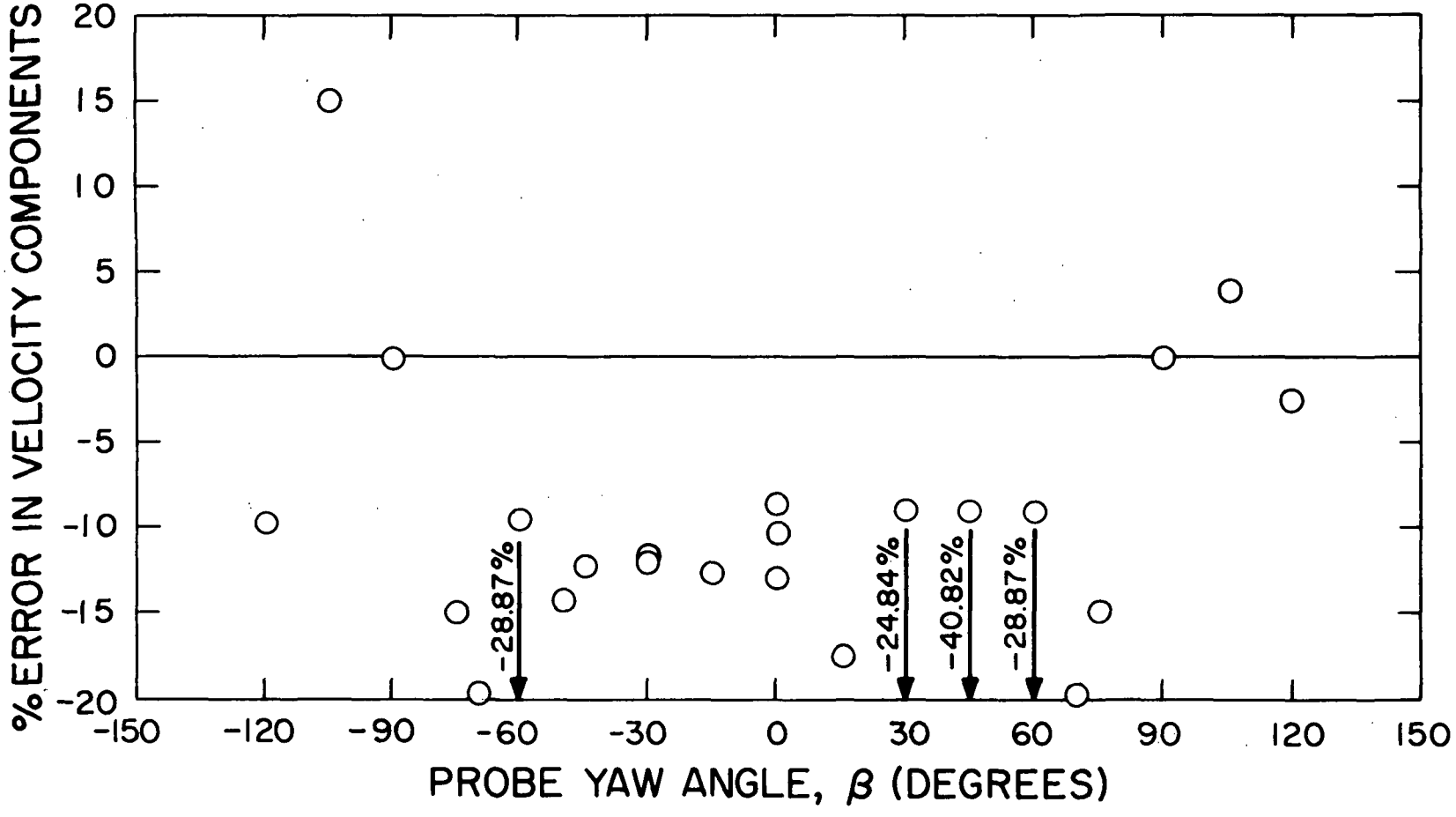

Figure 34: Percent Error in Velocity Component, U_A for ϕ-Method $U \simeq 30$fps, $\alpha=0°$. Probe #1193

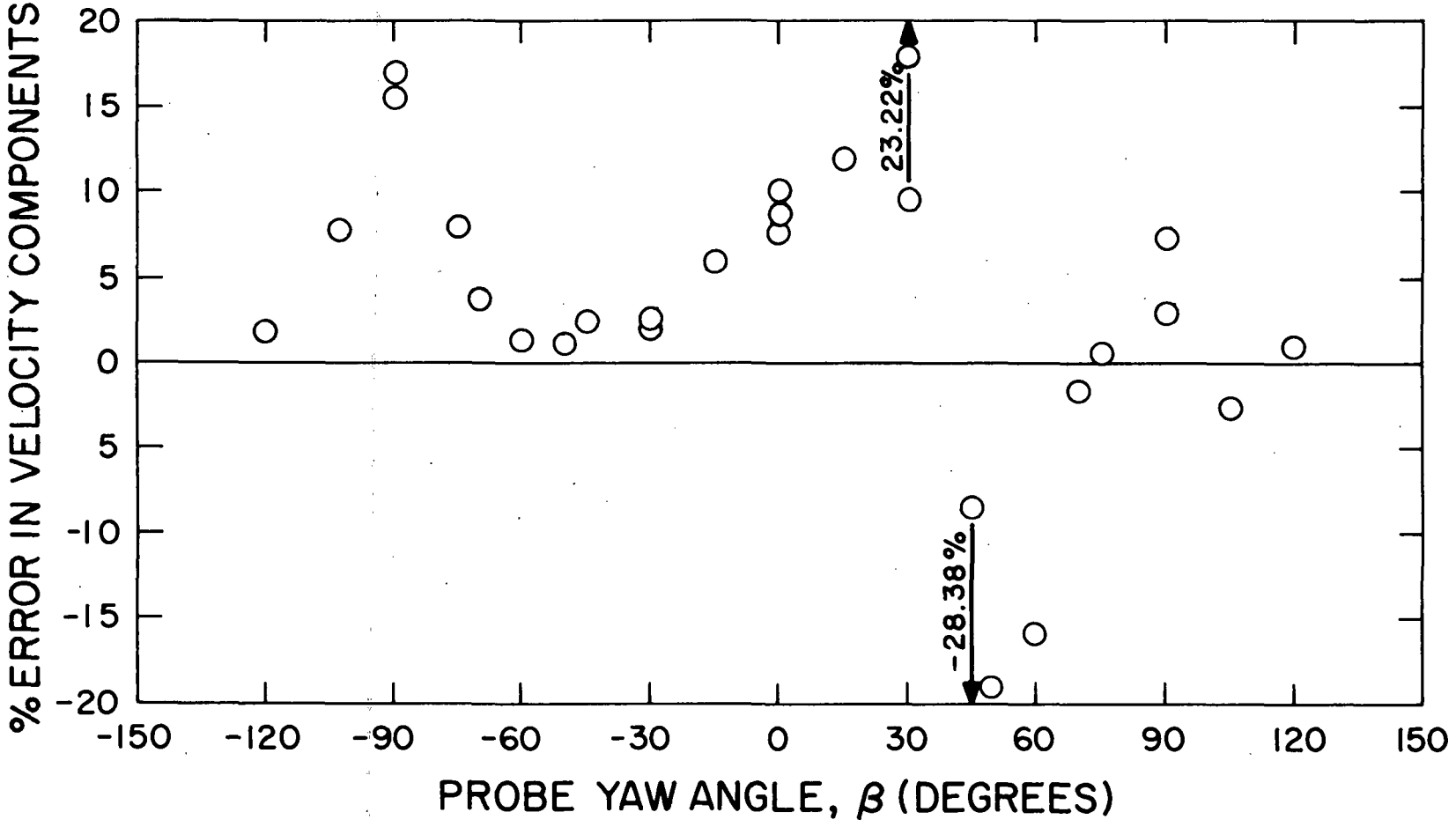

Figure 35: Percent Error in Velocity Component, U_B for ϕ-Method $U \simeq 30$fps, $\alpha=0°$. Probe #1193.

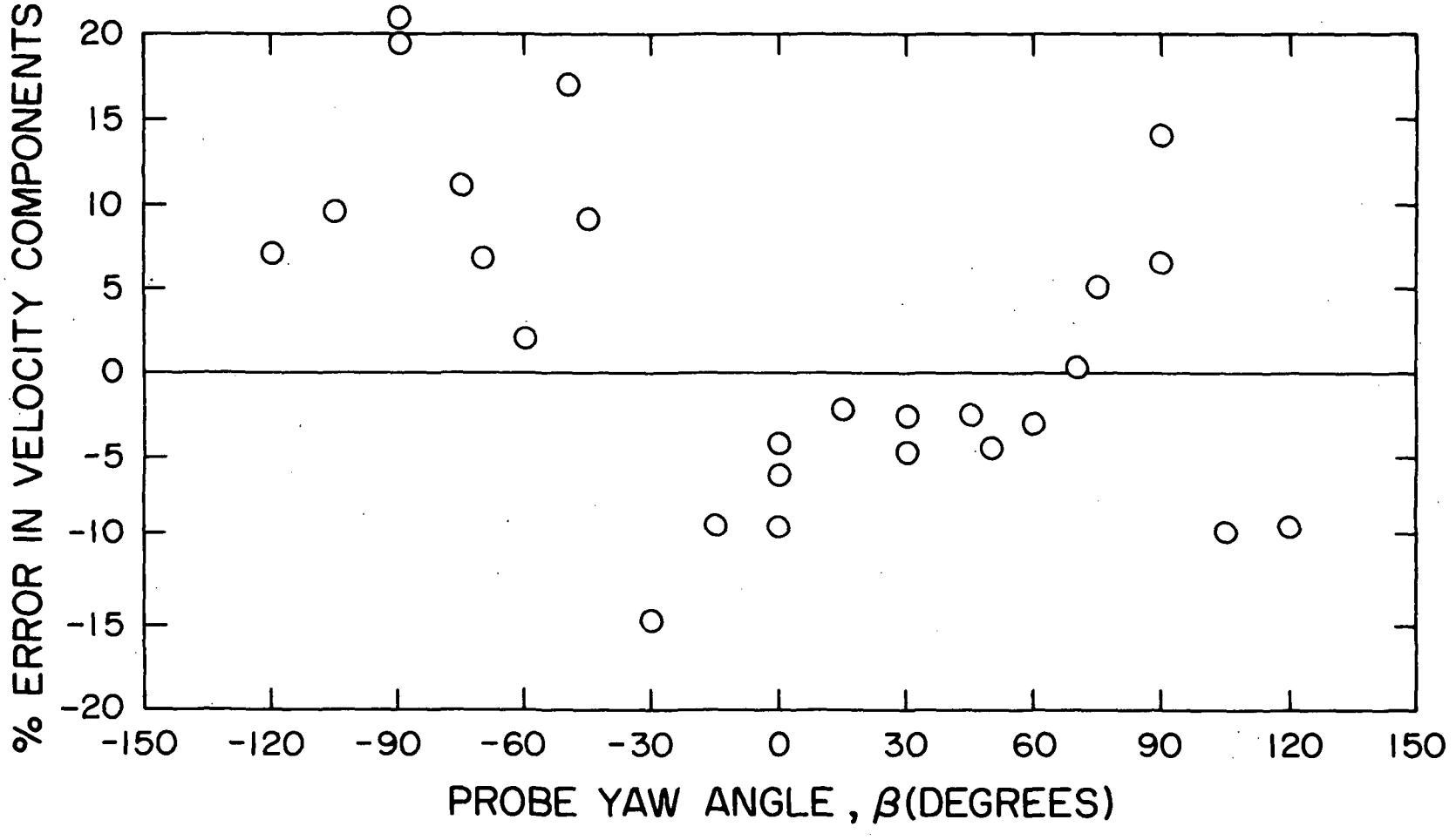

Figure 36: Percent Error in Velocity Component, U_C for ϕ-Method $U \simeq 30$fps, $\alpha=0°$. Probe #1193.

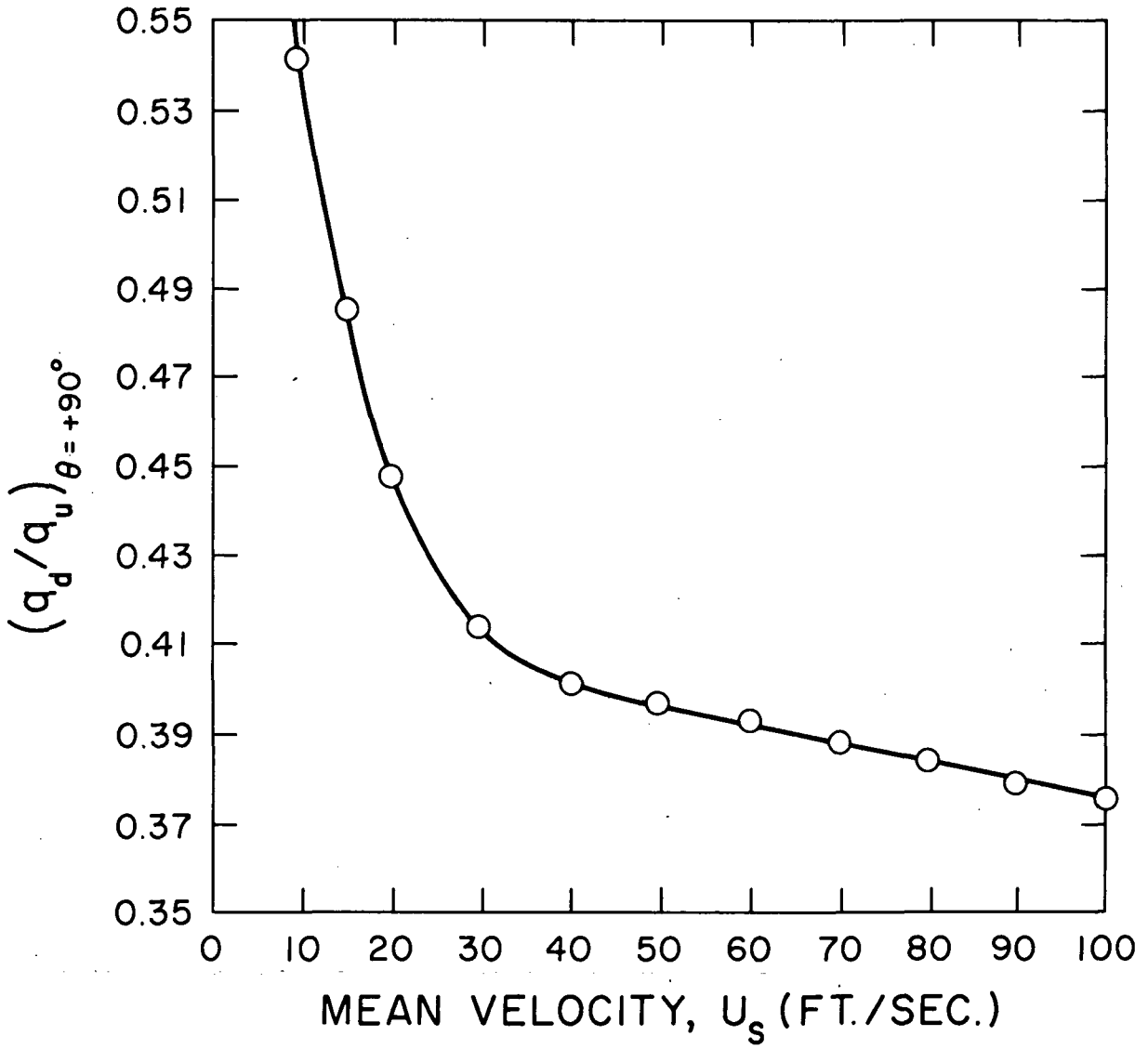

Figure 37: Ratio of Downstream Heat Transfer to Upstream Heat Transfer at $\theta=90°$ Vs. U_s.

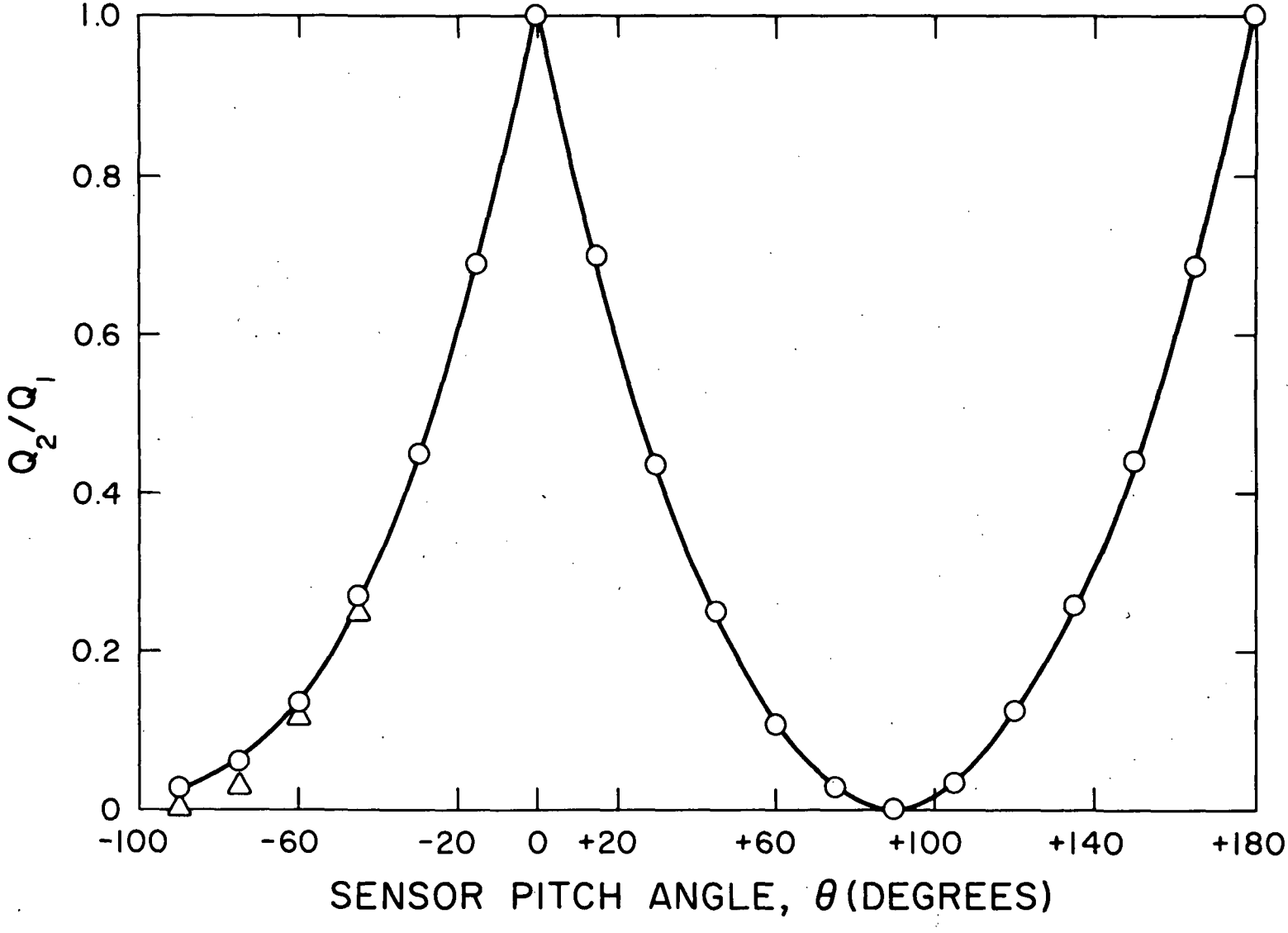

Figure 38: Typical Curve Used for Determination of Sensor Pitch Angle from the Ratio Q_2/Q_1. Sensor A, #1192.

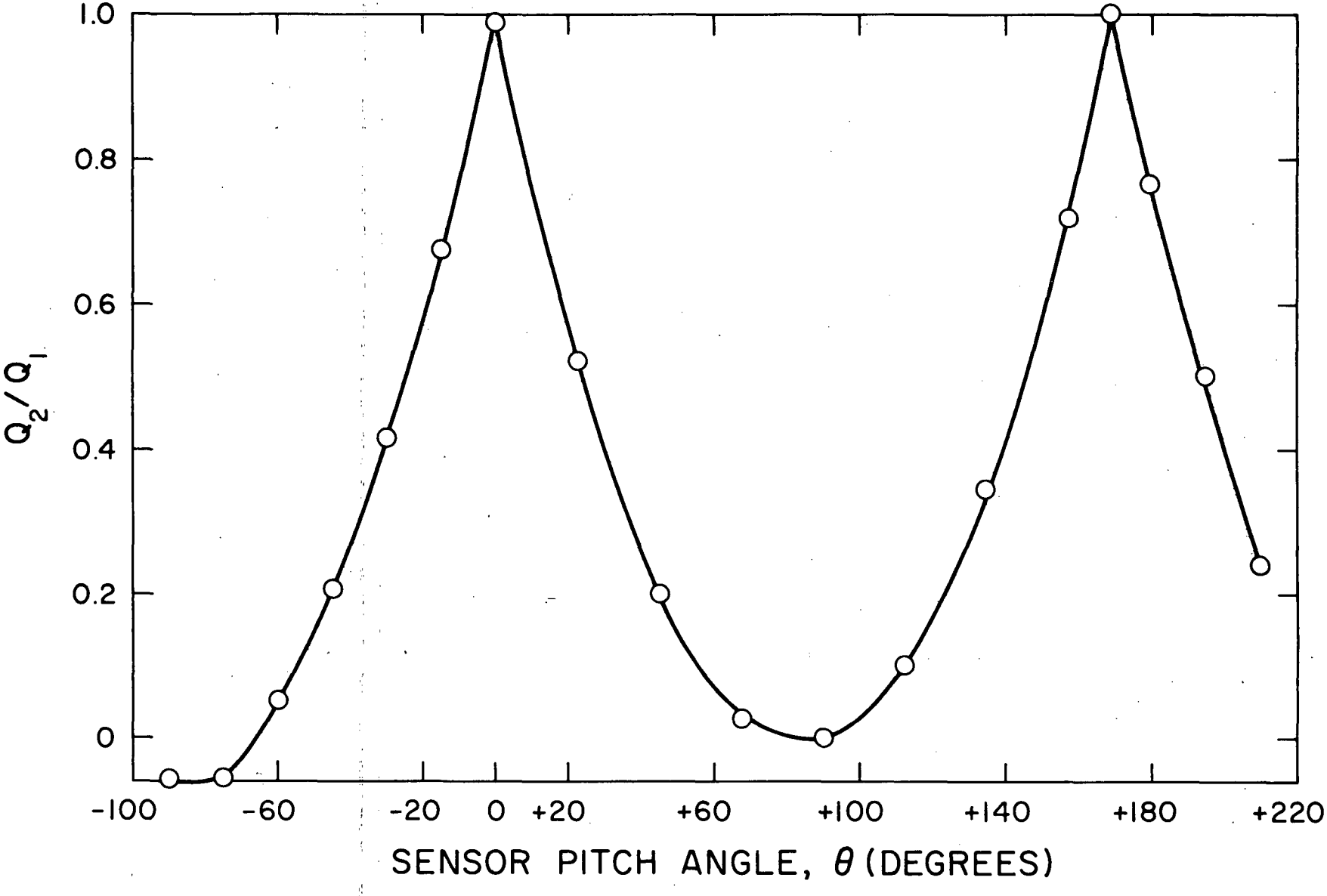

Figure 39: Curve Used for Determination of Sensor Pitch Angle Illustrating Asymmetry of the Sensor, Sensor C, #1192.

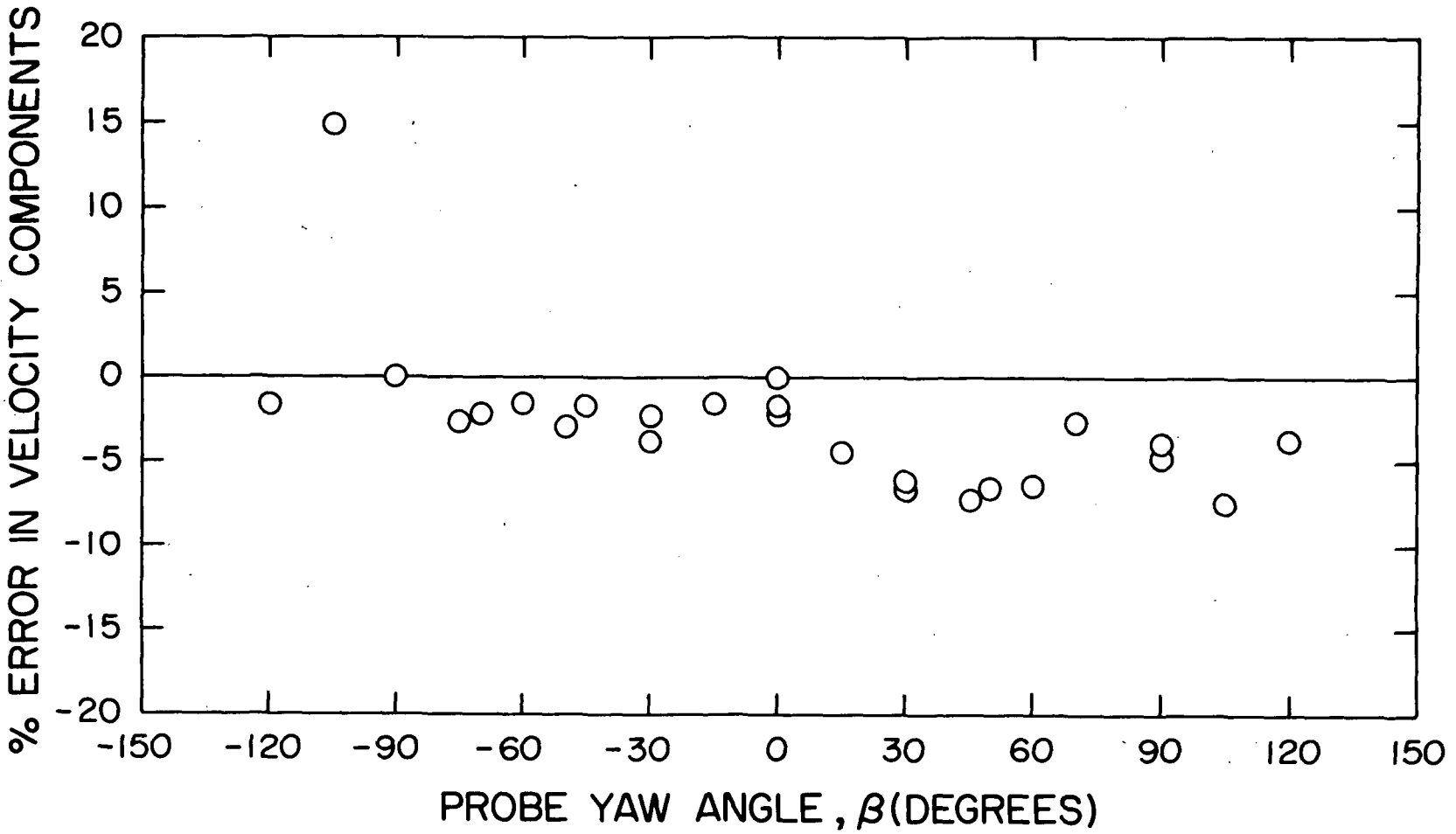

Figure 40: Percent Error in Velocity Component U_A for the θ-Method $U \simeq 30$fps, $\alpha=0°$. Probe #1193.

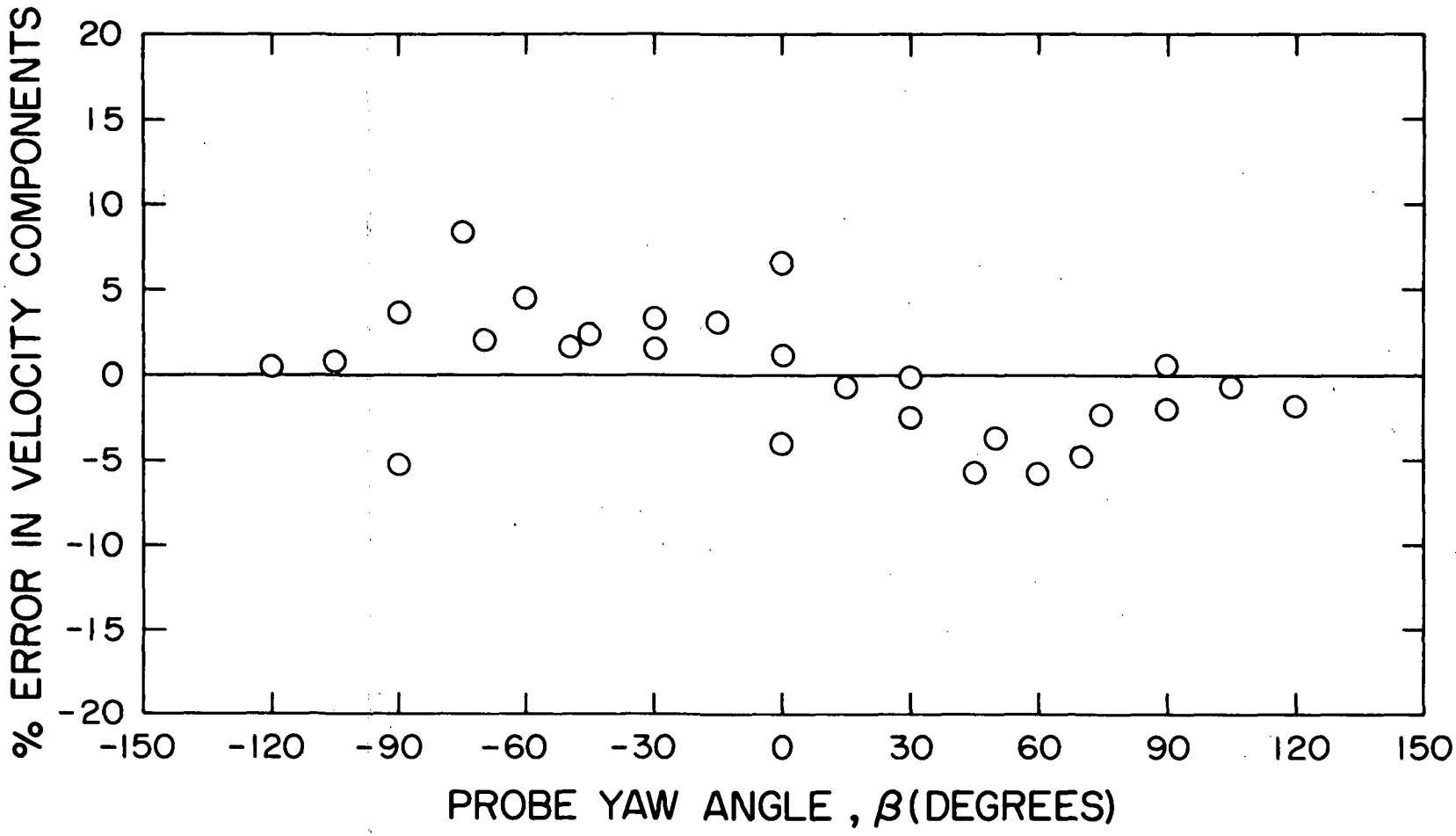

Figure 41: Percent Error in Velocity Component U_B for the θ-Method $U \simeq 30$fps, $\alpha=0°$. Probe #1193.

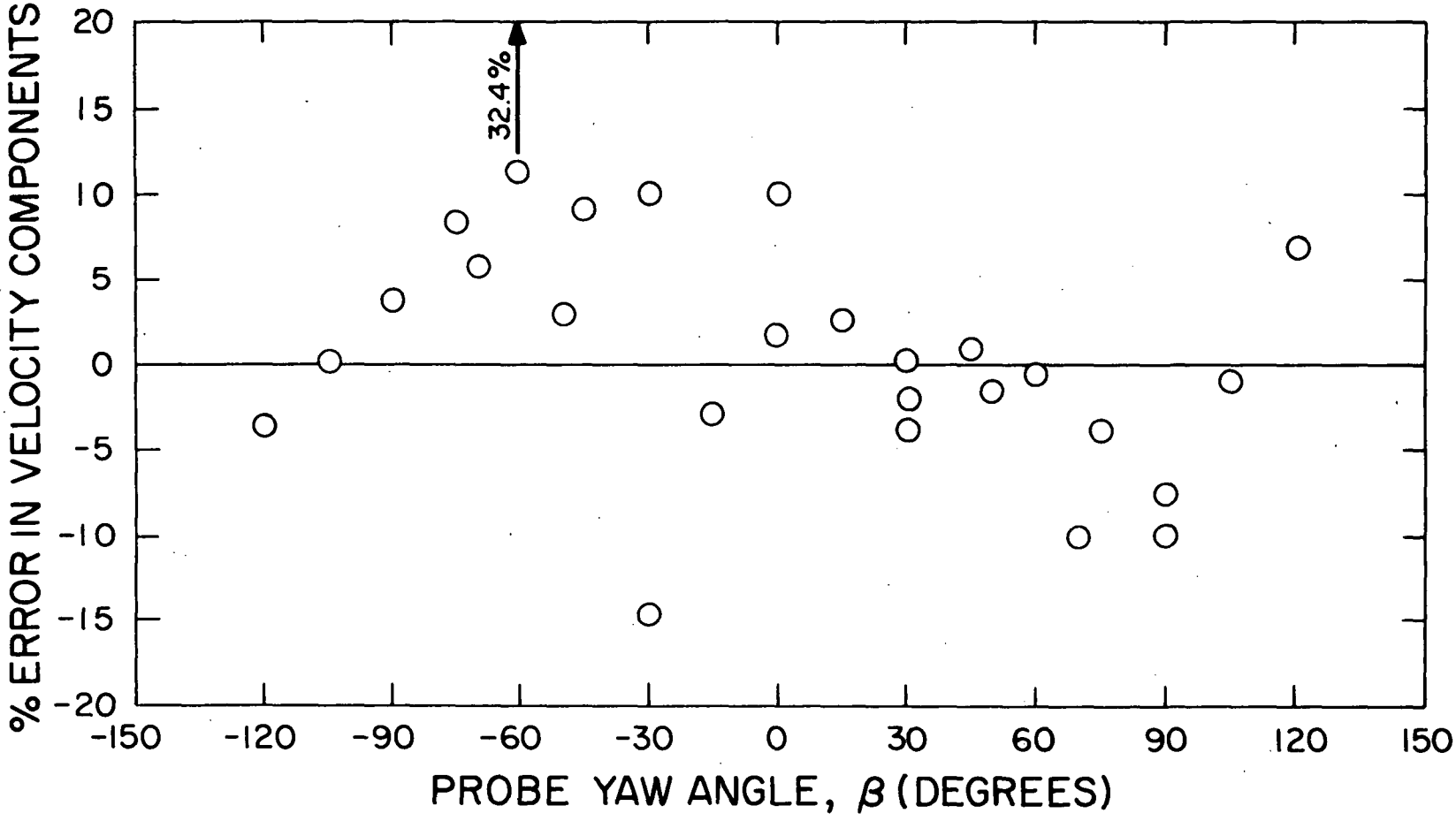

Figure 42: Percent Error in Velocity Component U_C for the θ-Method $U \simeq 30$fps, $\alpha=0°$. Probe #1193.

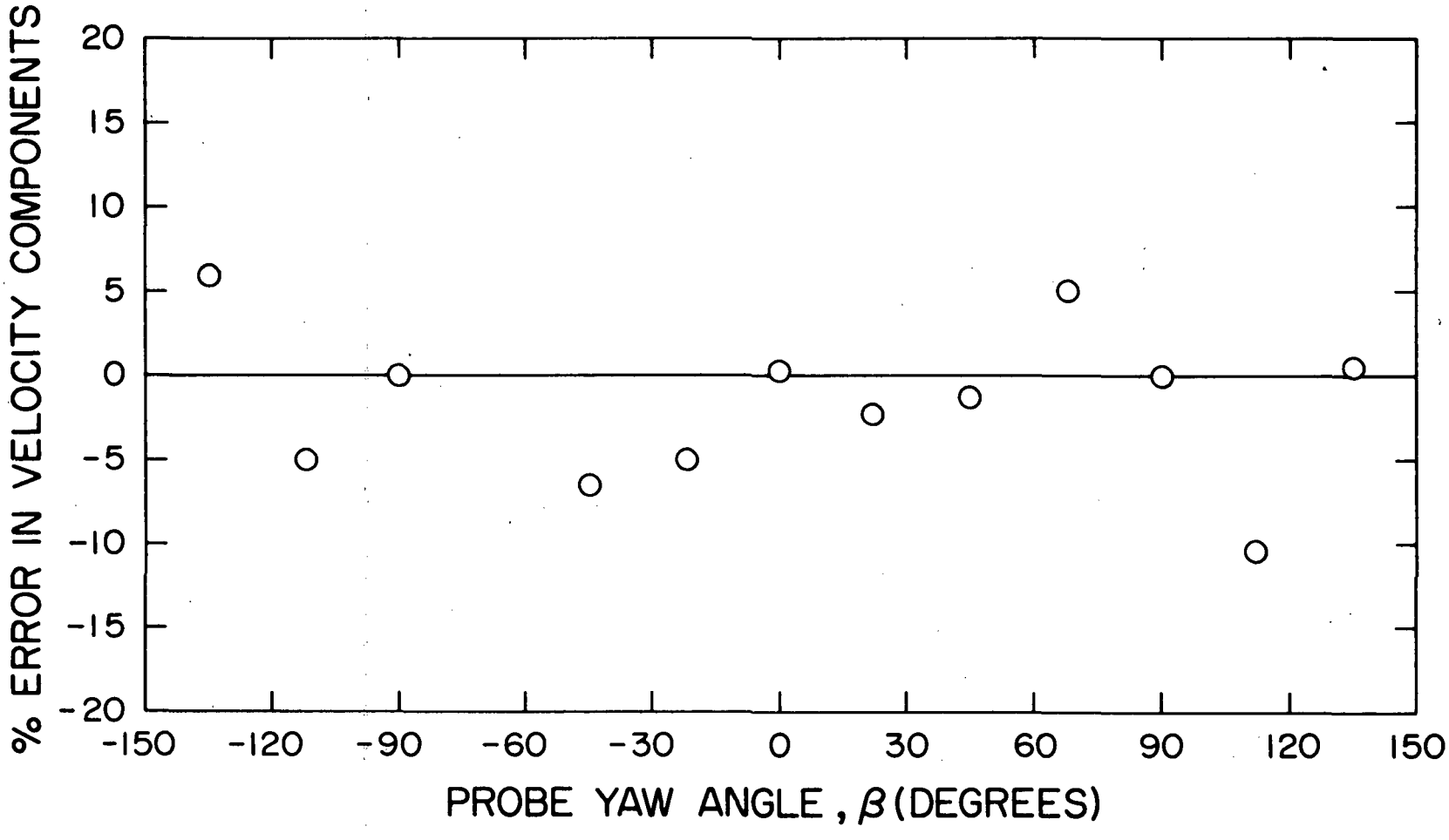

Figure 43: Percent Error in Velocity Component, U_A for First Approximation of T.S.I. Method $U \simeq 30$fps, $\alpha=0°$. Probe #1192.

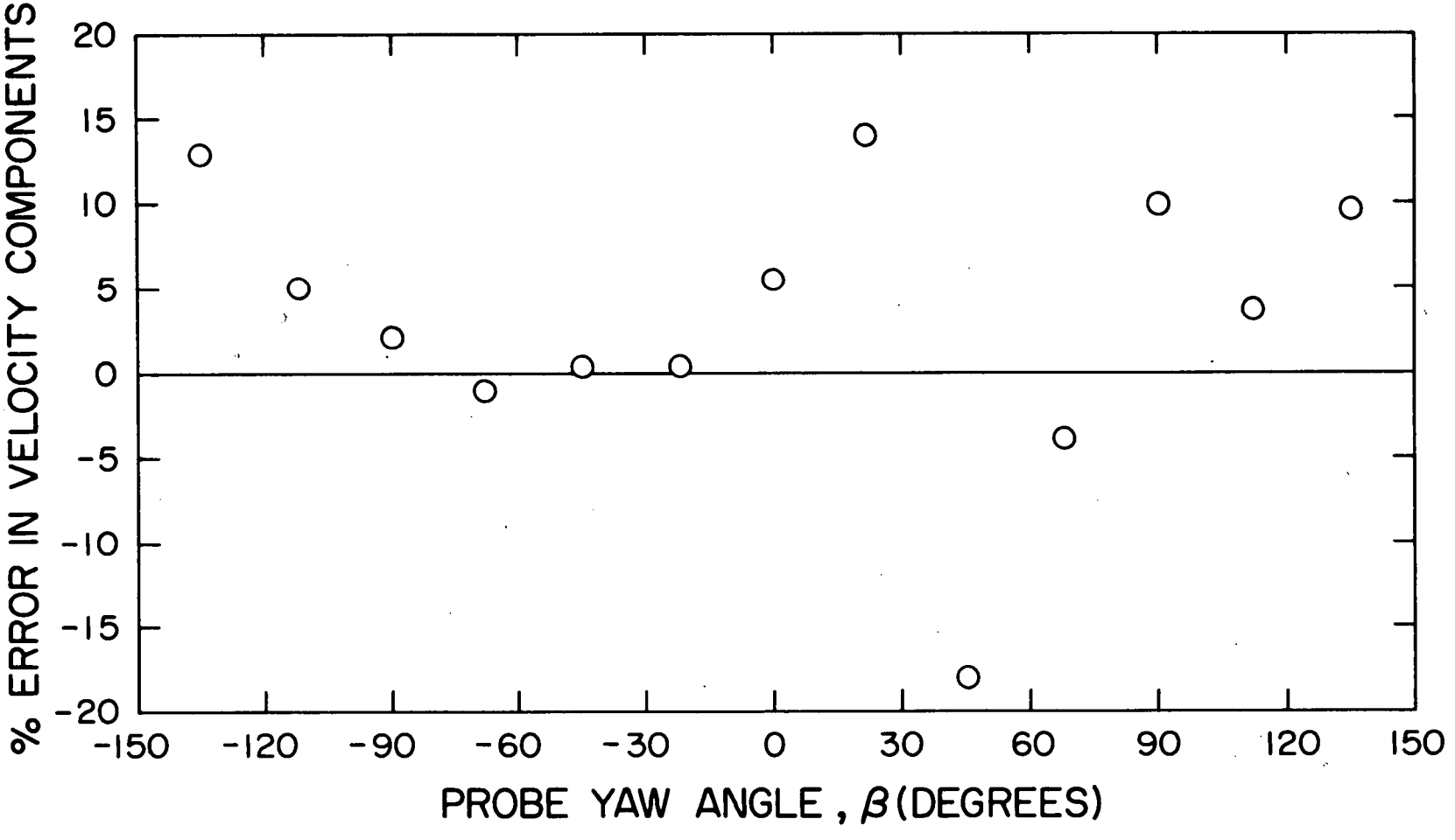

Figure 44: Percent Error in Velocity Component, U_B for First Approximation of the T.S.I. Method $U \simeq 30$fps, $\alpha=0°$. Probe #1192.

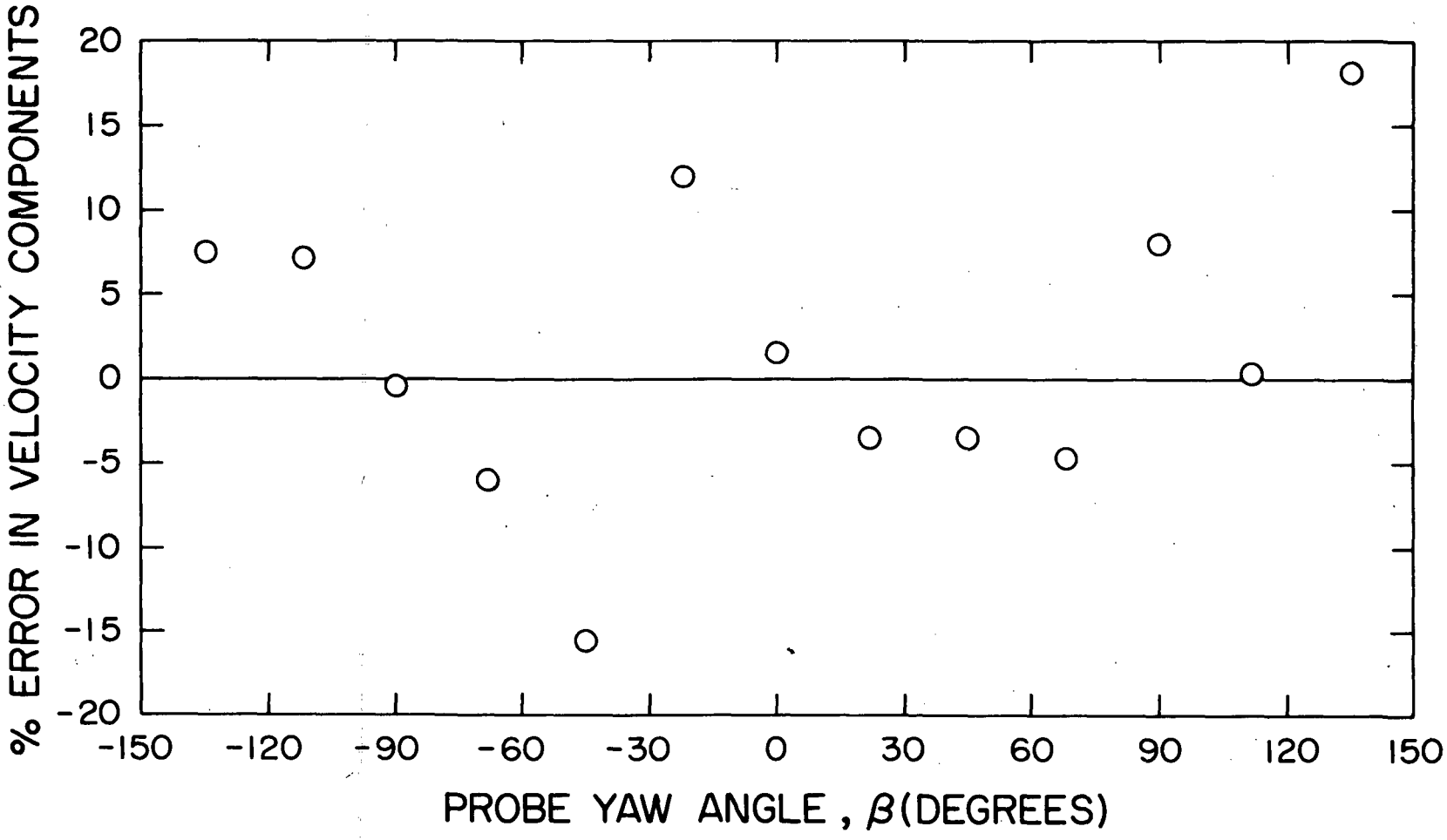

Figure 45: Percent Error in Velocity Component, U_C for First Approximation of the T.S.I. Method $U \simeq 30$fps, $\alpha=0°$. Probe #1192.

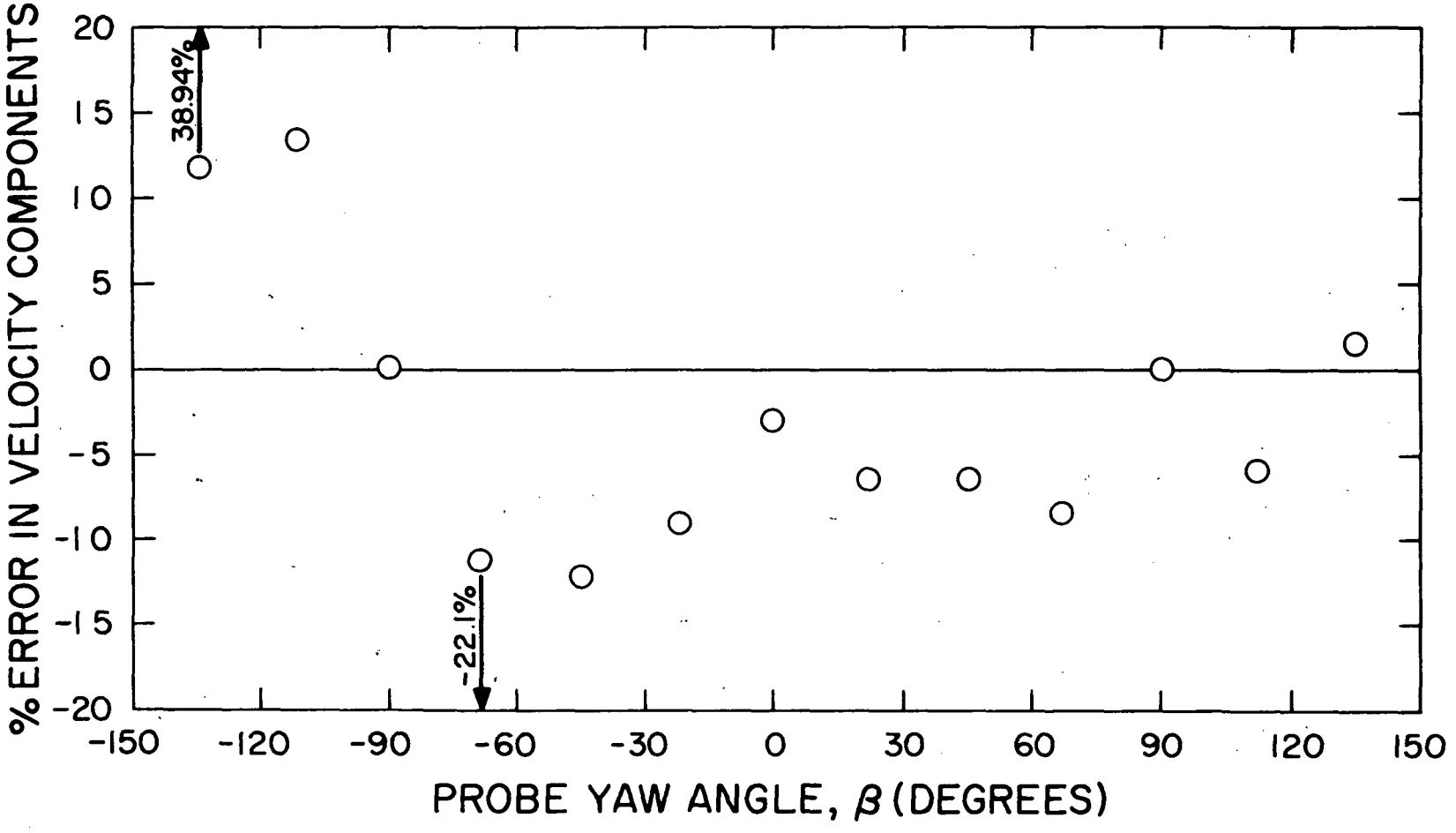

Figure 46: Percent Error in Velocity Component, U_A for ϕ-Method $U \simeq 30$fps, $\alpha=0°$. Probe #1192.

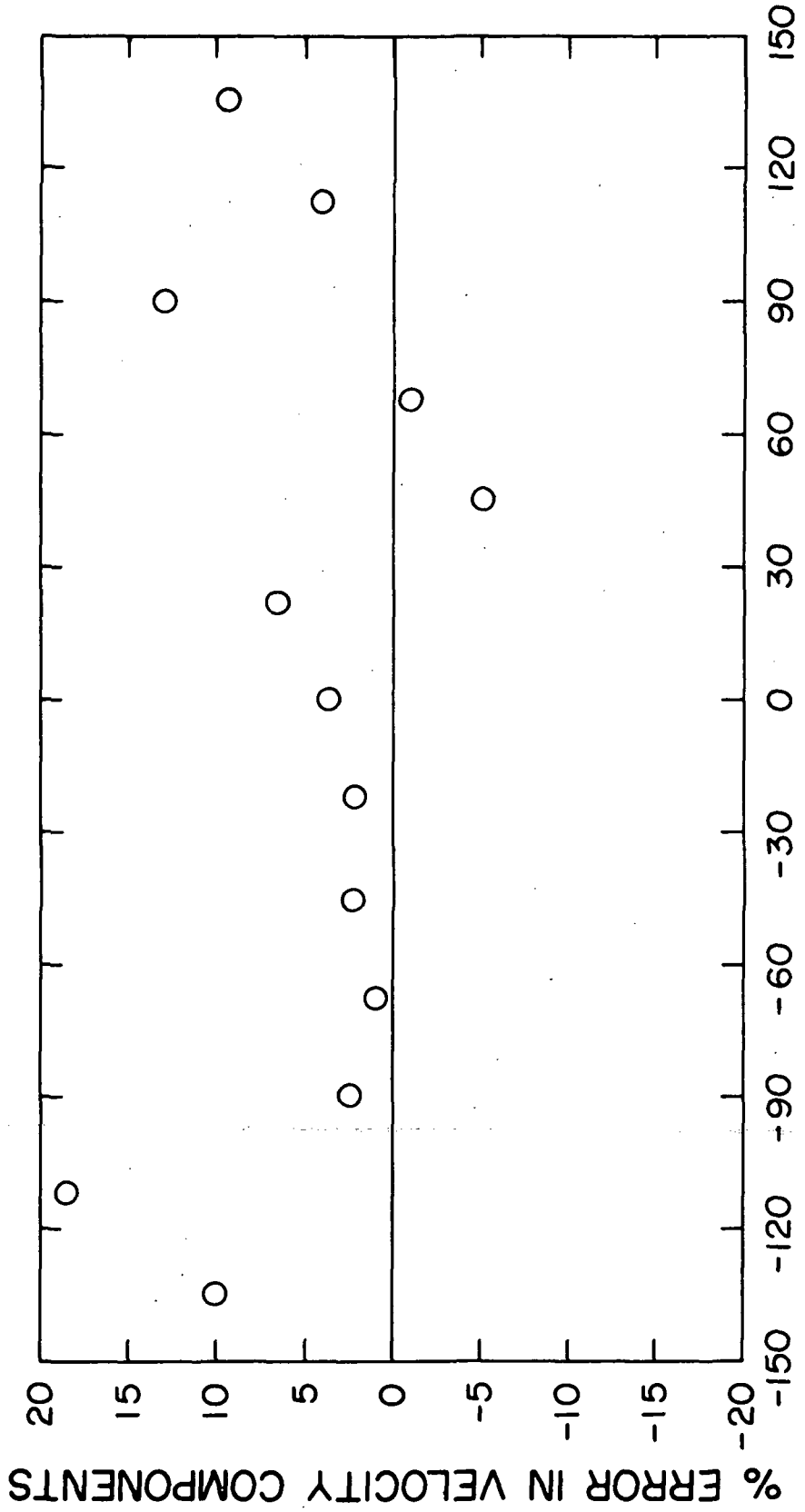

Figure 47: Percent Error in Velocity Component, U_B for ϕ-Method $U \simeq 30$fps, α=0°. Probe #1192.

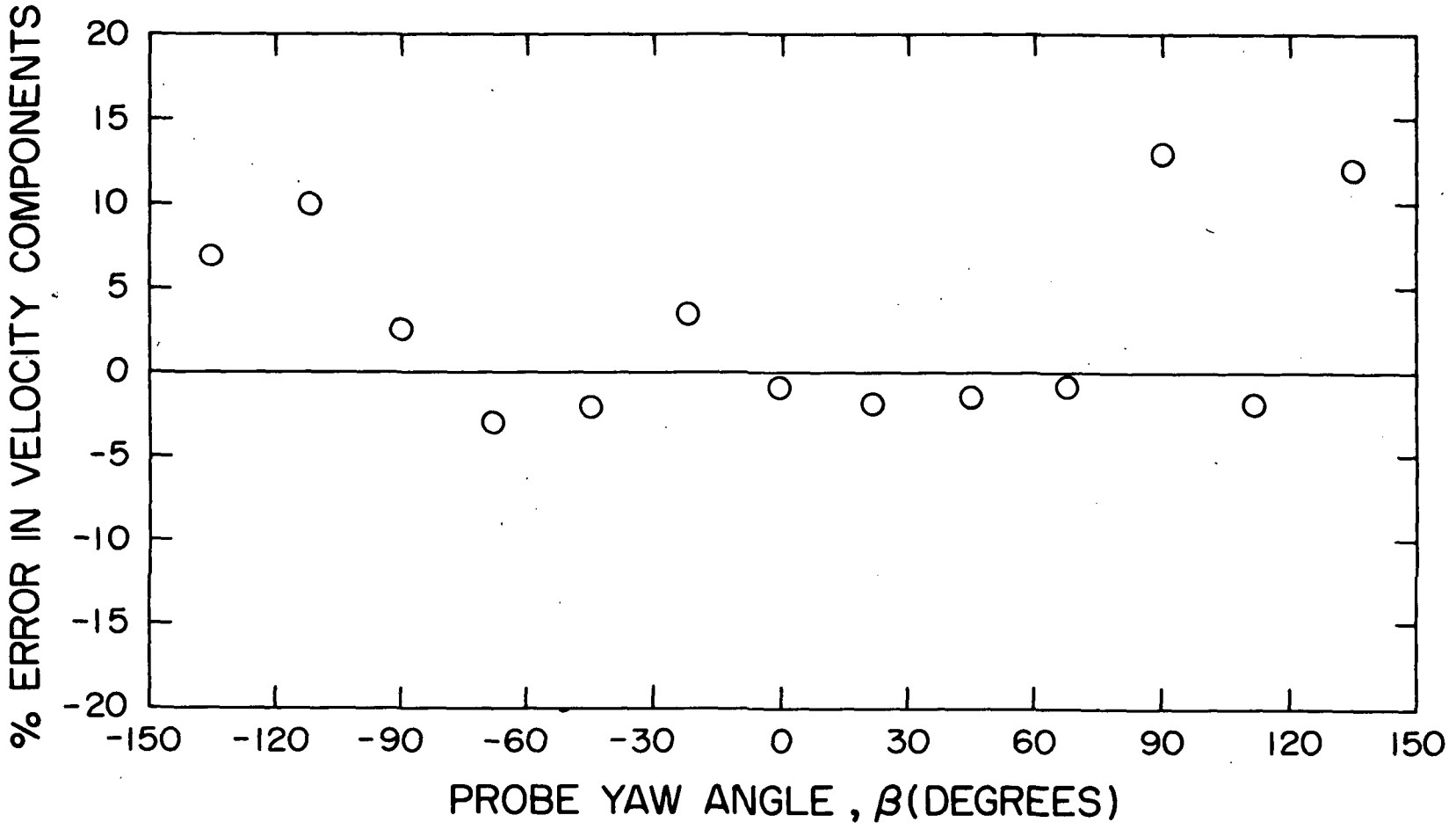

Figure 48: Percent Error in Velocity Component, U_C for ϕ-Method U $\simeq$ 30fps, α=0°. Probe #1192.

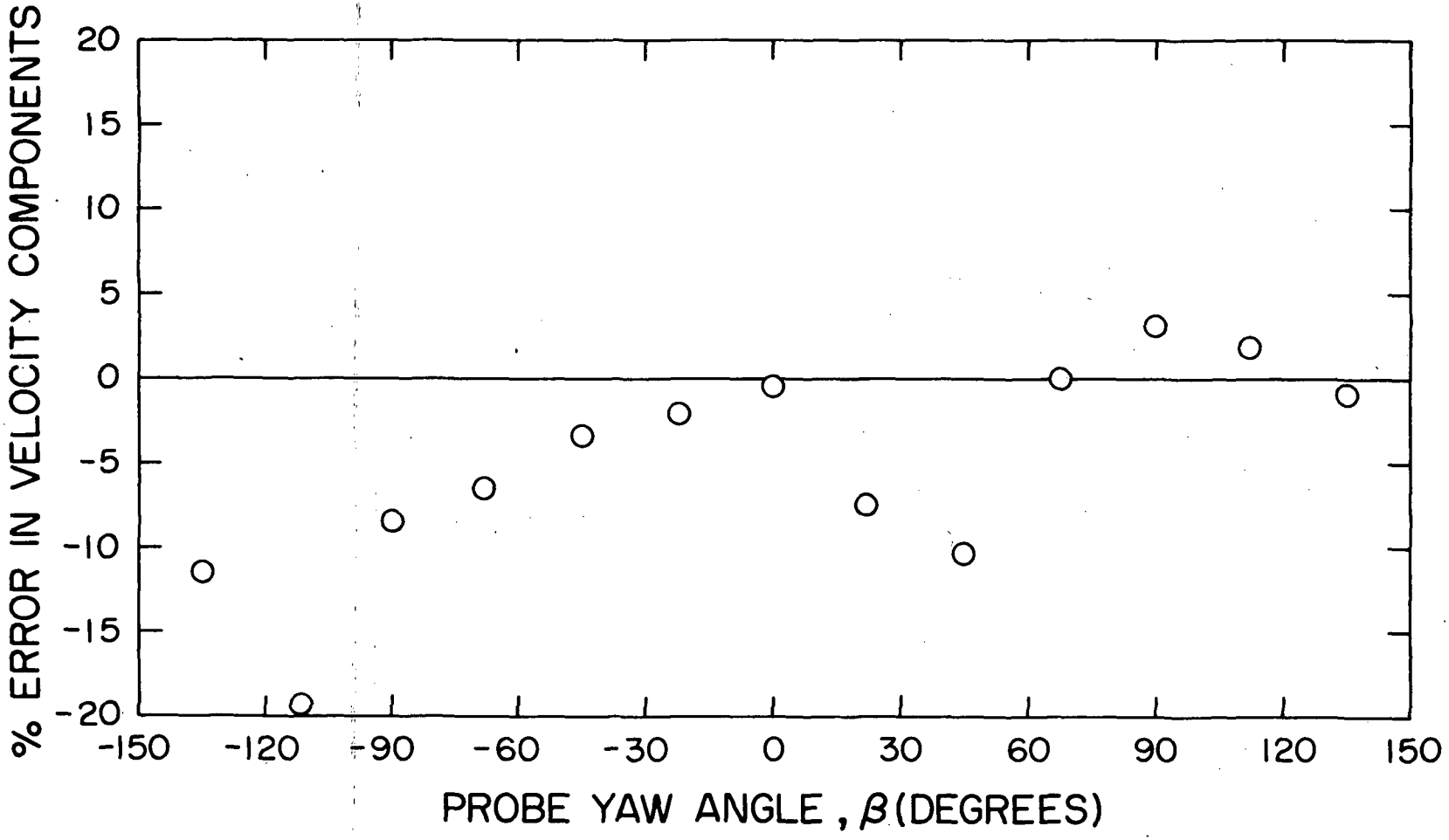

Figure 49: Percent Error in Velocity Component, U_A for the θ-Method $U \simeq 30$fps, $\alpha=0°$. Probe #1192.

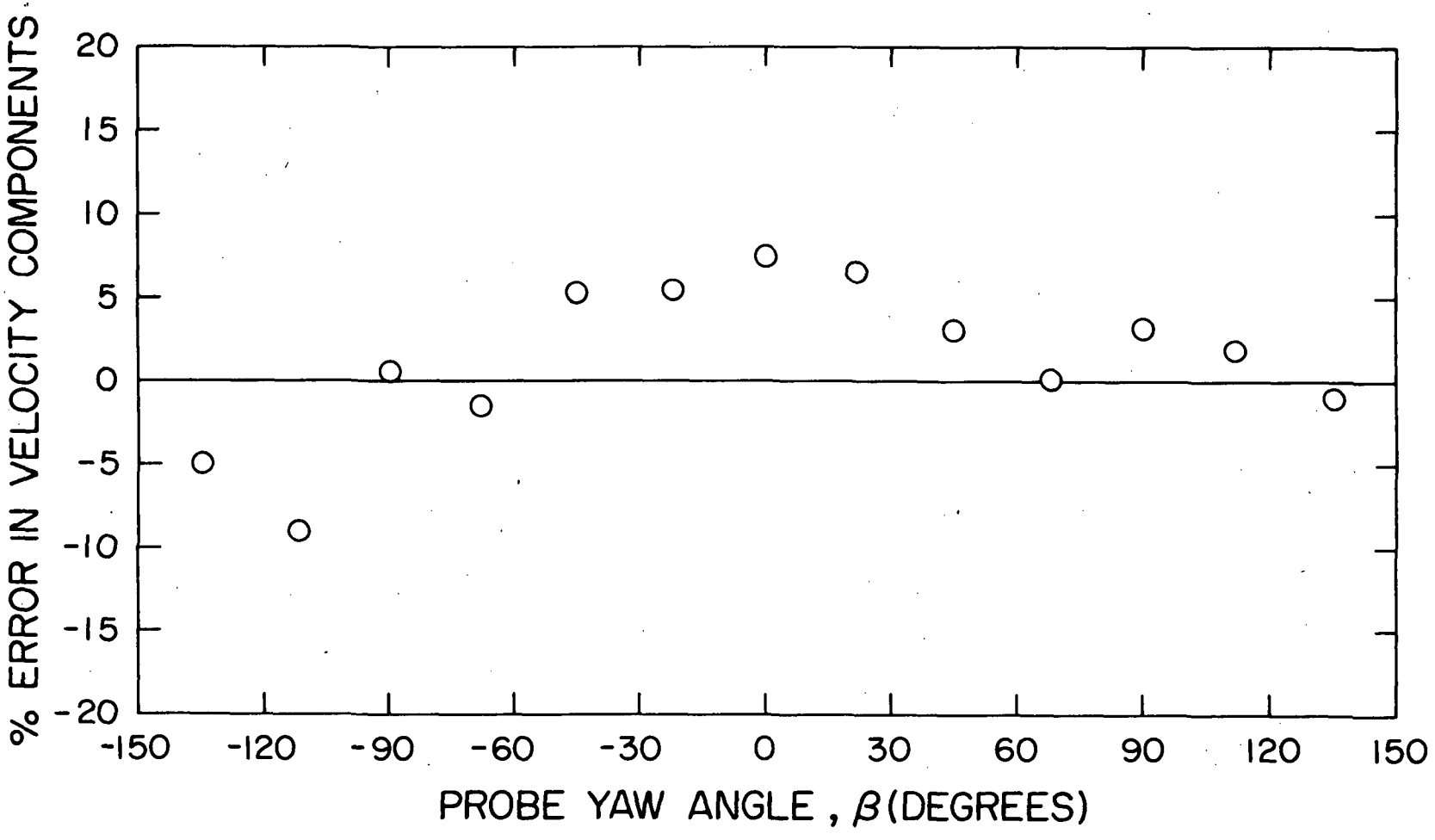

Figure 50: Percent Error in Velocity Component, U_B for the θ-Method $U \simeq 30$fps, $\alpha=0°$. Probe #1192.

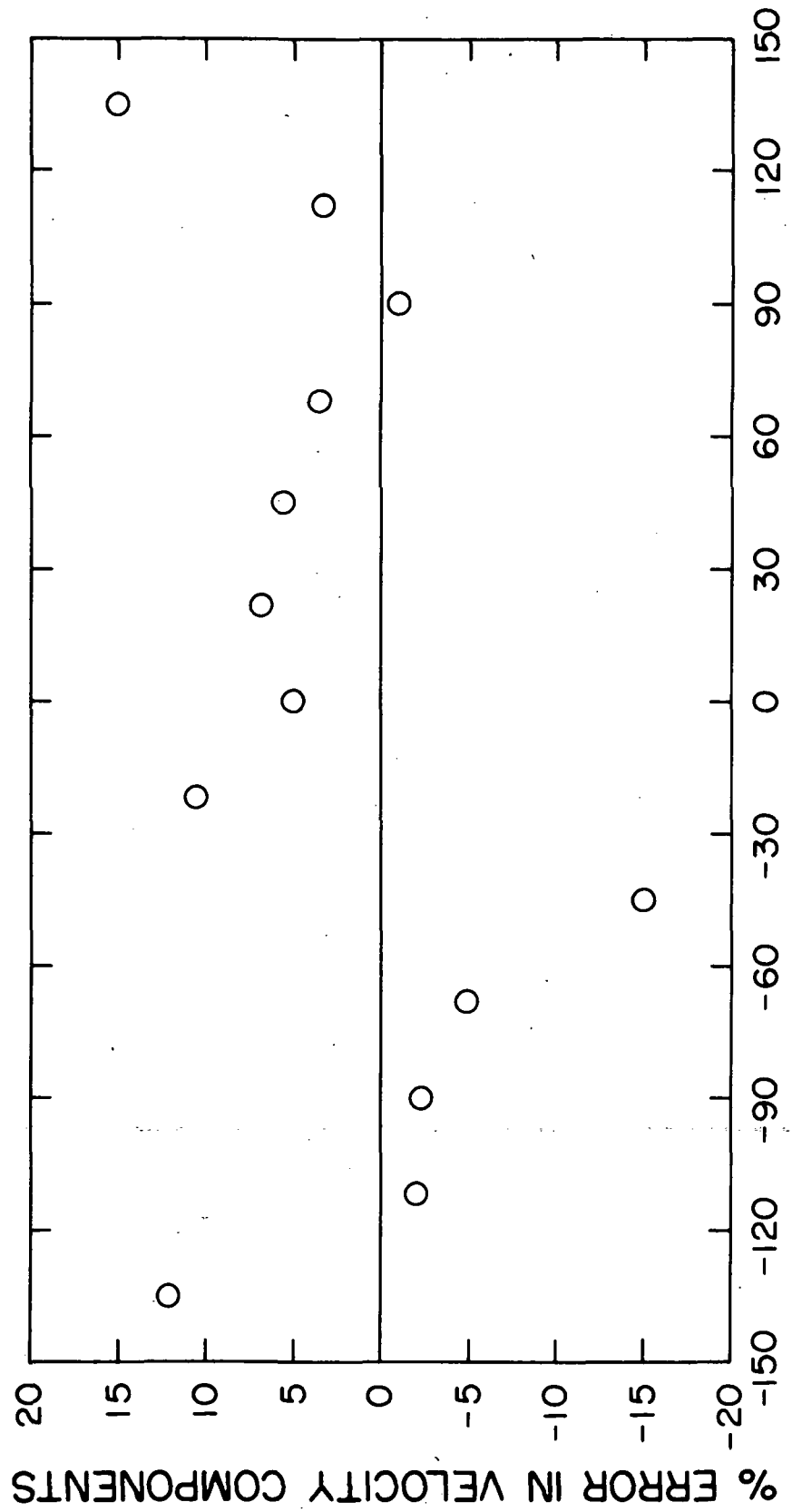

Figure 51: Percent Error in Velocity Component, U_C for the θ-Method $U \simeq 30$fps, $\alpha=0°$. Probe #1192.

TABLE I--CONSTANTS FOR EQUATION (2-1)

from Collis and Williams (3)

	n	A	B
$0.02 < R < 44$	0.45	0.24	0.56
$44 < R < 140$	0.51	0	0.48

TABLE II--RESULTS OF GRID TURBULENCE

MEASUREMENTS. T.S.I. #1192.

$U_{p.s.}$	α	β	β calc	$\left(\frac{u_x^2}{U^2}\right)^{1/2}$, % DISA	$\left(\frac{u_x^2}{U^2}\right)^{1/2}$, % T.S.I.
33.19	0	0	+ 2.96	12.0	10.8
32.82	0	+15	+16.25	12.0	10.9
33.33	0	+30	+31.01	12.0	10.5
33.55	0	+45	+47.74	12.0	9.56
33.54	0	+60	+61.15	12.0	9.83
33.90	0	-15	- 6.79	12.0	10.03
32.26	0	-30	-21.54	12.0	10.31
32.84	0	-45	-45.54	12.0	9.23
32.84	0	-45	-48.33	12.0	9.39
32.85	0	-60	-64.07	12.0	9.33

APPENDIX

Listing of Fortran Programs used to calculate velocity components.

I ϕ-method for #1192 and #1193

II θ-method for #1192

III θ-method for #1193

```
C  THIS PROGRAM WAS WRITTEN TO REDUCE DATA TAKEN MANUALLY
C  FROM THE TSI MODEL 1080 D ANEMOMETER SYSTEM. AN APRIL 24,
C  1972 REVISION
       DIMENSION HT(3),UES(3),PHI(4),ALPH(3),BETA(3),PHIP(4),
      1E(2,3),TA(3),AK(2,3),R(3),TEC(3),UAP(4),EIP(3,3),
      2,APRO(3),X(3),Y(3),PHID(3),PHIPD(3),GAMMA(3),AKAP(3),
      3C(3),D(3),CF(2,3),DELT(3),URAT(3),XXX(3),X51(3),VI(3),
      4VIII(3),IV11(7),E10(6),V11(7),V10(7)
       DIMENSION UA(3),EI(3,3),V(3),A(3),B(3),VII(3)
       DIMENSION UUC(3),PCTER(3)
       KKKK=1
       MMM=116
  109  READ(5,110)AL,BE,P,TROOM,DELH
  110  FORMAT(F6.2,F6.1,F7.2,F5.1,F7.4)
       BET=(BE*3.14159)/180.
       ALP=(AL*3.14159)/180.
       CALL ANGLE(ALP,BET,X51,XXX)
       READ(5,1) V11
    1  FORMAT(7F6.1)
       DO 998 III=1,7
  998  V10(III)=V11(III)*0.004882
       TE=V10(1)*40.
       WRITE(6,2)KKKK,AL,BE,TE
    2  FORMAT(/////,2X,'RUN NO.',I3,5X,'ALPHA=',F8.3,5X,'BETA
      1=',F8.3,5X,'AMB. TEMP=',F8.3,1X,'DEG. F')
       DO 999 I=2,7
  999  E10(I-1)=(V10(I)*2.)+3.
       E(1,1)=E10(1)
       E(2,1)=E10(2)
       E(1,2)=E10(3)
       E(2,2)=E10(4)
       E(1,3)=E10(5)
       E(2,3)=E10(6)
       WRITE(6,997)(E10(I),I=1,6)
  997  FORMAT(5X,'THE E ARE',6(3X,F7.3))
C   CONSTANTS ARE NOW READ IN FOR THE PROBE BEING USED.
C       HERE ARE THE 1192 CONSTANTS
       DELT(1)=468.
       DELT(2)=448.
       DELT(3)=408.
       R(1)=0.95627
       R(2)=1.00393
       R(3)=0.93912
       AK(1,1)=2.1308
       AK(2,1)=1.9484
       AK(1,2)=2.0298
       AK(2,2)=2.0458
       AK(1,3)=1.9573
       AK(2,3)=1.7262
C  CALCULATION OF CORRECTION FACTORS.
```

```
C CALCULATION OF Q/DELTA T'S.
      A1=59.4+(7.230-(7.230*(1.+(0.00377*(TROOM-74.)))))
      B1=A1-(39.6/(1.+(0.001067*(74.-TE))))
      CF(1,1)=(A1/59.4)*(19.8/B1)
      C1=70.4+(7.170-(7.170*(1.+(0.00377*(TROOM-74.)))))
      D1=C1-(46.9/(1.+(0.001067*(74.-TE))))
      CF(2,1)=(C1/70.4)*(23.5/D1)
      A(2)=62.4+(7.150-(7.150*(1.+(.00377*(TROOM-74.)))))
      B(2)=A(2)-(41.6/(1.+(.001067*(74.-TE))))
      C(2)=62.4+(7.180-(7.180*(1.+(.00377*(TROOM-74.)))))
      D(2)=C(2)-(41.6/(1.+(.001067*(74.-TE))))
      CF(1,2)=(A(2)/62.4)*(20.8/B(2))
      CF(2,2)=(C(2)/62.4)*(20.8/D(2))
      A(3)=71.2+(7.230-(7.230*(1.+(.00377*(TROOM-74.)))))
      B(3)=A(3)-(47.7/(1.+(.001067*(74.-TE))))
      C(3)=62.3+(7.080-(7.080*(1.+(.00377*(TROOM-74.)))))
      D(3)=C(3)-(41.7/(1.+(.001067*(74.-TE))))
      CF(1,3)=(A(3)/71.2)*(23.5/B(3))
      CF(2,3)=(C(3)/62.3)*(20.6/D(3))
      WRITE(6,1999) ((CF(I,J),I=1,2),J=1,3)
 1999 FORMAT(10X,'CF(I,J)=',6F10.5)
      DO 310 I=1,3
  310 R(I)=R(I)*(SQRT(CF(2,I)/CF(1,I)))
      DO 10 I=1,3
     1CF(2,I)*AK(2,I)))/DELT(I)
      HT(I)=(((E(1,I)**2)*CF(1,I)*AK(1,I))+((E(2,I)**2)*
      IF(HT(I)-0.530)3,4,4
    3 BA=0.1567
      GO TO 7
    4 BA=0.1271
    7 IF(BA-0.130)5,6,6
    5 AN=1./0.4425
      GO TO 8
    6 AN=1./0.3767
C CALCULATION OF EFFECTIVE COOLING VELOCITIES.
    8 UES(I)=(HT(I)/BA)**AN
   10 CONTINUE
      UPS1=DELH*(TE+460.)/P
      UPS=48.32098*(P/(TE+460.))*SQRT(UPS1)
      DO 120 I=1,3
  120 URAT(I)=UES(I)/UPS
      AKA=0.2
C CALCULATION OF STANDARDIZED VELOCITY.
   13 UT=(((UES(1)**2)+(UES(2)**2)+(UES(3)**2))/(2.040))
      US=SQRT(UT)
C CALCULATION OF ANGLES.
   14 DO 20 K=1,3
      Y(K)=((1.-(UES(K)**2)/(US**2))/(1.-AKA**2))
      IF(Y(K).LT.0.0000000)Y(K)=0.0
      PHI(K)=ARSIN(SQRT(Y(K)))
```

```
   20 CONTINUE
C  CALCULATION OF SIGNS OF ANGLES.
      IF((E(1,3)-(R(3)*E(2,3))).LT.0.0)PHI(1)=0.0-PHI(1)
      IF((E(1,1)-(R(1)*E(2,1))).LT.0.0)PHI(2)=0.0-PHI(2)
      IF((E(1,2)-(R(2)*E(2,2))).LT.0.0)PHI(3)=0.0-PHI(3)
C  NOW WE START THE IMPROVED ACCURACY ANALYSIS.
      DO 73 I=1,3
   73 PHID(I)=PHI(I)*180./3.14159
C  CALCULATION OF CONSTANTS.
      DO 70 I=1,3
      IF(PHID(I))59,61,61
   61 GAMMA(I)=0.0
      IF(US.LT.75.)GO TO 62
      AKAP(I)=0.2
      BETA(I)=30.0
      GO TO 69
   62 IF(US.LT.40.)GO TO 63
      AKAP(I)=0.36-(0.0021*US)
      BETA(I)=-18.7+(0.6493*US)
      GO TO 69
   63 IF(US.LT.25.)GO TO 64
      AKAP(I)=0.36-(0.0021*US)
      BETA(I)=21.068-(0.3448*US)
      GO TO 69
   64 IF(US.LT.20.)GO TO 65
      AKAP(I)=0.045+(0.0105*US)
      BETA(I)=-6.285+(0.7347*US)
      GO TO 69
   65 IF(US.LT.8.6)GO TO 66
      AKAP(I)=0.39-(0.0064*US)
      BETA(I)=-6.285+(0.7347*US)
      GO TO 69
   66 AKAP(I)=0.39-(0.0064*US)
      BETA(I)=0.0
   69 ALPH(I)=1.+(BETA(I)*((COS(PHI(I)))**3)*((SIN(PHI(I)))
     1**2))
      GO TO 70
   59 IF(US.LE.70.)GO TO 90
      AKAP(I)=0.175
      BETA(I)=5.+(0.033*US)
      IF(ABS(PHI(I)).LT.1.22173)GO TO 91
      GAMMA(I)=((TAN(ABS(PHI(I))-1.22173))**2)
      GO TO 89
   91 GAMMA(I)=0.0
      GO TO 89
   90 IF(US.LE.30.)GO TO 93
      AKAP(I)=0.2
      BETA(I)=5.+(0.033*US)
      IF(ABS(PHI(I)).LT.1.22173)GO TO 92
      GAMMA(I)=((TAN(ABS(PHI(I))-1.04720))**2)*0.375
```

```
      GO TO 89
   92 GAMMA(I)=0.0
      GO TO 89
   93 IF(US.LE.23.)GO TO 95
      AKAP(I)=0.2
      BETA(I)=-12.+(0.6*US)
      IF(ABS(PHI(I)).LT.1.22173)GO TO 94
      GAMMA(I)=((TAN(ABS(PHI(I))-1.04720))**2)*0.375
      GO TO 89
   94 GAMMA(I)=0.0
      GO TO 89
   95 AKAP(I)=0.25
      BETA(I)=0.0
      GAMMA(I)=0.0
   89 ALPH(I)=1.+(BETA(I)*((COS(PHI(I)))**2))
   70 CONTINUE
C  CALCULATION OF IMPROVED ACCURACY VELOCITY.
      UST=((UES(1)**2)+(UES(2)**2)+(UES(3)**2))/(2.+
     1(((AKAP(1)**2)*ALPH(1)*((SIN(PHI(1)))**2))+((AKAP(2)
     2**2)*ALPH(2)*((SIN(PHI(2)))**2))+((AKAP(3)**2)*ALPH(3)
     3*((SIN(PHI(3)))**2)))+GAMMA(1)+GAMMA(2)+GAMMA(3))
      USP=SQRT(UST)
      PS=29.92
      TS=530.
      T=TE+460.
      AP=(P*2.0884*12.)/(62.4*13.55)
C  CALCULATION OF TRUE VELOCITY.
      U=USP*(PS/AP)*(T/TS)
      U10=US*(PS/AP)*(T/TS)
      UP1=DELH*(TE+460.)/P
      UP=92.448819*SQRT(UP1)
      WRITE(6,45)US,USP,U,UP,UPS
   45 FORMAT(2X,'TSI STD. VEL.=',F9.4,5X,'IMPROVED STD. VEL.
     1=',F9.4,5X,'ACTUAL TSI VEL.=',F9.4/2X,'P-S TUBE ACTUAL
     2VEL.=',F9.4,5X,'STD. P-S TUBE VEL.=',F9.4)
C  IMPROVED ACCURACY ANGLES.
      DO 50 N=1,3,1
      X(N)=(1.-(UES(N)**2/(USP**2)))/(1.-ALPH(N)*(AKAP(N)**2
      IF(X(N).LT.0.0000000)X(N)=0.0
      IF (X(N) .GT. 1.000000) X(N)=1.0
      PHIP(N)=ARSIN(SQRT(X(N)))
   50 CONTINUE
      SUM=((SIN(PHIP(1)))**2)+((SIN(PHIP(2)))**2)+((SIN(
     1PHIP(3)))**2)
      WRITE(6,97)SUM,R(1),R(2),R(3)
   97 FORMAT(5X,4HSUM:,F8.5,5X,4HR'S:,1X,F8.5,5XF8.5,5X,
     1F8.5)
      WRITE(6,98)BETA(1),BETA(2),BETA(3),GAMMA(1),GAMMA(2),
     1GAMMA(3)
   98 FORMAT(5X,6HBETAS:,1X,F8.4,5X,F8.4,5X,F8.4,1X,
```

```
     17HGAMMAS:,1X,F8.5,5X,F8.5,5X,F8.5)
      WRITE(6,99)AKAP(1),AKAP(2),AKAP(3)
   99 FORMAT(5X,4HK'S:,1X,F8.5,5X,F8.5,5X,F8.5)
      IF((E(1,3)-(R(3)*E(2,3))).LT.0.0)PHIP(1)=0.0-PHIP(1)
      IF((E(1,1)-(R(1)*E(2,1))).LT.0.0)PHIP(2)=0.0-PHIP(2)
      IF((E(1,2)-(R(2)*E(2,2))).LT.0.0)PHIP(3)=0.0-PHIP(3)
      DO 51 I=1,3
   51 PHIPD(I)=PHIP(I)*180./3.14159
      DO 140 N=1,3,1
      UAP(N)=U*SIN(PHIP(N))
  140 CONTINUE
      DO 141 J=1,3
  141 UUC(J)=UP*SIN(X51(J))
      DO 142 I=1,3
  142 PCTER(I)=100.0*(UAP(I)-UUC(I))/UP
      WRITE(6,909)
  909 FORMAT(/7X,'Q/DT',8X,'UES',8X,'PHI(EXP)',5X,'PHI
     1(IST)',3X,'PHI(IMP)',5X,'VEL(ACT)',4X,'VEL(EXP)',
     24X,'PCTER')
      DO 200 I=1,3
  200 WRITE(6,201)HT(I),UES(I),XXX(I),PHID(I),PHIPD(I),
     1UAP(I),UUC(I),PCTER(I)
  201 FORMAT(/,4X,F9.6,7(3X,F9.4))
      KKKK=KKKK+1
      IF(KKKK.LE.MMM)GO TO 109
      STOP
      END
      SUBROUTINE ANGLE(ALP,BET,X51,XXX)
C     ALP AND BET ARE THE ANGLES OF ATTACK OF THE PROBE IN
C     RADIANS.THE X51'S ARE THE CALCULATED PHI'S IN RADIANS,
C     AND THE XXX'S ARE THE CALCULATED PHI'S IN DEGREES
      DIMENSION X51(3),XXX(3)
      XX=(0.57735*COS(ALP)*COS(BET))+(0.81650*COS(BET)*
     1SIN(ALP))
      YY=(0.57735*COS(BET)*COS(ALP))-(0.70711*SIN(BET))-
     1(0.40824*COS(BET)*SIN(ALP))
      ZZ=(0.57735*COS(BET)*COS(ALP))+(0.70711*SIN(BET))-
     1(0.40824*COS(BET)*SIN(ALP))
      IF (XX .GT. 1.000000) XX=1.0
      X51(1)=ARSIN(XX)
      IF (YY .GT. 1.000000) YY=1.0
      X51(2)=ARSIN(YY)
      IF (ZZ .GT. 1.000000) ZZ=1.0
      X51(3)=ARSIN(ZZ)
      XXX(1)=X51(1)*180./3.1415927
      XXX(2)=X51(2)*180./3.1415927
      XXX(3)=X51(3)*180./3.1415927
      RETURN
      END
```

```
C THIS PROGRAM WAS WRITTEN TO REDUCE DATA TAKEN BY THE TSI
C MODEL 1080-D TOTAL-VECTOR ANEMOMETER SYSTEM. IN THIS
C PROGRAM, NEW K'S HAVE BEEN USED AND THE PHI'S HAVE BEEN
C CALCULATED FROM THE THETA'S. THIS IS JULY 8,1972 REVISION.
      COMMON/SPLINE/AS(3,3),BS(3,3),CS(3,3)
      DIMENSION IV11(7),V11(7),V10(7),E10(6),DELT(3),R(3),
     1CF(2,3),E(2,3),QA(3),QB(3),HT(3),UES(3),RAT(3),R90(3),
     2THETA(3),THTR(3),PHI1(3),PHI2(3),PHIR1(3),PHIR2(3),
     3UCOMP(3),X(4),Y(3,4),XXX(3),X51(3),U1(3)
      DIMENSION PCTER(3),AK(2,3),QR(3),PHIR(3),PHI(3)
      MMM=116
      DO 101 I=1,3
      DO 101 J=1,3
  101 READ(5,103) AS(I,J),BS(I,J),CS(I,J)
  103 FORMAT(3E14.7)
      DO 100 KK=1,MMM
      READ(5,2) AL,BE,P,TROOM,DELH
    2 FORMAT(F6.2,F6.1,F7.2,F5.1,F7.4)
      BET=(BE*3.1415927)/180.
      ALP=(AL*3.1415927)/180.
C CALL 'ANGLE' TO OBTAIN PHI(CALC) FOR EACH SENSOR.
      CALL ANGLE(ALP,BET,X51,XXX)
C READ DECIMAL VALUES OF 0-5V OUTPUT VOLTAGES.
      READ(5,3)V11
    3 FORMAT(7F6.1)
      DO 4 II=1,7
    4 V10(II)=V11(II)*0.4882E-02
      TE=V10(1)*40.
      WRITE(6,5)KK,AL,BE,TE
    5 FORMAT(///2X,'RUN NO.',1X,I3,5X,'ALPHA=',F8.3,5X,'BETA
     1=',F8.3,5X,'AMB. TEMP=',F8.3,1X,'DEG.F')
      DO 6 I=2,7
    6 E10(I-1)=(V10(I)*2.)+3.
      E(1,1)=E10(1)
      E(2,1)=E10(2)
      E(1,2)=E10(3)
      E(2,2)=E10(4)
      E(1,3)=E10(5)
      E(2,3)=E10(6)
C #1192 CONSTANTS.
      DELT(1)=468.
      DELT(2)=448.
      DELT(3)=408.
      R(1)=0.95627
      R(2)=1.00393
      R(3)=0.93912
      AK(1,1)=2.174
      AK(2,1)=1.988
      AK(1,2)=2.030
      AK(2,2)=2.046
```

```
      AK(1,3)=1.982
      AK(2,3)=1.748
C CALCULATION OF CORRECTION FACTORS(CF).
      A1=  65.8+(7.136-(7.136*(1.+(0.00377*(TROOM-73.)))))
      B1=  A1  -(43.84/(1.+(0.001068*(73.-TE))))
      C1=  63.0+(7.086-(7.086*(1.+(0.00377*(TROOM-73.)))))
      D1=  C1  -(41.98/(1.+(0.001068*(73.-TE))))
      CF(1,1)=(A1  /65.8)*(21.96/B1)
      CF(2,1)=(C1  /63.0)*(21.02/D1)
      A2=  71.3+(7.056-(7.056*(1.+(0.00377*(TROOM-73.)))))
      B2=  A2  -(47.52/(1.+(0.001116*(73.-TE))))
      C2=  70.7+(7.046-(7.046*(1.+(0.00377*(TROOM-73.)))))
      D2=  C2  -(47.12/(1.+(0.001116*(73.-TE))))
      CF(1,2)=(A2  /71.3)*(23.78/B2)
      CF(2,2)=(C2  /70.7)*(23.58/D2)
      A3=  62.2+(7.116-(7.116*(1.+(0.00377*(TROOM-73.)))))
      B3=  A3  -(41.48/(1.+(0.001225*(73.-TE))))
      C3=  60.9+(6.977-(6.977*(1.+(0.00377*(TROOM-73.)))))
      D3=  C3  -(40.62/(1.+(0.001225*(73.-TE))))
      CF(1,3)=(A3  /62.2)*(20.72/B3)
      CF(2,3)=(C3  /60.9)*(20.28/D3)
      DO 8 I=1,3
    8 R(I)=R(I)*SQRT(CF(2,I)/CF(1,I))
C CALCULATION OF HEAT TRANSFERS(HT).
      DO 9 I=1,3
      QA(I)=(E(1,I)**2)*CF(1,I)*AK(1,I)
      QB(I)=(E(2,I)**2)*CF(2,I)*AK(2,I)
      HT(I)=(QA(I)+QB(I))/DELT(I)
C CALCULATION OF EFFECTIVE COOLING VELOCITIES (UES).
      IF(HT(I)-0.524)10,11,11
   10 BA=0.1547
      GO TO 12
   11 BA=0.12715
   12 IF(BA-0.130)13,14,14
   13 AN=1./0.44
      GO TO 15
   14 AN=1./0.3792
   15 UES(I)=(HT(I)/BA)**AN
    9 CONTINUE
C STANDARD VELOCITIES CALCULATION: UPS=PITOT-STATIC;US=TSI
      UPS1=DELH*(TE+460.)/P
      UPS=48.32098*(P/(TE+460.))*SQRT(UPS1)
      UT=((UES(1)**2)+(UES(2)**2)+(UES(3)**2))/2.04
      US=SQRT(UT)
      PS=1013.60
      TS=530.
      T=TE+460.
C NON-STANDARD VELOCITY CALCULATION: UP=PITOT-STATIC;UNS=TSI
      UNS=US*(PS/P)*(T/TS)
      UP1=DELH*(TE+460.)/P
```

```
      UP=92.448819*SQRT(UP1)
C CALCULATION OF QD/QU.
      DO 16 I=1,3
      IF(QA(I)-QB(I))17,17,18
   17 RAT(I)=QA(I)/QB(I)
      GO TO 16
   18 RAT(I)=QB(I)/QA(I)
   16 CONTINUE
      X(1)=10.
      X(2)=20.
      X(3)=30.
      X(4)=40.
C CALCULATION OF QD/QU AT THETA=90.
      DO 109 K=1,3
      IF(UES(K)-40.)107,108,108
  108 IF(K.EQ.1)R90(K)=0.4347-(0.000427*UES(K))
      IF(K.EQ.2)R90(K)=0.4192-(0.000444*UES(K))
      IF(K.EQ.3)R90(K)=0.3931-(0.000440*UES(K))
      GO TO 109
  107 IF(UES(K)-10.)110,111,111
  110 IF(K.EQ.1)R90(K)=1.-(0.0465*UES(K))
      IF(K.EQ.2)R90(K)=1.-(0.04665*UES(K))
      IF(K.EQ.3)R90(K)=1.-(0.0496*UES(K))
      GO TO 109
  111 CALL SPLIN2(K,X,Y,UES,R90)
  109 CONTINUE
      DO 19 I=1,3
C CALCULATION OF Q2/Q1.
      QR(I)=(RAT(I)-R90(I))/(1.-R90(I))
      IF(QR(I).LT.0.0)QR(I)=0.0
C CALCULATION OF THETA FOR EACH SENSOR.
      IF(I.NE.1)GO TO 20
      THETA(I)=(1.-SQRT(QR(I)))*90.
      IF(E(1,I)-R(I)*E(2,I))21,22,23
   21 THETA(I)=-THETA(I)
      GO TO 19
   22 THETA(I)=0.0
      GO TO 19
   23 IF(E(1,2)-R(2)*E(2,2))24,25,26
   24 THETA(I)=180.-THETA(I)
      GO TO 19
   25 THETA(I)=THETA(I)
      GO TO 19
   26 THETA(I)=THETA(I)
      GO TO 19
   20 IF(I.NE.2)GO TO 27
      THETA(I)=(1.-SQRT(QR(I)))*90.
      IF(E(1,I)-R(I)*E(2,I))28,29,19
   28 THETA(I)=-THETA(I)
      GO TO 19
```

```
   29 THETA(I)=0.0
      GO TO 19
   27 IF(E(1,I)-R(I)*E(2,I))200,201,201
  200 THETA(I)=-((1.-SQRT(QR(I)))*90.)
      GO TO 19
  201 IF(E(1,1)-R(1)*E(2,1))30,31,32
   30 THETA(I)=180.-((1.-SQRT(QR(I)/0.7919))*90.)
      GO TO 19
   31 THETA(I)=90.
      GO TO 19
   32 THETA(I)=(1.-SQRT(QR(I)))*90.
   19 CONTINUE
      DO 33 I=1,3
   33 THTR(I)=THETA(I)*3.1415927/180.
C START CALCULATION OF PHI FOR EACH SENSOR.
      SBC=1.-(((SIN(THTR(2)))**2)*((COS(THTR(3)))**2))
      SAB=1.-(((SIN(THTR(1)))**2)*((COS(THTR(2)))**2))
      SCA=1.-(((SIN(THTR(3)))**2)*((COS(THTR(1)))**2))
      PHI1(1)=(SIN(THTR(1))*SIN(THTR(3)))/SQRT(SCA)
      PHI2(1)=(COS(THTR(2))*COS(THTR(1)))/SQRT(SAB)
      PHI1(2)=(SIN(THTR(1))*SIN(THTR(2)))/SQRT(SAB)
      PHI2(2)=(COS(THTR(3))*COS(THTR(2)))/SQRT(SBC)
      PHI1(3)=(SIN(THTR(2))*SIN(THTR(3)))/SQRT(SBC)
      PHI2(3)=(COS(THTR(1))*COS(THTR(3)))/SQRT(SCA)
      DO 34 I=1,3
      IF (ABS(PHI1(I)) .GT. 1.000000) PHI1(I)=1.00000
      PHIR1(I)=ARSIN(PHI1(I))
      PHIR1(I)=ABS(PHIR1(I))
      IF (ABS(PHI2(I)) .GT. 1.000000) PHI2(I)=1.00000
      PHIR2(I)=ARSIN(PHI2(I))
      PHIR2(I)=ABS(PHIR2(I))
   34 CONTINUE
      IF(SCA-SAB)35,36,36
   35 PHIR(1)=PHIR2(1)
      GO TO 37
   36 PHIR(1)=PHIR1(1)
   37 IF(SAB-SBC)38,39,39
   38 PHIR(2)=PHIR2(2)
      GO TO 40
   39 PHIR(2)=PHIR1(2)
   40 IF(SBC-SCA)41,42,42
   41 PHIR(3)=PHIR2(3)
      GO TO 43
   42 PHIR(3)=PHIR1(3)
   43 IF(E(1,3).LT.(R(3)*E(2,3)))PHIR(1)=-PHIR(1)
      IF(E(1,1).LT.(R(1)*E(2,1)))PHIR(2)=-PHIR(2)
      IF(E(1,2).LT.(R(2)*E(2,2)))PHIR(3)=-PHIR(3)
C CALCULATION OF EXPECTED (U1) AND CALCULATED (UCOMP) PROBE
C -ORIENTED VELOCITIES.
      DO 44 I=1,3
```

```
      U1(I)=UP*SIN(X51(I))
      UCOMP(I)=UNS*SIN(PHIR(I))
   44 PHI(I)=PHIR(I)*180./3.1415927
      DO 142 I=1,3
  142 PCTER(I)=100.0*(UCOMP(I)-U1(I))/UP
      WRITE(6,45)E10
   45 FORMAT(5X,'E(I,J)',6(5X,F8.4))
      WRITE(6,46)CF
   46 FORMAT(5X,'CF(I,J)',6(5X,F8.4))
      WRITE(6,49)UP,UPS,UNS,US
   49 FORMAT(5X,'UP=',1X,F9.4,5X,'UPS=',1X,F9.4,5X,'UNS=',
     11X,F9.4,5X,'US=',1X,F9.4)
      WRITE(6,150)
  150 FORMAT(3X,'Q/DELTA T',6X,'UES',8X,'QD/QU',6X,'Q2/Q1',
     16X,'THETA',5X,'PHI(EXP)',3X,'PHI(CALC)',4X,'U(EXP)',
     29X,'U',3X,'PCTER')
      DO 50 I=1,3
   50 WRITE(6,47)HT(I),UES(I),RAT(I),QR(I),THETA(I),XXX(I),
     1PHI(I),U1(I),UCOMP(I),PCTER(I)
   47 FORMAT(3X,F8.5,3X,F10.5,3X,F8.5,3X,F8.5,3X,F9.4,3X,
     1F8.4,3X,F8.4,3X,F9.4,3X,F9.4.3X,F9.4)
  100 CONTINUE
      STOP
      END
      SUBROUTINE SPLIN2(N,X,Y,XARG,YARG)
C SUBROUTINE SPLIN2 CALCULATES THE VALUE OF QD/QU AT THETA=
C 90 FOR A SPECIFIC VALUE OF THE EFFECTIVE COOLING VELOCITY.
C ONE IS CALCULATED FOR EACH SENSOR. AS,BS, AND CS ARE THE
C COEFFICIENTS SPECIFIED BY AN EARLIER PROGRAM. N IS AN
C INDEX WHICH INDICATES WHICH VALUE OF QD/QU(I.E., WHICH
C SENSOR) TO USE. YARG(J) IS THE VALUE OF QD/QU AT THETA=90
C DESIRED.
      COMMON/SPLINE/AS(3,3),BS(3,3),CS(3,3)
      DIMENSION X(4),Y(3,4),XARG(3),YARG(3)
      Y(1,1)=0.535
      Y(1,2)=0.458
      Y(1,3)=0.429
      Y(1,4)=0.418
      Y(2,1)=0.5335
      Y(2,2)=0.4475
      Y(2,3)=0.4138
      Y(2,4)=0.4015
      Y(3,1)=0.504
      Y(3,2)=0.4185
      Y(3,3)=0.387
      Y(3,4)=0.376
      J=N
      DO 101 I=1,3
      IF(XARG(J)-X(I+1))102,101,101
  101 CONTINUE
```

```
  102 Q=(XARG(J)-X(I))/(X(I+1)-X(I))
      YARG(J)=Y(J,I)+AS(J,I)*Q+BS(J,I)*Q**2+CS(J,I)*Q**3
      RETURN
      END
      SUBROUTINE ANGLE(ALP,BET,X51,XXX)
C    ALP AND BET ARE THE ANGLES OF ATTACK OF THE PROBE IN
C RADIANS. THE X51'S ARE THE CALCULATED PHI'S IN RADIANS,
C AND THE XXX'S ARE THE CALCULATED PHI'S IN DEGREES.
      DIMENSION X51(3),XXX(3)
      XX=(0.57735*COS(ALP)*COS(BET))+(0.81650*COS(BET)*
     1SIN(ALP))
      YY=(0.57735*COS(BET)*COS(ALP))-(0.70711*SIN(BET))-
     1(0.40824*COS(BET)*SIN(ALP))
      ZZ=(0.57735*COS(BET)*COS(ALP))+(0.70711*SIN(BET))-
     1(0.40824*COS(BET)*SIN(ALP))
      X51(1)=ARSIN(XX)
      X51(2)=ARSIN(YY)
      X51(3)=ARSIN(ZZ)
      XXX(1)=X51(1)*180./3.1415927
      XXX(2)=X51(2)*180./3.1415927
      XXX(3)=X51(3)*180./3.1415927
      RETURN
      END
```

```
C THIS PROGRAM WAS WRITTEN TO REDUCE DATA TAKEN BY THE TSI
C MODEL 1080-D TOTAL-VECTOR ANEMOMETER SYSTEM. IN THIS
C PROGRAM, NEW K'S HAVE BEEN USED AND THE PHI'S HAVE BEEN
C CALCULATED FROM THE THETA'S. THIS IS JULY 8,1972 REVISION.
      COMMON/SPLINE/AS(3,3),BS(3,3),CS(3,3)
      DIMENSION IV11(7),V11(7),V10(7),E10(6),DELT(3),R(3),
     1CF(2,3),E(2,3),QA(3),QB(3),HT(3),UES(3),RAT(3),R90(3),
     2THETA(3),THTR(3),PHI1(3),PHI2(3),PHIR1(3),PHIR2(3),
     3UCOMP(3),X(4),Y(3,4),XXX(3),X51(3),U1(3)
      DIMENSION PCTER(3),AK(2,3),QR(3),PHIR(3),PHI(3)
      MMM=116
      DO 101 I=1,3
      DO 101 J=1,3
  101 READ(5,103) AS(I,J),BS(I,J),CS(I,J)
  103 FORMAT(3E14.7)
      DO 100 KK=1,MMM
      READ(5,2) AL,BE,P,TROOM,DELH
    2 FORMAT(F6.2,F6.1,F7.2,F5.1,F7.4)
      ALP=(AL*3.1415927)/180.
      BET=(BE*3.1415927)/180.
C CALL 'ANGLE' TO OBTAIN PHI(CALC) FOR EACH SENSOR.
      CALL ANGLE(ALP,BET,X51,XXX)
C READ DECIMAL VALUES OF 0-5V OUTPUT VOLTAGES.
      READ(5,3) (V11(I),I=1,7)
    3 FORMAT(7F6.1)
      DO 4 II=1,7
    4 V10(II)=V11(II)*0.4882E-02
      TE=V10(1)*30.
      WRITE(6,5)KK,AL,BE,TE
    5 FORMAT(///2X,'RUN NO.',1X,I3,5X,'ALPHA=',F8.3,5X,'BETA
     1=',F8.3,5X,'AMB. TEMP=',F8.3,1X,'DEG.F')
      DO 6 I=2,7
    6 E10(I-1)=(V10(I)*2.)+3.
      E(1,1)=E10(1)
      E(2,1)=E10(2)
      E(1,2)=E10(3)
      E(2,2)=E10(4)
      E(1,3)=E10(5)
      E(2,3)=E10(6)
C #1193 CONSTANTS.
      DELT(1)=470.
      DELT(2)=471.
      DELT(3)=459.
      R(1)=1.02941
      R(2)=1.04985
      R(3)=0.99658
      AK(1,1)=2.178
      AK(2,1)=2.308
      AK(1,2)=2.065
      AK(2,2)=2.276
```

```
      AK(1,3)=2.195
      AK(2,3)=2.180
C CALCULATION OF CORRECTION FACTORS(CF).
      A1=59.4+(7.230-(7.230*(1.+(0.00377*(TROOM-74.)))))
      B1=A1-(39.6/(1.+(0.001067*(74.-TE))))
      CF(1,1)=(A1/59.4)*(19.8/B1)
      C1=70.4+(7.170-(7.170*(1.+(0.00377*(TROOM-74.)))))
      D1=C1-(46.9/(1.+(0.001067*(74.-TE))))
      CF(2,1)=(C1/70.4)*(23.5/D1)
      A2=62.4+(7.150-(7.150*(1.+(0.00377*(TROOM-74.)))))
      B2=A2-(41.6/(1.+(0.001067*(74.-TE))))
      CF(1,2)=(A2/62.4)*(20.8/B2)
      C2=62.4+(7.180-(7.180*(1.+(0.00377*(TROOM-74.)))))
      D2=C2-(41.6/(1.+(0.001067*(74.-TE))))
      CF(2,2)=(C2/62.4)*(20.8/D2)
      A3=71.2+(7.230-(7.230*(1.+(0.00377*(TROOM-74.)))))
      B3=A3-(47.7/(1.+(0.001067*(74.-TE))))
      CF(1,3)=(A3/71.2)*(23.5/B3)
      C3=62.3+(7.080-(7.080*(1.+(0.00377*(TROOM-74.)))))
      D3=C3-(41.7/(1.+(0.001067*(74.-TE))))
      CF(2,3)=(C3/62.3)*(20.6/D3)
      WRITE(6,1999) ((CF(I,J),I=1,2),J=1,3)
 1999 FORMAT(10X,'CF(I,J)=',6F10.5)
      DO 8 I=1,3
    8 R(I)=R(I)*SQRT(CF(2,I)/CF(1,I))
C CALCULATION OF HEAT TRANSFERS(HT).
      DO 9 I=1,3
      QA(I)=(E(1,I)**2)*CF(1,I)*AK(1,I)
      QB(I)=(E(2,I)**2)*CF(2,I)*AK(2,I)
      HT(I)=(QA(I)+QB(I))/DELT(I)
C CALCULATION OF EFFECTIVE COOLING VELOCITIES (UES).
      IF(HT(I)-0.524)10,11,11
   10 BA=0.1547
      GO TO 12
   11 BA=0.12715
   12 IF(BA-0.130)13,14,14
   13 AN=1./0.44
      GO TO 15
   14 AN=1./0.3792
   15 UES(I)=(HT(I)/BA)**AN
    9 CONTINUE
C STANDARD VELOCITIES CALCULATION: UPS=PITOT-STATIC;US=TSI
      UPS1=DELH*(TE+460.)/P
      UPS=48.32098*(P/(TE+460.))*SQRT(UPS1)
      UT=((UES(1)**2)+(UES(2)**2)+(UES(3)**2))/2.04
      US=SQRT(UT)
      PS=1013.60
      TS=530.
      T=TE+460.
C NON-STANDARD VELOCITY CALCULATION: UP=PITOT-STATIC;UNS=TSI
```

```
      UNS=US*(PS/P)*(T/TS)
      UP1=DELH*(TE+460.)/P
      UP=92.448819*SQRT(UP1)
C CALCULATION OF QD/QU.
      DO 16 I=1,3
      IF(QA(I)-QB(I))17,17,18
   17 RAT(I)=QA(I)/QB(I)
      GO TO 16
   18 RAT(I)=QB(I)/QA(I)
   16 CONTINUE
      RAT(3)=QB(3)/QA(3)
      X(1)=10.
      X(2)=20.
      X(3)=30.
      X(4)=40.
C CALCULATION OF QD/QU AT THETA=90.
      DO 109 K=1,3
      IF(UES(K)-40.)107,108,108
  108 IF(K.EQ.1)R90(K)=-(0.00041*UES(K))+0.4224
      IF(K.EQ.2)R90(K)=-(0.00042*UES(K))+0.4188
      IF(K.EQ.3)R90(K)=-(0.00044*UES(K))+0.4396
      GO TO 109
  107 IF(UES(K)-10.)110,111,111
  110 IF(K.EQ.1)R90(K)=-(0.049*UES(K))+1.
      IF(K.EQ.2)R90(K)=-(0.047*UES(K))+1.
      IF(K.EQ.3)R90(K)=-(0.0451*UES(K))+1.
      GO TO 109
  111 CALL SPLIN2(K,X,Y,UES,R90)
  109 CONTINUE
      DO 19 I=1,3
C CALCULATION OF Q2/Q1.
      QR(I)=(RAT(I)-R90(I))/(1.-R90(I))
      IF(QR(I).LT.0.0)QR(I)=0.0
C CALCULATION OF THETA FOR EACH SENSOR.
      IF(I.NE.1)GO TO 20
      THETA(I)=(1.-SQRT(QR(I)))*90.
      IF(E(1,I)-R(I)*E(2,I))21,22,23
   21 THETA(I)=-THETA(I)
      GO TO 19
   22 THETA(I)=0.0
      GO TO 19
   23 IF(E(1,2)-R(2)*E(2,2))24,25,26
   24 THETA(I)=180.-THETA(I)
      GO TO 19
   25 THETA(I)=THETA(I)
      GO TO 19
   26 THETA(I)=THETA(I)
      GO TO 19
   20 IF(I.NE.2)GO TO 27
      THETA(I)=(1.-SQRT(QR(I)))*90.
```

```
      IF(E(1,I)-R(I)*E(2,I))28,29,19
   28 THETA(I)=-THETA(I)
      GO TO 19
   29 THETA(I)=0.0
      GO TO 19
   27 IF(E(1,1)-R(1)*E(2,1))30,31,32
   30 THETA(I)=180.-((1.-SQRT(QR(I)/1.3))*90.)
      GO TO 19
   31 THETA(I)=90.
      GO TO 19
   32 THETA(I)=(1.-QR(I)**(4./9.))*90.
   19 CONTINUE
      DO 33 I=1,3
   33 THTR(I)=THETA(I)*3.1415927/180.
C START CALCULATION OF PHI FOR EACH SENSOR.
      SBC=1.-(((SIN(THTR(2)))**2)*((COS(THTR(3)))**2))
      SAB=1.-(((SIN(THTR(1)))**2)*((COS(THTR(2)))**2))
      SCA=1.-(((SIN(THTR(3)))**2)*((COS(THTR(1)))**2))
      PHI1(1)=(SIN(THTR(1))*SIN(THTR(3)))/SQRT(SCA)
      PHI2(1)=(COS(THTR(2))*COS(THTR(1)))/SQRT(SAB)
      PHI1(2)=(SIN(THTR(1))*SIN(THTR(2)))/SQRT(SAB)
      PHI2(2)=(COS(THTR(3))*COS(THTR(2)))/SQRT(SBC)
      PHI1(3)=(SIN(THTR(2))*SIN(THTR(3)))/SQRT(SBC)
      PHI2(3)=(COS(THTR(1))*COS(THTR(3)))/SQRT(SCA)
      DO 34 I=1,3
      IF(ABS(PHI1(I)) .GT. 1.000000) PHI1(I)=1.0
      PHIR1(I)=ARSIN(PHI1(I))
      PHIR1(I)=ABS(PHIR1(I))
      IF(ABS(PHI2(I)) .GT. 1.000000) PHI2(I)=1.0
      PHIR2(I)=ARSIN(PHI2(I))
      PHIR2(I)=ABS(PHIR2(I))
   34 CONTINUE
      IF(SCA-SAB)35,36,36
   35 PHIR(1)=PHIR2(1)
      GO TO 37
   36 PHIR(1)=PHIR1(1)
   37 IF(SAB-SBC)38,39,39
   38 PHIR(2)=PHIR2(2)
      GO TO 40
   39 PHIR(2)=PHIR1(2)
   40 IF(SBC-SCA)41,42,42
   41 PHIR(3)=PHIR2(3)
      GO TO 43
   42 PHIR(3)=PHIR1(3)
   43 IF(E(1,3).LT.(R(3)*E(2,3)))PHIR(1)=-PHIR(1)
      IF(E(1,1).LT.(R(1)*E(2,1)))PHIR(2)=-PHIR(2)
      IF(E(1,2).LT.(R(2)*E(2,2)))PHIR(3)=-PHIR(3)
C CALCULATION OF EXPECTED (U1) AND CALCULATED (UCOMP) PROBE
C -ORIENTED VELOCITIES.
      DO 44 I=1,3
```

```
      U1(I)=UP*SIN(X51(I))
      UCOMP(I)=UNS*SIN(PHIR(I))
   44 PHI(I)=PHIR(I)*180./3.1415927
      DO 142 I=1,3
  142 PCTER(I)=100.0*(UCOMP(I)-U1(I))/UP
      WRITE(6,45)E10
   45 FORMAT(5X,'E(I,J)',6(5X,F8.4))
      WRITE(6,46)CF
   46 FORMAT(5X,'CF(I,J)',6(5X,F8.4))
      WRITE(6,49)UP,UPS,UNS,US
   49 FORMAT(5X,'UP=',1X,F9.4,5X,'UPS=',1X,F9.4,5X,'UNS=',
     11X,F9.4,5X,'US=',1X,F9.4)
      WRITE(6,150)
  150 FORMAT(3X,'Q/DELTA T',6X,'UES',8X,'QD/QU',6X,'Q2/Q1',
     16X,'THETA',5X,'PHI(EXP)',3X,'PHI(CALC)',4X,'U(EXP)',
     29X,'U',3X,'PCTER')
      DO 50 I=1,3
   50 WRITE(6,47)HT(I),UES(I),RAT(I),QR(I),THETA(I),XXX(I),
     1PHI(I),U1(I),UCOMP(I),PCTER(I)
   47 FORMAT(3X,F8.5,3X,F10.5,3X,F8.5,3X,F8.5,3X,F9.4,3X,
     1F8.4,3X,F8.4,3X,F9.4,3X,F9.4.3X,F9.4)
  100 CONTINUE
      STOP
      END
      SUBROUTINE SPLIN2(N,X,Y,XARG,YARG)
C SUBROUTINE SPLIN2 CALCULATES THE VALUE OF QD/QU AT THETA=
C 90 FOR A SPECIFIC VALUE OF THE EFFECTIVE COOLING VELOCITY.
C ONE IS CALCULATED FOR EACH SENSOR. AS,BS, AND CS ARE THE
C COEFFICIENTS SPECIFIED BY AN EARLIER PROGRAM. N IS AN
C INDEX WHICH INDICATES WHICH VALUE OF QD/QU(I.E., WHICH
C SENSOR) TO USE. YARG(J) IS THE VALUE OF QD/QU AT THETA=90
C DESIRED.
      COMMON/SPLINE/AS(3,3),BS(3,3),CS(3,3)
      DIMENSION X(4),Y(3,4),XARG(3),YARG(3)
      Y(2,1)=0.530
      Y(2,2)=0.4463
      Y(2,3)=0.4129
      Y(2,4)=0.4018
      Y(1,1)=0.51
      Y(1,2)=0.439
      Y(1,3)=0.414
      Y(1,4)=0.406
      Y(3,1)=0.549
      Y(3,2)=0.458
      Y(3,3)=0.432
      Y(3,4)=0.422
      J=N
      DO 101 I=1,3
      IF(XARG(J)-X(I+1))102,101,101
  101 CONTINUE
```

```
  102 Q=(XARG(J)-X(I))/(X(I+1)-X(I))
      YARG(J)=Y(J,I)+AS(J,I)*Q+BS(J,I)*Q**2+CS(J,I)*Q**3
      RETURN
      END
      SUBROUTINE ANGLE(ALP,BET,X51,XXX)
C    ALP AND BET ARE THE ANGLES OF ATTACK OF THE PROBE IN
C RADIANS. THE X51'S ARE THE CALCULATED PHI'S IN RADIANS,
C AND THE XXX'S ARE THE CALCULATED PHI'S IN DEGREES.
      DIMENSION X51(3),XXX(3)
      XX=(0.57735*COS(ALP)*COS(BET))+(0.81650*COS(BET)*
     1SIN(ALP))
      YY=(0.57735*COS(BET)*COS(ALP))-(0.70711*SIN(BET))-
     1(0.40824*COS(BET)*SIN(ALP))
      ZZ=(0.57735*COS(BET)*COS(ALP))+(0.70711*SIN(BET))-
     1(0.40824*COS(BET)*SIN(ALP))
      X51(1)=ARSIN(XX)
      X51(2)=ARSIN(YY)
      X51(3)=ARSIN(ZZ)
      XXX(1)=X51(1)*180./3.1415927
      XXX(2)=X51(2)*180./3.1415927
      XXX(3)=X51(3)*180./3.1415927
      RETURN
      END
```

SPECIAL DISTRIBUTION

Scientific and Technical Information Facility (5 copies)
National Aeronautics and Space Administration
P. O. Box 33
College Park, Maryland 20740

Wallops Station
National Aeronautics and Space Administration
Wallops Island, Virginia 23337

Mr. R. L. Krieger, Director	(1 copy)
Mr. A. D. Spinak, Associate Director	(1 copy)
Mr. M. W. McGoogan	(1 copy)
Mr. W. H. West	(1 copy)
Mr. J. W. Gray	(1 copy)
Mr. J. F. Spurling	(1 copy)

Dr. G. H. Fichtl (1 copy)
George C. Marshall Space Flight Center
Aerospace Environment Division
Huntsville, Alabama 35812

Mr. R. M. Henry (1 copy)
ESSD Planetary Atmospheres Section
NASA
Langley Research Center - Mail Stop 160
Hampton, Virginia 23365

Dr. E. C. Kindle (2 copies)
Assistant Dean, School of Sciences
Old Dominion University
Norfolk, Virginia 23508

Dr. M. Hoshiya (1 copy)
Masashi Institute of Technology
Tokyo, JAPAN

Engineering Research Center
Colorado State University
Fort Collins, Colorado 80521

Dr. J. E. Cermak	(1 copy)
Professor V. A. Sandborn	(1 copy)

Dr. R. D. Marshall (1 copy)
National Bureau of Standards
Building Research Division
Washington, D. C. 20234